International School for Advanced Studies

Dissertation Submitted for the Degree of
"Doctor Philosophiæ"

Magnetism and Superconductivity in the Two-Band Hubbard Model

A Variational Monte Carlo Perspective

Supervisors:

Dr. Federico Becca

Dr. Luca F. Tocchio

Candidate:

Caterina De Franco

October 2018

Acknowledgement

Trieste, October 2018

I would like to thank SISSA for giving me the opportunity to study here and I am also grateful to Federico and Luca for their guidance, help and patience.

Introduction

More than thirty years after the historical discovery of Cuprate high-temperature superconductors (Bednorz and Müller 1986), understanding their underlying pairing mechanism remains one of the biggest challenges in condensed matter physics. The more recent discovery of Iron-based superconductors (Kamihara, Watanabe, Hirano, and Hosono 2008) provides a great opportunity to identify the important ingredients that are common to both families of high-temperature superconductor materials and to test the theoretical approaches that have been formulated for Cuprates.
Both in Iron-based compounds and in Cuprates, the low-energy properties are determined by the electrons in d orbitals, in which the competition between kinetic energy and electron-electron repulsion plays a central role in determining the ultimate physical properties. The simplest model that describes this behavior is the single-band Hubbard model (Hubbard 1963). Despite its simplicity, the Hubbard model shows the occurrence of a variety of phenomena, such as Mott metal-insulator transition, magnetic order and possibly superconductivity. It is widely recognized that the one-band Hubbard model or its strong coupling version (namely the $t-J$ model) can capture the main features of the superconductive pairing of Cuprates (Lee, Nagaosa, and Wen 2006). By contrast, keeping a single orbital is not adequate for describing generic transition-metal compounds in which d shell multiplets are partially filled and, therefore, orbital fluctuations cannot be neglected. For instance, in Iron-based superconductors, all five d orbitals are expected to play an important role in conducting properties and only the inclusion of multi-orbital effects can correctly characterize their nature (Fernandes and Chubukov 2016).

The particular aspects of the band structure, including the symmetry properties of the d orbitals, are certainly important to obtain a detailed description of these materials; however, their main features at low temperatures should be triggered by the existence of strong electron-electron correlations, e.g., the on-site Coulomb potential and the Hund coupling. In this regard, it is important to understand the interplay between kinetic and potential terms in a simplified model, in which the kinetic part is the same for all the

orbitals. Therefore, we will concentrate on a multi-orbital model with degenerate bands. Besides being interesting *per se* as natural and simple extension of the one-band model, the two-band Hubbard model is the minimal model that can capture various forms of collective fluctuations among spin, charge, and orbital degrees of freedom. In particular, in this thesis we show that the presence of more than one electronic band, together with the non-trivial effects of Hund coupling, brings to a scenario that is different from the one emerging from the one-band model.

Our investigations are based on the Variational Monte Carlo method. Nowadays, drastic improvements of computer facilities gave us the opportunity to use Quantum Monte Carlo approaches with great numerical accuracy. An important part of this thesis is devoted to the definition of the Jastrow-Slater variational wave function and the technical details on how to optimize the variational parameters in order to better approximate the ground state properties. By varying the variational wave function, we are able to assess the zero-temperature properties in different physical regimes, also including the case where no magnetic/orbital order is present, in order to compare our findings with previous Dynamical Mean-Field Theory calculations.
The starting point is the theoretical understanding of the Mott metal-insulator transition, which takes place when increasing the Coulomb interaction U. Here, the presence of the Hund coupling J has some important consequences that manifest in different ways when changing the electron density. For example, in the paramagnetic sector, while J clearly favors the Mott insulator at half filling, by lowering the critical value U_{MIT}, for other integer fillings the critical U_{MIT} is pushed towards higher values. When including magnetic/orbital order, the Mott insulator acquires antiferromagnetic order at half filling, whereas for quarter filling (i.e., one electron per site) it turns out to have ferromagnetic and antiferro-orbital orders.

Another remarkable difference with respect to the one-band model concerns the superconductive pairing state. When more than one band is present, several distinct channels (symmetries) can be realized, including intra- and inter-orbital pairing, with singlet or triplet character. Our results show that the on-site spin-triplet superconductivity is predominant in a large part of the phase diagram. This kind of pairing can be easily understood in the presence of the ferromagnetic Hund coupling that favors high-spin states. Moreover, unlike in the one-band Hubbard model, a nearest-neighbor intra-orbital singlet pairing cannot be stabilized away from half-filling. The interplay among various degrees of freedom that are present when more than one orbital is taken into account, brings to a fascinating phase diagram where superconductivity, magnetic, and orbital orders are present.

The outline of the thesis will be as follows:

- in Chapter I we will review the basic ideas behind the physics of Mott insulators, stressing the underling concept of electron-electron correlation. We will elucidate the peculiarities of the two families of high temperature superconductors, Cuprates and Iron-based superconductors, exposing also the basics of BCS theory. Finally we will present our model.

- in Chapter II we will analyze the computational method we used, Variational Monte Carlo. After having clarified the variational principle and the Metropolis algorithm, we will explain the details of minimization algorithm. We will conclude the chapter by examining the Jastrow-Slater variational wavefunction.

- in Chapter III we will present our results on the two degenerate band Hubbard model, focusing on the case when the Hund coupling is present. We will also demonstrate that, for some particular cases, the addition of another degenerate band, does not change the general conclusions we draw for the two-band case. We will show how the phase diagram changes when orbital or magnetic orders are allowed in the wave function and which kind of superconductive pairing arises upon doping the Mott insulating state. Finally, we will summarize the obtained results in two phase diagrams.

Contents

Chapter 1

Mott insulators and high-temperature superconductivity: models and materials

Band theory was the first successful theoretical description of metals and insulators. Indeed, it was able to predict the metallic or insulating character of a given material by simple inspection of the electronic spectrum. The solution of the Schrödinger equation, in the presence of the periodic potential, generated by the lattice, gives rise to a band structure, namely a set of electronic states specified by $E_n(\mathbf{q})$ (where $\mathbf{q}$ is the momentum and n is an integer that labels the band) (Ashcroft and Mermin 2011). At zero temperature, the many-body ground state is obtained by populating the lowest-energy levels, in accordance with the Pauli principle. Then, the distinction between metals and insulators is determined by the filling of the electronic bands: whenever the highest occupied band is completely filled and there is a finite gap to the lowest unoccupied one, the system is an insulator; otherwise, in the presence of partially filled electronic bands, the system is a metal.

The foundations of the band theory rely on a strong approximation in which electrons behave as independent particles. Here, the Coulomb interaction is replaced by an effective single-particle potential that represents the average (mean-field) interaction felt by each electrons and generated by all the other ones. In the early years of quantum mechanics the band picture was already well established, however, a few transition-metal

oxides with partially-filled d-electron bands were reported as insulators. As already pointed out by Mott and Peierls 1937, the missing ingredient of the band theory is the lack of a proper description of electronic interaction. These observations set off the long and continuing history of strongly-correlated electron systems.

1.1 Metal-insulator transition

A milestone in the field of strongly-correlated electron systems was reached by the definition of the Mott insulator (Mott 1949), which describes a situation where a material should be metallic according to band theory, but instead it is insulating due to a strong electron-electron repulsion that dominates over the kinetic energy. The paradigm of a Mott insulator can be pictured by considering a lattice made by Hydrogen atoms. For concreteness, we can consider a three-dimensional cubic lattice with N sites; whenever only the lowest-energy $1s$ orbital is included in the calculation, there is a single band, hosting at most $2N$ electrons (here, the factor 2 is due to the spin degeneracy). When the total number of electrons is N the band is half filled and, according to band theory, the ground state should be a metal. However, the bandwidth decreases exponentially with the distance between neighboring atoms and, at large distances, the Coulomb repulsion prevails over the kinetic energy. As a consequence, it is natural to expect that electrons localize on different sites, in order to minimize the potential energy. Notice that the insulating behavior is not accompanied by any symmetry breaking phenomenon, such as the appearence of charge or spin density waves. In this respect, the Mott insulator is genuinely different from what can be obtained within the band theory by breaking some symmetry. For instance, within the previous example with N electrons on N sites, an insulator can be obtained by allowing antiferromagnetic order, which leads to an enlarged unit cell with two atoms. In this case, there will be two electronic bands separated by a finite gap: the lowest band would be completely filled, while the highest one would be empty, thus leading to a band insulator.

In general, the band theory predicts a metallic behavior for all cases with an odd number of electrons per unit cell, while an insulator is only possible for an even number of particles in the unit cell (in the previous example with antiferromagnetic order at half filling, we have two electrons per unit cell). By contrast, a Mott insulator is possible for an odd number of particles per unit cell, because they can localize thanks to the (strong) electron-electron repulsion. Indeed, the band theory fails to predict the nature of materials like the transition-metal oxides (e.g., CoO, V_2O_3, NiO) that have an odd number of electrons per unit cell and, therefore, cannot be insulating when only the band

filling is considered. The breakdown of the band theory becomes clear when the electron-electron interaction is not negligible. Let us consider a single atom with an electron in the $1s$ orbital with energy $\epsilon_{\rm at}$. When adding a second electron, the total energy turns out to be $2\epsilon_{\rm at}+U$ where U is the Coulomb interaction between the two electrons (see Fig. 1.1). These energy levels are fundamentally different from the usual single-electron spectrum. Indeed, the upper level at $\epsilon_{\rm at}+U$ exists only because there is already an electron occupying the lower level at $\epsilon_{\rm at}$. When a lattice is considered instead of a single atom, electrons become delocalized; then, the energy levels at $\epsilon_{\rm at}$ and $2\epsilon_{\rm at}+U$ acquire some broadening (see Fig. 1.2), giving rise to the concept of the Hubbard "bands", which are related to the incoherent part of the one-particle spectral function. Notice that the Hubbard bands should not be confused with standard electronic bands, which give rise to a coherent peak in the spectral weight. By increasing the Coulomb interaction U, a gap is developing between the lower and upper Hubbard bands, thus switching the system from a metal to a Mott insulator: this is the so-called Mott metal-insulator transition (MIT).

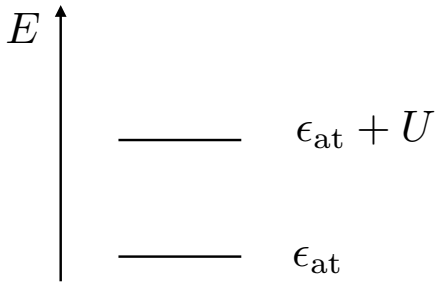

Figure 1.1: Single site spectrum in the presence of the electron-electron interaction.

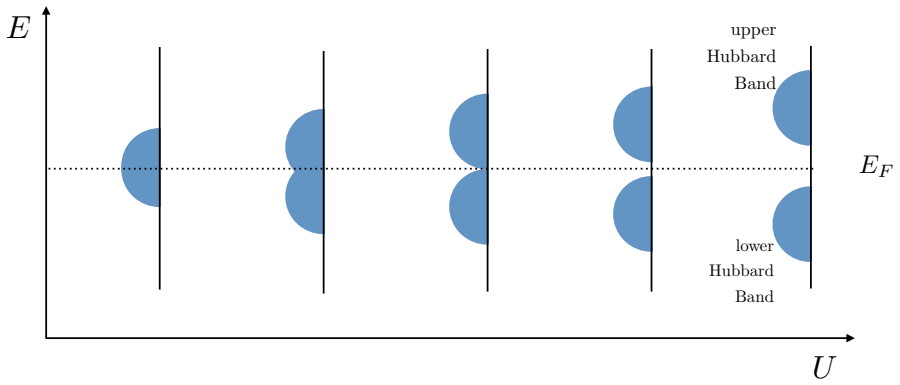

Figure 1.2: Sketch of a Mott transition: due to the increase of the Coulomb interaction U, the metallic band separates into the lower Hubbard band and the upper Hubbard band.

1.2 The Hubbard model

A clear prototype of a Mott transition is described by the Hubbard model, which gives a simplified descrition of interacting electrons on a lattice. The Hubbard Hamiltonian was written down by Hubbard 1964, Gutzwiller 1963 and Kanamori 1963. Its form arises quite naturally from considering a lattice of L atoms (sites) on which the fermions move. Let us derive the Hubbard Hamiltonian from general principles. Our starting point is the many-body Hamiltonian for N interacting electrons in a periodic potential provided by the ions in a lattice within the Born-Oppenheimer approximation (Giuliani and Vignale 2005):

$$\begin{aligned}\mathcal{H} =&\mathcal{H}_{\text{kin}} + \mathcal{H}_{\text{el-ion}} + \mathcal{H}_{\text{int}} = \\ =&-\frac{\hbar^2}{2m}\sum_{n=1}^{N}\nabla_n^2 + \sum_{n=1}^{N}\sum_{i=1}^{L}V_1(\mathbf{x}_n - \mathbf{R}_i) + \frac{1}{2}\sum_{n\neq n'}V_2(\mathbf{x}_n - \mathbf{x}_{n'})\end{aligned} \tag{1.1}$$

where $\mathbf{x}_n$ is the positions of the $n-th$ electron, while $\mathbf{R}_i$ indicates the position of the i-th ion on the lattice. V_1 and V_2 are the electron-ion potential and electron-electron interaction, respectively.

In order to obtain the Hamiltonian in second quantization formalism, we introduce a basis set of single-particle wave functions for every site $\mathbf{R}$ of the lattice, $\chi_{\alpha,\mathbf{R}}(\mathbf{x},\sigma)$. Since the Hamiltonian (1.1) is spin-independent we can work with factorized wave functions, i.e., $\chi_{\alpha,\mathbf{R}}(\mathbf{x},\sigma) = \chi_{\alpha,\mathbf{R}}(\mathbf{x})\omega_\sigma$. The spatial part is given by localized Wannier orbitals, satisfying the following conditions:

$$\begin{aligned}&\int d\mathbf{x}\,\chi_{\alpha,\mathbf{R}_1}(\mathbf{x})\,\chi_{\beta,\mathbf{R}_2}(\mathbf{x}) = \delta_{\alpha,\beta}\delta_{\mathbf{R}_1,\mathbf{R}_2}\\ &\sum_{\alpha,\mathbf{R}}\chi^\star_{\alpha,\mathbf{R}}(\mathbf{x})\,\chi_{\alpha,\mathbf{R}}(\mathbf{y}) = \delta(\mathbf{x}-\mathbf{y})\end{aligned} \tag{1.2}$$

Then, the Fermi fields for the electrons whit spin σ in real space read:

$$\Phi_\sigma(\mathbf{x}) = \sum_{\alpha,\mathbf{R}}\chi_{\alpha,\mathbf{R}}(\mathbf{x})\,c_{\alpha,\mathbf{R},\sigma}, \qquad \Phi^\dagger_\sigma(\mathbf{x}) = (\Phi_\sigma(\mathbf{x}))^\dagger \tag{1.3}$$

where $c_{\alpha,\mathbf{R},\sigma}$ ($c^\dagger_{\alpha,\mathbf{R},\sigma}$) are the annihilation (creation) operators that destroy (create) a fermion in the Wannier state $\chi_{\alpha,\mathbf{R}}(\mathbf{x})$.

The second-quantization form of the non-interacting part of the Hamiltonian be-

comes:

$$\begin{aligned}\mathcal{H}_{\rm kin}+\mathcal{H}_{\rm el-ion} &= \sum_{\sigma}\int d\mathbf{x}\,\Phi^{\dagger}_{\sigma}(\mathbf{x})\left[-\frac{\hbar^2}{2m}\nabla^2+\sum_i V_1(\mathbf{x}-\mathbf{R}_i)\right]\Phi_{\sigma}(\mathbf{x}) = \\ &= \sum_{\sigma}\sum_{\alpha,\beta}\sum_{\mathbf{R}_1,\mathbf{R}_2} t^{\alpha,\beta}_{\mathbf{R}_1,\mathbf{R}_2}\, c^{\dagger}_{\alpha,\mathbf{R}_1,\sigma}c_{\beta,\mathbf{R}_2,\sigma}\end{aligned} \tag{1.4}$$

where the matrix elements $t^{\alpha,\beta}_{\mathbf{R}_1,\mathbf{R}_2}$ are given by:

$$t^{\alpha,\beta}_{\mathbf{R}_1,\mathbf{R}_2} = \int d\mathbf{x}\,\chi^{\star}_{\alpha,\mathbf{R}_1}(\mathbf{x})\left[-\frac{\hbar^2}{2m}\nabla^2+\sum_i V_1(\mathbf{x}-\mathbf{R}_i)\right]\chi_{\beta,\mathbf{R}_2}(\mathbf{x}) \tag{1.5}$$

with $t^{\alpha,\beta}_{\mathbf{R}_1,\mathbf{R}_2} = (t^{\beta,\alpha}_{\mathbf{R}_2,\mathbf{R}_1})^{\star}$.

Upon Fourier transforming the fermion operators, the non-interacting Hamiltonian (1.4) becomes:

$$\mathcal{H}_{\rm kin}+\mathcal{H}_{\rm el-ion} = \frac{1}{L}\sum_{\sigma}\sum_{\alpha,\beta}\sum_{\mathbf{R}_1,\mathbf{R}_2}\sum_{\mathbf{q}_1,\mathbf{q}_2} e^{-i\mathbf{q}_1\mathbf{R}_1}e^{i\mathbf{q}_2\mathbf{R}_2}t^{\alpha,\beta}_{\mathbf{R}_1,\mathbf{R}_2}\, c^{\dagger}_{\alpha,\mathbf{q}_1,\sigma}c_{\beta,\mathbf{q}_2,\sigma} \tag{1.6}$$

Within a regular lattice structure, the hopping matrix $t^{\alpha,\beta}_{\mathbf{R}_1,\mathbf{R}_2}$ depends upon the relative distance $|\mathbf{R}_1-\mathbf{R}_2|$, so that:

$$t^{\alpha,\beta}_{\mathbf{R}_1,\mathbf{R}_2} = \frac{1}{L}\sum_{\mathbf{q}} e^{i\mathbf{q}(\mathbf{R}_1-\mathbf{R}_2)}t^{\alpha,\beta}_{\mathbf{q}} \tag{1.7}$$

Therefore, Eq. (1.6) becomes:

$$\mathcal{H}_{\rm kin}+\mathcal{H}_{\rm el-ion} = \sum_{\sigma}\sum_{\alpha,\beta}\sum_{\mathbf{q}} t^{\alpha,\beta}_{\mathbf{q}}\, c^{\dagger}_{\alpha,\mathbf{q},\sigma}c_{\beta,\mathbf{q},\sigma} \tag{1.8}$$

Similarly, the interaction part can be written as:

$$\mathcal{H}_{\rm int} = \frac{1}{2}\sum_{\sigma\sigma'}\sum_{\alpha,\beta,\gamma,\delta}\sum_{\mathbf{R}_1\mathbf{R}_2\mathbf{R}_3\mathbf{R}_4} U^{\alpha,\beta,\gamma,\delta}_{\mathbf{R}_1,\mathbf{R}_2,\mathbf{R}_3,\mathbf{R}_4}\, c^{\dagger}_{\alpha,\mathbf{R}_1,\sigma}c^{\dagger}_{\beta,\mathbf{R}_2,\sigma'}c_{\gamma,\mathbf{R}_3,\sigma'}c_{\delta,\mathbf{R}_4,\sigma} \tag{1.9}$$

where

$$U^{\alpha,\beta,\gamma,\delta}_{\mathbf{R}_1,\mathbf{R}_2,\mathbf{R}_3,\mathbf{R}_4} = \int d\mathbf{x}d\mathbf{y}\,\chi^{\star}_{\alpha,\mathbf{R}_1}(\mathbf{x})\chi^{\star}_{\beta,\mathbf{R}_2}(\mathbf{y})\,V_2(\mathbf{x}-\mathbf{y})\,\chi_{\gamma,\mathbf{R}_3}(\mathbf{y})\chi_{\delta,\mathbf{R}_4}(\mathbf{x}) \tag{1.10}$$

So far everything is exact. The Hubbard model was proposed for the description

of electrons in narrow bands, where Wannier orbitals have a noticeable local character. Here, the first approximation consists in considering only one orbital (with s character for simplicity) on each site (atom); this fact can be justified whenever inter-orbital processes can be neglected because of large energy gaps among the d levels, like in the Cuprates where the relevant charge fluctuations involve only the $d_{x^2-y^2}$ orbital. Therefore, in the following, we will drop the orbital indices and keep only the ones related to the atomic position. The second important approximation is given by neglecting all the interaction terms but the local one with $\mathbf{R} \equiv \mathbf{R}_1 = \mathbf{R}_2 = \mathbf{R}_3 = \mathbf{R}_4$. This defines the Hubbard U interaction $U = U_{\mathbf{R},\mathbf{R},\mathbf{R},\mathbf{R}}$, which triggers the electronic repulsion when two particles reside on the same atom (with opposite spins). Finally, in the simplest version of the model, only nearest-neighbor hoppings are kept, i.e., $t = -t_{\mathbf{R}_1,\mathbf{R}_2}$ for nearest-neighbor sites $\mathbf{R}_1$ and $\mathbf{R}_2$ and zero otherwise. The hopping parameter is negative, in order to have the minimum of energy in the totally symmetric Γ point. Thus, the Hubbard model is described by two parameters, the electron correlation strength U and the hopping (or tunneling) t:

$$\mathcal{H} = -t \sum_{\langle i,j\rangle\sigma} c^\dagger_{i,\sigma} c_{j,\sigma} + \text{h.c.} + U \sum_i n_{i,\uparrow} n_{i,\downarrow} \tag{1.11}$$

where $\langle i,j\rangle$ indicates that i and j are nearest-neighbor sites and $n_{i,\sigma} = c^\dagger_{i,\sigma} c_{i,\sigma}$ is the electronic density per spin σ on site i.

The Mott insulator can be realized at half filling, namely when the number of electrons N equals the number of sites L. How does the Mott insulator come out of the Hubbard model? Let us analyze the two dimensional case at half filling for $U \gg t$. In this case we should start from the configuration which minimizes the Coulomb repulsion U and treats the kinetic term by perturbation theory. The lowest energy configuration is the one in which each site is singly occupied. Indeed, the energy cost of having just an empty site and a doubly occupied one instead of two singly occupied sites is given by:

$$E(2) + E(0) - 2E(1) = U \tag{1.12}$$

which is much larger than the energy gain due to the kinetic term, which is of order t. Therefore, there is a finite energy gap to create charge excitations. Still, the configuration with one electron per site is largely degenerate, since there are 2^L degenerate states with one electron per site due to the spin of every electron. The hopping term is able to split the degeneracy within second order in perturbation theory, giving rise to a large-U effective Hamiltonian describing localized spins coupled together by the super-exchange $J = 4t^2/U$. Indeed, for a given pair of neighbouring sites the four ground states in the

atomic limit are

Singlet state	Triplet state
	$\|\uparrow,\uparrow\rangle$
$\frac{1}{\sqrt{2}}(\|\uparrow,\downarrow\rangle - \|\downarrow,\uparrow\rangle)$	$\|\downarrow,\downarrow\rangle$
	$\frac{1}{\sqrt{2}}(\|\uparrow,\downarrow\rangle + \|\downarrow,\uparrow\rangle)$

When the hopping t is introduced perturbatively, there is a virtual transition from the singlet state to intermediate (doubly-occupied) configurations:

$$\frac{(|\uparrow,\downarrow\rangle - |\downarrow,\uparrow\rangle)}{\sqrt{2}} \longrightarrow \frac{(|\uparrow\downarrow,0\rangle + |0,\uparrow\downarrow\rangle)}{\sqrt{2}} \nearrow \frac{(|\downarrow,\uparrow\rangle - |\uparrow,\downarrow\rangle)}{\sqrt{2}}$$
$$\qquad\qquad\qquad\qquad\qquad\qquad\qquad\qquad\qquad\qquad \searrow \frac{(|\uparrow,\downarrow\rangle - |\downarrow,\uparrow\rangle)}{\sqrt{2}}$$

Instead, the triplet states cannot give rise to such virtual transitions, because of the Pauli principle. This process results in an energy gain of the order $4t^2/U$.

The effective Hamiltonian that is obtained within this perturbation approach is called Heisenberg or super-exchange model.

$$\mathcal{H} = J \sum_{\langle ij \rangle} \mathbf{S}_i \cdot \mathbf{S}_j = J \sum_{\langle ij \rangle} \left(S_i^x S_j^x + S_i^y S_j^y + S_i^z S_j^z \right) \tag{1.13}$$

where $\mathbf{S}_i = (S_i^x, S_i^y, S_i^z)$ denotes the spin operator on the site i.

Therefore, an effective antiferromagnetic super-exchange coupling $J = 4t^2/U$ is generated within the insulating regime. This fact can lead to magnetic order, thus spoiling the nature of the Mott insulator, which would become an ordinary band insulator with magnetic order. For example, on the square lattice, the quantum fluctuations generated by $(S_i^x S_j^x + S_i^y S_j^y)$ terms only marginally affect the classical state, which is obtained by minimizing the $S_i^z S_j^z$ terms. In this case, the ground state of the Heisenberg model has a finite magnetization at zero temperature, being described as a "dressed" (by quantum fluctuations) classical antiferromagnet. In order to enhance quantum fluctuations and drive the system into a pure Mott insulator with no broken symmetries down to zero temperature, it is important to consider *frustrated* lattices, where the classical ground

state is not unique. Another option, is to increase quantum fluctuations by incorporating more than one orbital per site, thus generating orbital fluctuations that may destabilize the classical order. In this context, Anderson 1973 and Fazekas and Anderson 1974 gave a milestone contribution to define a wave function that may capture the essence of Mott insulators. This is the so-called resonating-valence-bond (RVB) state, which is constructed by considering a superposition of singlets formed by electrons on different sites (in the simplest version, we can consider the case where electrons reside on nearest-neighbor sites). Notice that the number of these configurations is exponentially large with the system size. Like in the benzene molecule, where singlets "resonate" between the two different Kekulé configurations, in the RVB state all the possible singlet configurations resonate through a tunneling procedure; nowadays, we know that different superpositions of singlet configurations give RVB states with different topological properties (Wen 2004). At half filling, the strong electron-electron repulsion prevents an electric current and, therefore, the RVB state describes a Mott insulator. Although this kind of wave function may be not adequate to describe the correct ground state of the microscopic model (which may possess magnetic long-range order), it may be eventually stabilized when few electrons are removed, leaving empty sites (holes). In this context, superconductivity emerges naturally from the Mott insulator, since electrons are already paired together to form singlets; when holes are present in the system, they can move around without any penalty due to the strong correlation, giving rise to superconductivity. We would like to notice that this kind of RVB state, with coherent mobile carriers, is indistinguishable, in terms of symmetry, from a standard superconductor (Lee, Nagaosa, and Wen 2006). Anderson a suggested practical way to describe the RVB state by considering a BCS wave function where all configurations with one or more doubly occupied sites are eliminated. Soon after the original Anderson's suggestion, intensive numerical calculations based on his idea, enlightened the importance of the RVB theory in the understanding of high-temperature superconductors.

1.3 The origin of attractive interaction

At the beginning of the 20th century, the Dutch physicist Kamerlingh Onnes made a groundbreaking step forward in low-temperature physics: he succeeded to liquify helium (Van Delft and Kes 2010). At that time, it was known that the electric conductance was due to the motion of electrons while the resistivity to their scattering by the ions. Therefore, the question of greatest importance was: upon approach 0K, which of the two would be the first to decrease? The scattering amplitude, leading to no resistivity or the electron

mobility bringing to no conductivity? By using a cryostat filled with liquid helium, he reported the jump of the resistance of an ultrapure mercury sample from about 12Ω to less than $10^{-6}\Omega$ within an interval of 0.01K, thus reporting the first evidence for a superconducting phase of matter. In the years after Onnes' discovery, physicists, seeking for the microscopic mechanism to explain superconductivity, focused on how to treat properly Coulomb interaction or to define the role of the crystal in the superconducting process. For a long time, people did not consider the possibility that phonons could have a role until the isotopic effect was discovered in 1950 (Maxwell 1950; Reynolds, Serin, Wright, and Nesbitt 1950), showing that transition temperature depends on the isotopic mass. Soon after this important fact, it became clear that the screening by the ionic motion can yield an attractive interaction between electrons with energies sufficienlty close together (namely separated by less than the typical phonon energy). Armed with this discovery, Cooper (Cooper 1956) showed that this attractive interaction naturally leads to the creation of electron pairs, now known as Cooper pairs. Finally, within a year, Bardeen, Cooper, and Schrieffer 1957 (BCS) developed a microscopic description of the superconducting state as a condensate state of Cooper pairs.

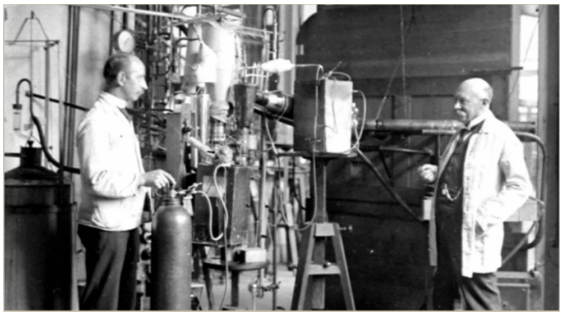

Figure 1.3: Heike Kamerlingh Onnes (right) and Gerrit Flim, his chief technician, at the helium liquefier in Leiden, circa 1911 (Van Delft and Kes 2010).

Although the phonon mechanism is the foundation for electron pairing in standard superconductors, it is important to recognize that the BCS model only requires an attractive interaction, no matter what is its origin. Different pairing mechanisms may be responsible for superconductivity in high-temperature superconductors (Monthoux, Pines, and Lonzarich 2007), nonetheless, the macroscopic phenomenology of the resulting superconducting state changes only very little. The superconducting order parameter captures the essence of the macroscopic condensation of Cooper pairs, even in the absence of detailed knowledge about the microscopic origin of superconductivity. Hence, the basic BCS model is expected to capture the fundamental properties of all superconductors.

1.3.1 The BCS theory

The great achievement obtained by Bardeen, Cooper and Schrieffer was to write down a simple and insightful variational wave function that describes the superconducting phase. Here, the ground state can be pictured as a superposition of states where the pair with momenta $(\mathbf{q}, -\mathbf{q})$ and opposite spins is either occupied or empty:

$$|\Psi_{BCS}\rangle = \prod_q (u_q + v_q c^\dagger_{q,\uparrow} c^\dagger_{-q,\downarrow}) \, |0\rangle \tag{1.14}$$

where $|0\rangle$ represents the vacuum, $c^\dagger_{q,\sigma}$ creates an electron with momentum $\mathbf{q}$ and spin σ; u_q and v_q are variational parameters. Without loss of generality, we can take $|u_q|^2+|v_q|^2=1$, in order to enforce the normalization of the BCS wave function. Indeed, we have that:

$$\begin{aligned}
&\langle \Psi_{BCS} \,|\, \Psi_{BCS} \rangle = \langle 0| \prod_q (u^\star_q + v^\star_q c_{-q,\downarrow} c_{q,\uparrow}) \prod_{q'} (u_{q'} + v_{q'} c^\dagger_{q',\uparrow} c^\dagger_{-q',\downarrow}) \, |0\rangle = \\
&= \langle 0| \prod_q \prod_{q'} (u^\star_q u_{q'} + u^\star_q v_{q'} c^\dagger_{q',\uparrow} c^\dagger_{-q',\downarrow} + v^\star_q u_{q'} c_{-q,\downarrow} c_{q,\uparrow} + v^\star_q v_{q'} c_{-q,\downarrow} c_{q,\uparrow} c^\dagger_{q',\uparrow} c^\dagger_{-q',\downarrow} \, |0\rangle = \\
&= \prod_q (|u_q|^2+|v_q|^2)
\end{aligned} \tag{1.15}$$

Notice that the BCS wave function does not describe a state with a fixed number of particles and therefore we have

$$\left\langle \Psi_{BCS} \left| \, c^\dagger_{q,\uparrow} c^\dagger_{-q,\downarrow} \, \right| \Psi_{BCS} \right\rangle \neq 0 \tag{1.16}$$

Microscopically, the electron pairing is originated from the attraction mediated by the electron-phonon interaction. As originally proposed by Bardeen, Cooper, and Schrieffer 1957, we can consider an effective Hamiltonian for the reduced problem of electron pairs with total momentum $\mathbf{P} = 0$:

$$\mathcal{H}_{BCS} = \sum_{q,\sigma} \epsilon_q c^\dagger_{q,\sigma} c_{q,\sigma} + \frac{1}{N} \sum_{q,q'} V_{q,q'} c^\dagger_{q,\uparrow} c^\dagger_{-q,\downarrow} c_{-q'\downarrow} c_{q'\uparrow} \tag{1.17}$$

where ϵ_q is the electron dispersion and $V_{q,q'} = -V$ if $|\epsilon_q| \leq \omega_D$ and $|\epsilon_{q'}| \leq \omega_D$ and zero otherwise. This kind of Hamiltonian can be viewed as a low-energy model describing the residual interactions $V_{q,q'}$ between the quasi-particles in the normal phase. By in-

troducing the "pairon" operators:

$$b_q^\dagger = c_{q,\uparrow}^\dagger c_{-q,\downarrow}^\dagger \tag{1.18}$$

$$b_q = c_{-q,\downarrow} c_{q,\uparrow} \tag{1.19}$$

and $n_{q,\sigma} = c_{q,\sigma}^\dagger c_{q,\sigma}$, the effective Hamiltonian (1.17) can be written as:

$$\mathcal{H}_{BCS} = \sum_{q,\sigma} \epsilon_q n_{q,\sigma} + \frac{1}{N} \sum_{q,q'} V_{q,q'} b_q^\dagger b_{q'} \tag{1.20}$$

For an attractive potential, the ground state of $\mathcal{H}_{BCS}$ has no pairs $(\mathbf{q},\uparrow;-\mathbf{q},\downarrow)$ occupied by a single electron. In this case, the operator $n_{q,\uparrow} + n_{-q,\downarrow}$ can be replaced by $2b_q^\dagger b_q$, leading to:

$$\mathcal{H}_{BCS} = 2\sum_{q} \epsilon_q b_q^\dagger b_q + \frac{1}{N} \sum_{q,q'} V_{q,q'} b_q^\dagger b_{q'} \tag{1.21}$$

Then, whenever $n_{q,\uparrow} + n_{-q,\downarrow} = 2b_q^\dagger b_q$, the "pairon" operators are equivalent to hard-core boson creation and destruction operators; therefore, the effective BCS Hamiltonian (1.21) corresponds to a problem of hard-core bosons on a lattice, which is expected to give rise to condensation and superfuidity. The BCS approach boils down to find a variational estimate of the ground state energy by using the wave function of Eq. (1.14), which is equivalent to solve the mean-field problem given by:

$$\mathcal{H}_{BCS}^{MF} = \sum_{q,\sigma} \epsilon_q c_{q,\sigma}^\dagger c_{q,\sigma} + \frac{1}{N} \sum_{q,q'} V_{q,q'} \langle (c_{q,\uparrow}^\dagger c_{-q,\downarrow}^\dagger \rangle c_{-q',\downarrow} c_{q',\uparrow} + c_{q,\uparrow}^\dagger c_{-q,\downarrow}^\dagger \langle c_{-q',\downarrow} c_{q',\uparrow} \rangle \rangle) \tag{1.22}$$

here, we dropped constant terms and included standard Hartree-Fock contributions inside the electron dispersion ϵ_q. By defining the superconducting parameter:

$$\Delta_q = \frac{1}{N} \sum_{q'} V_{q,q'} \langle c_{q',\uparrow}^\dagger c_{-q',\downarrow}^\dagger \rangle \tag{1.23}$$

and neglecting all the constant terms, Eq. (1.22) becomes:

$$\mathcal{H}_{BCS}^{MF} = \sum_{q,\sigma} \epsilon_q c_{q,\sigma}^\dagger c_{q,\sigma} + \sum_{q} \left(\Delta_q c_{-q,\downarrow} c_{q,\uparrow} + \Delta_q^\star c_{q,\uparrow}^\dagger c_{-q,\downarrow}^\dagger \right) \tag{1.24}$$

Solving Eq. (1.24) self-consistently, we obtain that Δ_q satisfies:

$$\Delta_q = -\sum_{q'} \frac{\Delta_{q'}}{2E_{q'}} V_{q,q'} \tag{1.25}$$

where

$$E_q = \sqrt{\epsilon_q^2 + \Delta_q^2} \tag{1.26}$$

Then, the self-consistent parameter Δ_q plays the role of an energy gap, which changes the electronic spectrum. Indeed, a finite Δ_q may open a full gap in the excitation spectrum, for example, this is the case when Δ_q is constant ($\Delta_q = \Delta$). Finally, the variational parameters of the BCS wave function u_q and v_q can be easily found and are given by:

$$u_q^2 = \frac{1}{2}\left(1 + \frac{\epsilon_q}{E_q}\right) \tag{1.27}$$

$$v_q^2 = \frac{1}{2}\left(1 - \frac{\epsilon_q}{E_q}\right) \tag{1.28}$$

1.3.2 The meaning of the gap parameter Δ_q

Within the BCS approach, the gap parameter Δ_q is independent of the energy and only depends upon the momentum $\mathbf{q}$. In general, Δ_q may have a non-trivial $\mathbf{q}$ dependence, which reflects the symmetry of the underlying lattice. For instance, the crystal structures of existing superconductors are all characterized by a center of inversion, then Δ_q must be even ($\Delta_{-q} = \Delta_q$) or odd ($\Delta_{-q} = -\Delta_q$) under the inversion through the origin of the $\mathbf{q}$ space (Tsuei and Kirtley 2000). Therefore, the gap parameter Δ_q does not necessarily have the same sign everywhere along the Fermi surface: in general regions of opposite sign will be separated by nodal lines. Such states correspond to Cooper pairs with non-zero internal angular momentum (allowed by the point group symmetry of the lattice). The absence of nodes corresponds to a state with s symmetry, one nodal line to a p state, two nodal lines to a d state and so on, see Fig. 1.4. While an s-wave superconductor has a fully gapped Fermi surface, in a d-wave superconductor, the presence of the nodes implies gapless excitations.

The symmetry of the superconducting gap function determines also the spin of the Cooper pair (which can be either singlet or triplet). Because fermions obey anticommutation relations, an even symmetry in the orbital part (e.g., s or d-wave) is associated to a singlet wave function, while an odd orbital part (p-wave) corresponds to a triplet. A mixture of spin-singlet and -triplet pair states in not possible as long as the spin-orbit interaction is small.

In sumamry, the gap parameter Δ_q is a well defined quantity, whose symmetry can be experimentally determined and the pair amplitude $\langle c^\dagger_{q,\uparrow} c^\dagger_{-q,\downarrow} \rangle$ captures the essence of the macroscopic phase coherence in all the superconducting states.

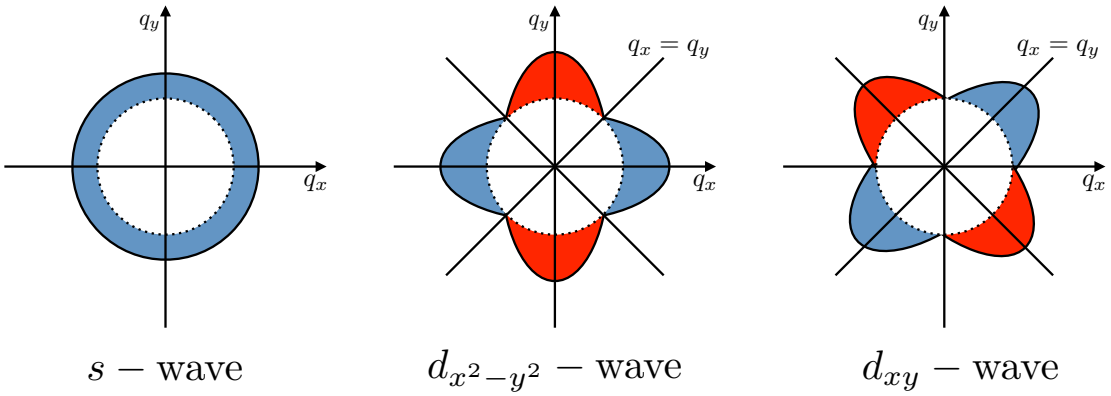

Figure 1.4: s, $d_{x^2-y^2}$ and d_{xy} symmetries of the gap function in the two-dimensional square lattice. The Fermi surface is represented by a dashed line, while the solid curves denote the first excited states. s-wave has an isotropic gap, whereas $d_{x^2-y^2}$ (d_{xy}) presents a gap which is maximum (identically zero) along the Brillouin zone boundary and zero (maximum) in diagonal directions.

1.4 Mottness and high-temperature superconductivity

Since the discovery of high-temperature superconductors in 1987, it has become clear that superconductivity may arise from injecting charge carriers into a Mott insulator (this procedure is called *doping*). Most importantly, the strength of the electronic pairing seems not to be proportional to the electron-phonon coupling, as in the standard BCS theory, but the superconducting mechanism seems to take benefit from the presence of strong electronic correlations. Therefore, a lot of effort has been focused to understand to what extent superconductivity may emerge from a doped Mott insulator within microscopic models such the Hubbard model or its strong-coupling limit, the so-called $t-J$ model (Lee, Nagaosa, and Wen 2006).

One important family of high-temperature superconductors is given by Cuprates, in which CuO_2 planes are separated by other layers of atoms (Ba, La, O...) that act as charge reservoirs that may dope electrons or holes into the CuO_2 planes. Superconductivity is due to processes occuring in these planes. Another relevant family of materials, which attracted a lot of interest in the recent years, is given by the Iron-based superconductors, including the so-called Pnictides and Chalcogenides (Stewart 2011). Also

in these compounds, the relevant building blocks are given by planes defined by the Iron atoms. As far as the Cuprates is concerned, it is now widely recognized that superconductivity is intimately related to doped Mott insulators (Lee, Nagaosa, and Wen 2006). Instead, for Iron-based superconductors, different approaches have been pursued, also including the possibility that superconductivity may be due to the presence of a concomitant Mott insulator (Song et al. 2016).

A general feature of these materials is that they contain transition metals, such as Copper or Iron, whose properties are triggered by the presence of partially filled d orbitals. The latter ones have total angular momentum $L = 2$, leading to a 10-fold degenerate shell in the atom (when including the spin degrees of freedom). In these compounds, the transition-metal ion is generally surrounded by ligand atoms (like Oxygens) to form the solid. According to the symmetry of the cage formed by these atoms, the crystal field splits the degeneracy in different ways. For example, within the tetragonal symmetry, the 5-fold degeracy of the $L = 2$ shell is split into e_g and t_{2g} levels, with 2 and 3-fold degeneracy, respectively (not counting the spin). These can be further split within the cubic or orthorhombic environments:

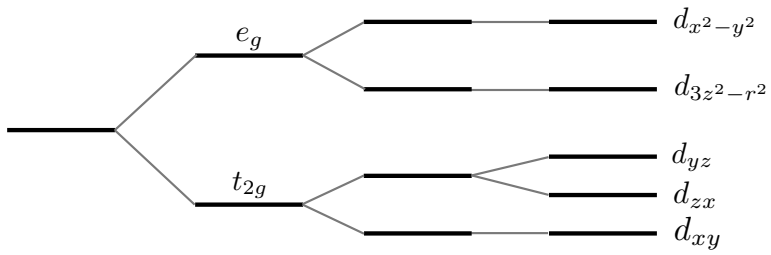

The (quasi) orbital degeneracy of these systems plays a very important role, being the ultimate source of their complicated behavior. Here, charge, spin, and orbital fluctuations are usually strong and determine the actual ground-state properties; in some cases, when a sizable spin-orbit coupling is present, they are entangled, inducing peculiar properties (Winter et al. 2017). One prominent role is played by the Hund coupling, which may quench orbital fluctuations, favoring states with the highest possibile spin on each transition metal ion.

1.4.1 Cuprate superconductors

The first Copper-oxide superconductor was discovered in a Lanthanum-Barium-Copper oxide material (Bednorz and Müller 1986). This compound showed the highest transition temperature (high-T_c) ever recorded at that time: 30K (see Fig. 1.5). This outcome, as well as the relatively small electron-phonon coupling constant, the fact that the material was somehow "unexpected" (e.g., being a transition-metal oxide), and other anomalous features (like for example the extraordinary linear behavior of the resistivity down to low temperatures) made it clear that a different mechanism, with respect to the standard superconductivity, was at work.

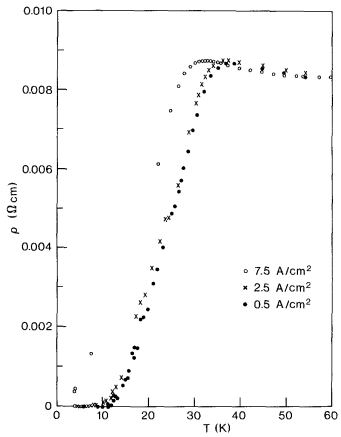

Figure 1.5: Temperature dependence of resistivity of $Ba_xLa_{5-x}O_{5(3-y)}$ with $x = 0.75$ and $y > 0$, recorded for different current densities (Bednorz and Müller 1986).

Cuprates have been the subject of an uncountable number of works. One of the most studied materials is $La_{2-x}Sr_xCuO_4$, which shows superconductivity in a wide range of doping x (that can be achieved by atomic substitution, namely substituting La with Sr). The undoped material with $x = 0$ (which is usually called *parent compound*) has a layered perovskite structure, in which the crystalline environment experienced by Cu atoms is tetragonal (see Fig. 1.6); it is an insulator with antiferromagnetic order (with a pitch vector $\mathbf{Q} = (\pi, \pi)$ in the CuO_2 plane). Still, the Mott physics is believed to be relevant since many aspects cannot be understood within a simple band theory approach. Its phase diagram, changing doping and temperature, fits into a universal scenario that is reported in Fig. 1.7. Here, the antiferromagnetic order present in the parent compound is rapidly suppressed and eventually disappears by doping with holes or electrons and superconductivity appears. Quite interestingly, the metallic state above the superconductos shows very anomalous features that cannot be described by the

Landau theory of standard Fermi liquids. Finally, by further doping superconductivity disappears and a conventional metallic phase is stabilied. It is generically believed that the strong electronic correlation is the driving force to determine their physical properties.

Within the undoped compound, every Copper atom has 9 electrons (with very small fluctuations), namely there is one hole in the d shell. This hole predominantly occupies the $d_{x^2-y^2}$ orbital, which has a finite overlap with the p orbitals of the four neighboring oxygen atoms in the CuO_2 planes, giving rise to Wannier orbitals centered around the Copper atoms. The low-energy properties of Copper oxides are believed to be well described by a single-band model (F. C. Zhang and Rice 1988). Then, the presence of a strong on-site repulsion, due to the fact that the configurations with zero or two holes are highly suppressed, gives rise to a microscopic description in terms of the Hubbard model or its strong-coupling version.

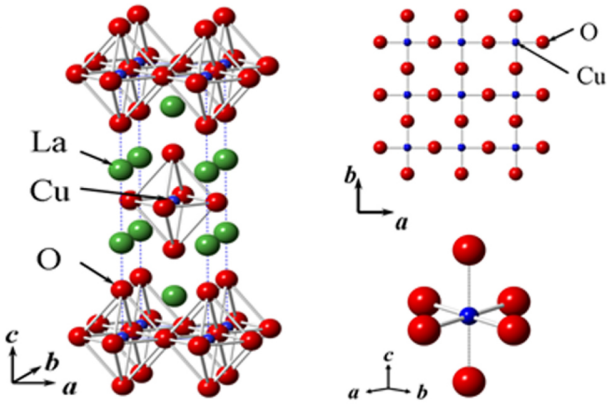

Figure 1.6: Crystal structure of the tetragonal phase of La_2CuO_4 (left). The top view (top-right) and CuO_6 octahedron (bottom-right) are also reported. Figure reproduced from Hosono et al. 2015.

The discovery of high-temperature superconductivity in doped Mott insulators generated a great interest in RVB states, following a pioneering work by Anderson 1987, who suggested that this kind of approach may capture the essence of electron pairing within Cuprates. Remarkably, the RVB theory was found successful to describe the $d_{x^2-y^2}$ nature of the superconducting Cuprates state (Gros, Poilblanc, Rice, and F. C. Zhang 1988; F. C. Zhang, Gros, Rice, and Shiba 1988; Kotliar and Liu 1988; Suzumura, Hasegawa, and Fukuyama 1988; Gros 1988), even before the pairing symmetry was experimentally established (Tsuei, Kirtley, et al. 1994; Hardy, Bonn, Morgan, Liang, and K. Zhang 1993).

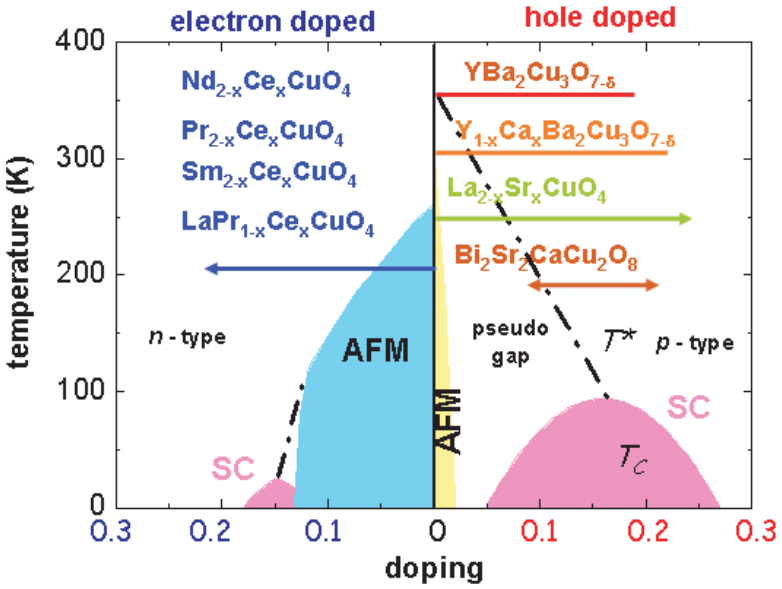

Figure 1.7: Accessible regions of the phase diagram for the different copper oxides superconductors. (Figure reproduced from Erb, Lambacher, Habel, and Gross 2018.)

1.4.2 Iron-based superconductors

For almost 20 years, the Copper oxides seemed to offer the only way to get high-temperature superconductivity. Then, in 2008, a new superconductor containing Iron was discovered (Kamihara, Watanabe, Hirano, and Hosono 2008). In some way, the story resembled what had been found earlier in the Cuprates. Subsequent data seemed to strengthen the connection between Cuprates and the Iron-based superconductors (Norman 2008 and Hu 2016). The parent compound was not superconducting but superconductivity is obtained upon chemical substitution. Even the crystal structure made of well separated layers was reminiscent of the one of Cuprates: in analogy with CuO_2 planes in Cuprates, also the Fe atoms form a square lattice (see Fig. (1.8)). However, the environment surrounding the Fe atoms is such that all five d orbitals are close in energy. Therefore, while Cuprates may be well described by considering a single electronic band close to the Fermi level, Iron-based superconductors are intrinsically multi-orbital systems with orbital fluctuations that involve the entire d shell of Iron. In this respect, the Hund coupling is expected to play an important role, beside the standard Hubbard U interaction (Georges, de'Medici, and Mravlje 2013). Moreover, the parent compounds of the Iron-based superconductors are not antiferromagnetic insulators but metals. More specifically, they are "bad" metals, meaning that they show a finite conductivity but vio-

late the Ioffe-Mott-Regel limit (Emery and Kivelson 1995). Still, most of the Iron-based superconductors show magnetically ordered phases, even if FeSe and some compounds in the LaFePO family do not show any evidence of long-range magnetic ordering (Song et al. 2016).

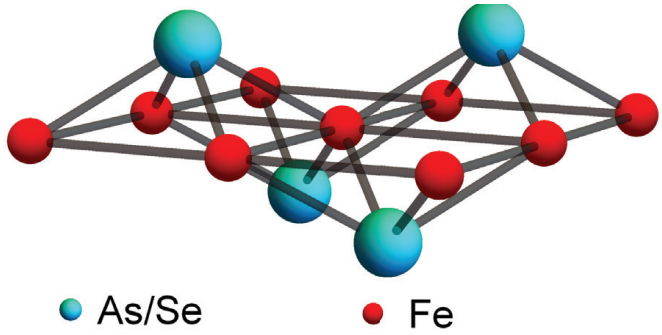

Figure 1.8: Schematic crystal structure of an FeAs or FeSe plane, displaying the puckering of the As/Se atoms above and below the square Fe plane. (Figure reproduced from Fernandes and Chubukov 2016.)

In contrast to Cuprates, where the magnetic order is characterized by the $\mathbf{Q} = (\pi, \pi)$ pitch vector, here the ordering vector is $\mathbf{Q} = (\pi, 0)$ [or $(\pi, 0)$]; In other words, the spins on the Fe ions are ferromagnetically aligned along one direction and antiferromagnetically aligned along the other (Si, Yu, and Abrahams 2016). Moreover, while Cuprates are generally believed to fall within a strong-coupling regime, where the Hubbard U term is larger than the average kinetic energy, Iron-based superconductors inhabit in an intermediate region, which is neither weak nor strong coupling. Still, different works have highlighted the existence of strong electron-electron interactions, suggesting that the correct starting point should be a multi-band Hubbard model (Si, Yu, and Abrahams 2016). A possible explanation for the observed behavior, including both weak- and strong-coupling aspects, can be given by the existence of an orbital-selective Mott transition (de'Medici, Giovannetti, and Capone 2014). Here, the Hund coupling effectively decouples the charge excitations in different orbitals, which are also differently populated. In this case, the effective Coulomb interaction may be different for different orbitals, thus leading to a mixed behavior in which strongly-correlated electrons coexist with weakly-correlated ones.

1.5 Multi-band Hubbard models

The minimal model that captures the interplay between kinetic energy, which favors delocalized electrons over the whole lattice, and potential energy, which instead reduces the mobility leading to a localization of the charge degrees of freedom, is given by the single-band Hubbard model. However, limiting to the case in which there is a single active orbital on each atom is often a very crude approximation, which cannot capture the correct low-energy behavior of the majority of materials. For example, as discussed before for generic transition-metal oxides, where there are unfilled d orbitals, orbital fluctuations represent an important aspect that determine the ultimate physical properties. The generalization of the single-band model to include multi-orbital (multi-band) effects is straightforward (Kanamori 1963). The case with two orbitals per atom (e.g., relevant to describe the e_g doublet) represents the simplest example. The model takes into account Hund's exchange coupling as well as the intra- and inter-orbital Coulomb interactions. Still, the study of the Mott physics in multi-orbital systems lacks a complete understanding and requires substantial investigations in the future.

In the same spirit of the single-band Hubbard model, starting from the interacting term (1.10), we can make the approximation in which only on-site terms with $\mathbf{R}_1 = \mathbf{R}_2 = \mathbf{R}_3 = \mathbf{R}_4$ are kept, while all the other ones are dropped. At this stage, we can distinguish various term depending on the values of the band indices. In particular, for the two-band model, we have

- The case with $\alpha = \beta = \gamma = \delta$, leading to the intra-band Coulomb repulsion U:

$$\frac{U}{2}\sum_{\sigma,\sigma'}\sum_{\alpha}\sum_{i} c^{\dagger}_{i,\alpha,\sigma}c^{\dagger}_{i,\alpha,\sigma'}c_{i,\alpha,\sigma'}c_{i,\alpha,\sigma} = U\sum_{i}\left(n_{i,1,\uparrow}n_{i,1,\downarrow} + n_{i,2,\uparrow}n_{i,2,\downarrow}\right) \tag{1.29}$$

- The case with $\alpha = \delta \neq \beta = \gamma$, leading to the inter-band Coulomb repulsion U':

$$\frac{U'}{2}\sum_{\sigma,\sigma'}\sum_{i}\sum_{\alpha\neq\beta} c^{\dagger}_{i,\alpha,\sigma}c^{\dagger}_{i,\beta,\sigma'}c_{i,\beta,\sigma'}c_{i,\alpha,\sigma} = U'\sum_{\sigma,\sigma'}\sum_{i} n_{i,1,\sigma}n_{i,2,\sigma'} \tag{1.30}$$

- The case with $\alpha = \gamma \neq \beta = \delta$, leading to the Hund coupling term J:

$$\frac{J}{2}\sum_{\sigma,\sigma'}\sum_{i}\sum_{\alpha\neq\beta} c^{\dagger}_{i,\alpha,\sigma}c^{\dagger}_{i,\beta,\sigma'}c_{i,\alpha,\sigma'}c_{i,\beta,\sigma} = -J\sum_{\sigma,\sigma'}\sum_{i} c^{\dagger}_{i,1,\sigma}c_{i,1,\sigma'}c^{\dagger}_{i,2,\sigma'}c_{i,2,\sigma} \tag{1.31}$$

- The case with $\alpha = \beta \neq \gamma = \delta$, leading to the pair-hopping term J':

$$\frac{J'}{2}\sum_{\sigma,\sigma'}\sum_{i}\sum_{\alpha\neq\gamma} c^{\dagger}_{i,\alpha,\sigma}c^{\dagger}_{i,\alpha,\sigma'}c_{i,\gamma,\sigma'}c_{i,\gamma,\sigma} = -J'\sum_{i} c^{\dagger}_{i,1,\uparrow}c^{\dagger}_{i,1,\downarrow}c_{i,2,\uparrow}c_{i,2,\downarrow} + \text{H.c.} \quad (1.32)$$

All other terms in the interaction tensor, e.g., with $\alpha = \beta = \gamma \neq \delta$, vanish by symmetry (Georges, de'Medici, and Mravlje 2013). By choosing real-valued wave functions, the spin-exchange and pair-hopping integrals are equal, namely $J = J'$. In addition, the Hamiltonian is tailored for describing the physical e_g orbitals. In this context, cubic symmetry implies (Georges, de'Medici, and Mravlje 2013):

$$U' = U - 2J \quad (1.33)$$

As far as the hopping parameters are concerned, $t^{\alpha,\beta}_{i,j}$ depend on the geometry of the lattice and the form of the d orbitals that are considered. In the following, we will make a simplified choice of the kinetic terms in which we will consider the same hopping for the two orbitals and no inter-orbital contributions, i.e., $t^{\alpha,\beta}_{i,j} = -\delta_{\alpha,\beta}t$ for nearest-neighbor sites i, j and zero otherwise.

Therefore, the final Hamiltonian for the two-band model reads as:

$$\begin{aligned}\mathcal{H} = &-t\sum_{\langle i,j\rangle,\alpha,\sigma} c^{\dagger}_{i,\alpha,\sigma}c_{j,\alpha,\sigma} + \text{H.c.} + \\ &+ U\sum_{i,\alpha} n_{i,\alpha,\uparrow}n_{i,\alpha,\downarrow} + (U-2J)\sum_{i,\sigma\neq\sigma'} n_{i,1,\sigma}n_{i,2,\sigma'} + (U-3J)\sum_{i,\sigma} n_{i,1,\sigma}n_{i,2,\sigma} \\ &- J\sum_{i,\sigma\neq\sigma'} c^{\dagger}_{i,1,\sigma}c_{i,1,\sigma'}c^{\dagger}_{i,2,\sigma'}c_{i,2,\sigma} \\ &- J\sum_{i}(c^{\dagger}_{i,1,\uparrow}c^{\dagger}_{i,1,\downarrow}c_{i,2,\uparrow}c_{i,2,\downarrow} + \text{H.c.})\end{aligned} \quad (1.34)$$

Following the same arguments, the three-band model the Hamiltonian reads:

$$\begin{aligned}\mathcal{H} = &-t \sum_{\langle i,j\rangle,\alpha,\sigma} c^{\dagger}_{i,\alpha,\sigma} c_{j,\alpha,\sigma} + \text{H.c.} + \\ &+ U \sum_{i,\alpha} n_{i,\alpha,\uparrow} n_{i,\alpha,\downarrow} + (U-2J) \sum_{i,\sigma\neq\sigma'} \sum_{\alpha<\beta} n_{i,\alpha,\sigma} n_{i,\beta,\sigma'} + (U-3J) \sum_{i,\sigma} \sum_{\alpha<\beta} n_{i,\alpha,\sigma} n_{i,\beta,\sigma} \\ &- J \sum_{i,\sigma\neq\sigma'} \sum_{\alpha<\beta} c^{\dagger}_{i,\alpha,\sigma} c_{i,\alpha,\sigma'} c^{\dagger}_{i,\beta,\sigma'} c_{i,\beta,\sigma} \\ &- J \sum_{i} \sum_{\alpha<\beta} (c^{\dagger}_{i,\alpha,\uparrow} c^{\dagger}_{i,\alpha,\downarrow} c_{i,\beta,\uparrow} c_{i,\beta,\downarrow} + \text{H.c.})\end{aligned} \tag{1.35}$$

where, here, the condition $U' = U - 2J$ is imposed to have rotationally invariance (Georges, de'Medici, and Mravlje 2013).

One key point that has been addressed in the past is to understand how the Mott metal-insulator transition at integer fillings is affected by orbital degeneracy, inter-orbital Coulomb interaction, and Hund coupling. In this context, many works have been performed in the "symmetric sector", namely disregarding any possible magnetic or orbital long-range order, in order to capture the correlation effects that are not spoiled by weak-coupling effects. This approach is justified by the choice of describing the physical picture that can be realized when magnetic and orbital order is suppressed by the presence of competing interactions, i.e., frustration (without including it explicitly in the model). For the multi-orbital Hubbard model, in the absence of the Hund coupling J, it has been observed by means of different computational methods that the value of the Coulomb interaction, for which the metal-insulator transition occurs at commensurate filling, reaches its maximum at half filling. This result has been obtained by using the Gutzwiller approximation (Lu 1994), Dynamical Mean Field Theory (Rozenberg 1997 and Ono, Potthoff, and Bulla 2003) and quantum Monte Carlo techniques (Koch, Gunnarsson, and Martin 1999). The presence of a finite J reduces the value of the critical U at half filling (Han, Jarrell, and Cox 1998) while, recent studies (de'Medici, Mravlje, and Georges 2011 and de'Medici 2011), have highlighted the opposite trend for all the other (integer) fillings, where the presence of a finite J increases U_{MIT}.

One important issue that has been addressed in multi-orbital Hubbard models is the nature of the MIT. Indeed, while in the single-orbital model different numerical methods (Brinkman and Rice 1970, Georges, Kotliar, Krauth, and Rozenberg 1996, Capello, Becca, Fabrizio, Sorella, and Tosatti 2005) established that the Mott metal-insulator transition is continuous at zero temperature, former studies of multi orbital

models, based on the Gutzwiller approximation, suggested that the transition, at half filling, becomes first order whenever $J > 0$, while it remains continuous only at $J = 0$ (Bünemann and Weber 1997 and Bünemann, Weber, and Gebhard 1998). Similar results have been obtained more recently by means of the Dynamical Mean Field Theory (DMFT) method (Ono, Potthoff, and Bulla 2003 and Facio, Vildosola, Garcia, and Cornaglia 2017).

The analysis of the role of band degeneracy and Hund coupling in the development of superconductivity in multi orbital Hubbard models represents another topic of great interest, particularly relevant for Iron-based superconductors. However, treating nonlocal pairing beyond perturbative approximations is particularly difficult. A recent DMFT study on a three-orbital Hubbard model highlighted the emergence of on-site triplet superconductivity at finite doping for $J > 0$ (Hoshino and Werner 2015), in agreement with previous results obtained in the large J/U limit, within an Hartree-Fock-Bogoliubov approach (Spałek 2012) and the Gutzwiller approximation (Spałek and Bünemann 2013). Here, spin-triplet superconductivity is related to the emergence of local magnetic moments, which originate from the Hund coupling and are enhanced by an Ising anisotropy that suppresses fluctuations among different spin configurations. The presence of pairing with d-wave symmetry is much more difficult to assess within the standard Dynamical Mean Field Theory, because, in infinite spatial dimensions, it is not possible to deal with spatial dependence of a pairing state.

In addition to superconductivity, long-range magnetic order may be stabilized in a relatively large region of the phase diagram for $J > 0$. Within the two-band model, various calculations highlighted the existence of itinerant ferromagnetism for $1 < n < 2$, which can be stabilized by the double-exchange mechanism for $J > 0$ (Held and Vollhardt 1998, Momoi and Kubo 1998, Kubo 2009 and Peters and Pruschke 2010). In addition, recent DMFT calculations on the three-band model (Hoshino and Werner 2015) suggested the possibility to have antiferromagnetism close to half filling and ferromagnetism in a wide doping region at large values of the Coulomb repulsion.

In order to investigate the role of the inter-orbital Coulomb repulsion and Hund coupling, in this thesis we consider the two- and three-band Hubbard model with degenerate bands on a square lattice with only nearest-neighbor hopping. We will show that, despite the apparent simplicity of our model, the physics behind the phase-diagram can be very rich.

Chapter 2

Variational Monte Carlo

Quantum Monte Carlo methods are a class of computational algorithms whose common aim is to provide reliable and accurate solutions for interacting bosonic or fermionic systems (Becca and Sorella 2017 and Gubernatis, Kawashima, and Werner 2016). The core of these numerical approaches is based upon the construction of a stochastic sampling in which a bunch of relevant configurations are selected according to a given probability distribution.

Among quantum Monte Carlo methods, the Variational Monte Carlo (VMC) allows us to obtain the physical properties of a *given* many-body state, whose modulus square defines the probability distribution. The major advantage of VMC is that it does not suffer from the sign problem, thus allowing stable numerical simulations even for a large number of particles. In addition, it satisfies the variational principle, i.e., the expectation value of the Hamiltonian is bounded from below by the exact ground-state energy. The main drawback comes from the fact that there is a potential bias due to the choice of the variational state, which may miss the correct physical properties of the true ground state. Still, remarkably accurate estimations of ground-state energies can be achieved in a wide class of physical systems by optimizing the so-called Jastrow-Slater wave functions that contain a large number of parameters (Becca and Sorella 2017). Furthermore, an important advantage of the VMC approach is that quite general Hamiltonians may be considered, without a dramatic increase of the computational cost; for example, we can easily consider lattice models with long-range interactions and/or different atomic orbitals, including Hund and spin-orbit coupling among them. Finally, VMC is easily scalable to a large number of processors and, therefore, allows calculations on relatively large cluster sizes.

In this chapter, we present the statistical formulation of the VMC approach. Specif-

ically, we will focus on the Metropolis algorithm and the energy optimization scheme. We conclude the chapter by describing the wave function used in this work, namely the Jastrow-Slater wave function.

2.1 Variational Principle

In order to approximate the ground state of a quantum system, VMC takes advantage of the variational principle, which we will describe in detail in the following. Let us consider the time-independent Schrödinger equation with a discrete energy spectrum $\{E_i\}$. Then, any quantum state $|\Psi\rangle$ can be expanded in terms of the eigenstates $\left|\Psi_i^{\text{exact}}\right\rangle$ of the Hamiltonian $\mathcal{H}$:

$$|\Psi\rangle = \sum_i a_i \left|\Psi_i^{\text{exact}}\right\rangle \tag{2.1}$$

where $a_i = \left\langle \Psi_i^{\text{exact}} \middle| \Psi \right\rangle$. The normalization condition of the wave function $\langle \Psi \,|\, \Psi \rangle = 1$ implies that $\sum_i |a_i|^2 = 1$. It is easy to show that the variational energy, computed as the expectation value of the Hamiltonian over $|\Psi\rangle$

$$E = \frac{\langle \Psi | \, \mathcal{H} \, | \Psi \rangle}{\langle \Psi \,|\, \Psi \rangle} \tag{2.2}$$

is bounded from below by the actual ground-state energy E_0. Indeed, by using the expansion of (2.1) and the normalization condition, we have that

$$E = \sum_i E_i |a_i|^2 \geq E_0 \sum_i |a_i|^2 = E_0 \tag{2.3}$$

Clearly, if we were able to vary $|\Psi\rangle$ over all possible states within the Hilbert space, minimizing the expectation value of $\mathcal{H}$, then the lowest value would be E_0 and the corresponding state would be the ground state of $\mathcal{H}$. However, this kind of procedure is not affordable in realistic computations on large sizes where the Hilbert space is huge. Therefore, a subspace of the entire Hilbert space is chosen, making an *ansatz* for the wave function, namely choosing a functional form (e.g., the Jastrow-Slater one, see below) that depends on a set of variational parameters. In general, the choice of the *ansatz* is crucial to capture the presence of long-range order: for example, simple Hartree-Fock states cannot describe a superconducting phase, even when the Jastrow factor is included and, in this respect, a BCS wave function is necessary (in other words, there is no way to get superconductivity if the approximate wave function does not contain some pairing term like in the BCS wave function!). Still, some exceptions to this rule are known; in

fact, it has been shown that charge-density waves may develop whenever a sufficiently strong electron-electron repulsion is included in the Jastrow factor, without an explicit symmetry breaking in the wave function (Kaneko, Tocchio, Valentì, Becca, and Gros 2016).

The best approximation of the true ground state can be chosen by comparing the variational energies of different wave functions and taking the one with the lowest possible value, since the variational principle ensures the best *ansatz* to have the minimal energy. In this regard, the analytical evaluation of (2.2) is only possible in a few cases, like for example when $|\Psi\rangle$ is an uncorrelated Slater determinant constructed from single-electron orbitals. Otherwise, we have to devise a numerical technique to compute the variational energy and determine the lowest-energy solution. To this purpose Markov chains and the Metropolis algorithm are invaluable tools to compute quantum expectation values over a given wave function (Becca and Sorella 2017). In addition, the evaluation of the energy derivatives with respect to the variational parameters allows us to minimize E and optimize the variational wave function.

In the following, we will consider the case where the Hilbert space is discrete, since we will focus on interacting electrons on the lattice. Let us first define a many-body basis $\{|x\rangle\}$ (orthogonal and normalized) for the Hilbert space, where each element is specified by giving the positions (lattice site and orbital occupation) and the component of the spin along the z axis of every electron. A statistical approach to evaluate the quantum expectation value of (2.2) is obtained by inserting a completeness relation of the basis set, i.e., $\sum_x \langle x \,|\, x\rangle = \mathbb{1}$:

$$E = \frac{\sum_x \langle \Psi \,|\, x\rangle \langle x| \,\mathcal{H}\, |\Psi\rangle}{\sum_x \langle \Psi \,|\, x\rangle \langle x \,|\, \Psi\rangle} = \frac{\sum_x |\langle \Psi \,|\, x\rangle|^2 \frac{\langle x \,|\, \mathcal{H} \,|\, \Psi\rangle}{\langle x \,|\, \Psi\rangle}}{\sum_x |\langle \Psi \,|\, x\rangle|^2} = \sum_x P(x) E_L(x) \tag{2.4}$$

Here, the variational energy is written as a sum over all the configurations of the basis set of a probability distribution $P(x)$ times the observable $E_L(x)$, which is called *local energy*. In fact, we have that

$$P(x) = \frac{|\langle x \,|\, \Psi\rangle|^2}{\sum_x |\langle x \,|\, \Psi\rangle|^2} \tag{2.5}$$

defines a bona-fide probability distribution, since it satisfies the conditions that $P(x) \geq 0$ for every electron configuration and $\sum_x P(x) = 1$. Then, the local energy

$$E_L(x) = \frac{\langle x \,|\, \mathcal{H} \,|\, \Psi\rangle}{\langle x \,|\, \Psi\rangle} \tag{2.6}$$

can be evaluated by inserting a completeness relation

$$E_L(x) = \sum_{x'} \langle x \,|\, \mathcal{H} \,|\, x' \rangle \, \frac{\langle x' \,|\, \Psi \rangle}{\langle x \,|\, \Psi \rangle} \tag{2.7}$$

since, for any local Hamiltonian, only a small number (i.e., proportional to the total number of electrons N_e) of matrix elements $\langle x \,|\, \mathcal{H} \,|\, x' \rangle$ are finite within our choice of a local basis set.

Whenever we are able to extract configurations according to $P(x)$ and compute $E_L(x)$, a statistical estimation of the variational energy E can be obtained, as well as its errorbar. A similar derivation can be done for any other observable. In the next sections, we will discuss a practical way to implement an efficient Monte Carlo sampling of the relevant electron configurations.

Finally, let us consider the variance of the variational state, which is defined by:

$$\sigma^2 = \frac{\langle \Psi | \, (\mathcal{H} - E)^2 \, | \Psi \rangle}{\langle \Psi \,|\, \Psi \rangle} = \frac{\langle \Psi | \, \mathcal{H}^2 \, | \Psi \rangle}{\langle \Psi \,|\, \Psi \rangle} - E^2 \tag{2.8}$$

Again, by inserting a completeness relation of the basis set, we obtain (assuming a real wave function and then a real local energy):

$$\sigma^2 = \frac{\sum_x \langle \Psi | \, \mathcal{H} \, | x \rangle \, \langle x | \, \mathcal{H} \, | \Psi \rangle}{\sum_x \langle \Psi \,|\, x \rangle \, \langle x \,|\, \Psi \rangle} - E^2 = \sum_x P(x) E_L^2(x) - \left(\sum_x P(x) E_L(x) \right)^2 \tag{2.9}$$

which shows that σ^2 is related to the variance of the statistical variable $E_L(x)$.

It should be noticed that, whenever the variational state $|\Psi\rangle$ is an eigenstate of the Hamiltonian, $E_L(x)$ is constant. This fact, which goes under the name of *zero-variance property*, is particularly important because it implies the reduction of the statistical fluctuations of $E_L(x)$ when $|\Psi\rangle$ approaches the actual ground state eigenfunction $\left|\Psi_0^{\text{exact}}\right\rangle$.

2.2 Markov Chains

A Markov chain is a stochastic procedure to construct a sequence of configurations x (usually, defined at discrete time steps t_M) whose probability distribution $p(x, t_M)$ converges to the desired probability $P(x)$. It should be emphasized that the time evolution is not related to the actual dynamics of the system, but it is an artificial process to reach a steady state from which static properties may be obtained. At every time, the configuration depends only on the previous one and, therefore, the time evolution is determined

by a transition probability $\omega(x', x)$, which gives the probability that the configuration x at time t_M evolves into x' at time t_{M+1}. Its normalization is given by:

$$\sum_{x'} \omega(x', x) = 1 \tag{2.10}$$

For the sake of simplicity, we will consider the case in which $\omega(x', x)$ is time-independent (i.e., it does not depend upon the time t_M). In the case of VMC, every configuration x along the stochastic process denotes an element of the basis set $\{|x\rangle\}$ that has been fixed at the beginning (see above). Finding a suitable transition probability to quickly converge to $P(x)$ is the core of the iterative Markov process.

Given $p(x, t_M)$ at time t_M, the probability $p(x', t_{M+1})$ at time t_{M+1} can be calculated by considering the amount of probability that flows from x to x':

$$p(x', t_{M+1}) = p(x', t_M) + \sum_x \left[p(x, t_M)\omega(x', x) - p(x', t_M)\omega(x, x') \right] \tag{2.11}$$

which is called Master equation for the Markov chains. In order to reach a steady evolution, in which the probability distribution converges to the desired probability $P(x)$ (i.e., $p(x, t_M) \to P(x)$ for $t_M \to \infty$), it is sufficient to require the so-called *detailed balance* condition:

$$P(x)\omega(x', x) = P(x')\omega(x, x') \tag{2.12}$$

which states that there is no net flux of probability along $x \leftrightarrow x'$, implying that the distribution is stationary. A necessary condition for a Markov chain to reach a unique equilibrium distribution, starting from an arbitrary initial probability distribution, is a property called *ergodicity*. A process can be defined ergodic if it is possible to reach any state from any other state with a finite number of applications of the Markov process (Van Kampen 1992). This fact imposes constraints on the choice of the transition probability $\omega(x', x)$.

Formally, the equilibrium distribution is reached only in the limit $t_M \to \infty$; however, in practice, we can imagine that configurations are distributed according to $P(x)$ for large (but finite) times, i.e., after a *thermalization* time t_{therm}. Therefore, averages to estimate observables can be computed starting from t_{therm}, for a suitable number of steps.

2.3 Metropolis Monte Carlo Algorithm

Within the detailed balance condition, a simple solution for the transition probability $\omega(x', x)$ can be obtained, which goes under the name of Metropolis algorthim (Metropolis, A. W. Rosenbluth, M. N. Rosenbluth, A. H. Teller, and E. Teller 1953). In order to do that, we split the probability $\omega(x', x)$ by taking:

$$\omega(x', x) = T(x', x)A(x', x) \tag{2.13}$$

where $T(x', x)$ and $A(x', x)$ are the trial and acceptance probability distributions, respectively. Then, the Metropolis algorithm can be described as follows: for a given configuration x, we propose a new (trial) configuration x' based on $T(x', x)$, which can be chosen in an arbitrary way (it should be as simple as possible in order to have an efficient process). Then, the configuration x' is accepted or rejected according to $A(x', x)$, which is obtained from the detailed balance condition (2.12):

$$\frac{A(x', x)}{A(x, x')} = \frac{P(x')T(x, x')}{P(x)T(x', x)} \tag{2.14}$$

The Metropolis solution of this set of equations (for every configurations x and x') is given by

$$A(x', x) = \min\{1, q(x', x)\} \tag{2.15}$$

where

$$q(x', x) = \frac{P(x')T(x, x')}{P(x)T(x', x)} \tag{2.16}$$

Therefore, a new configuration is accepted or rejected according to the value of $q(x', x)$. A simplified version of this algorithm consists in taking a symmetric trial probability, i.e., $T(x, x') = T(x', x)$, such that:

$$q(x', x) = \frac{P(x')}{P(x)} \tag{2.17}$$

It is worth noting that in VMC it is not necessary to know the normalization constant $\sum_x |\langle \Psi \,|\, x \rangle|^2$ to generate configurations according to the probability distribution $P(x)$. Indeed, only ratios of weights $P(x')/P(x) = |\Psi(x')|^2/|\Psi(x)|^2$ between different configurations are needed.

In our case, where x represents the full many-electron configuration, the basic procedure is described as follows:

1) Generate random numbers to select two sites i and j and the component of the spin σ along the quantization axis, this defines the trial probability $T(x', x)$;

2) If one electron with spin σ can hop from i to j, compute the acceptance probability $A(x', x)$; otherwise go back to the 1);

3) Generate a uniform random number $u \in (0, 1]$;

4) Accept the new configuration if $A(x', x) \geq u$ otherwise reject it;

5) Every N_e steps (where N_e is the number of electrons), compute the local energy (or other correlation functions) for the configuration x'

6) Go to 1)

After a suitable thermalization time, configurations are distributed according to $P(x)$ and, denoting by $\{x_1 \dots x_N\}$ the set of equilibrated configurations, the final estimation of the variational energy is given by:

$$E = \lim_{N \to \infty} \epsilon_N \tag{2.18}$$

where

$$\epsilon_N = \frac{1}{N} \sum_{i=1}^{N} E_L(x_i) \tag{2.19}$$

Whenever the values of the local energy $E_L(x_i)$ are uncorrelated (corresponding to considerably different electronic configurations), the errorbar $\Delta\epsilon_N$ associated to ϵ_N can be estimated by computing

$$\Delta\epsilon_N = \sqrt{\frac{1}{N-1}(\eta_N - \epsilon_N^2)} \tag{2.20}$$

where

$$\eta_N = \frac{1}{N} \sum_{i=1}^{N} E_L^2(x_i) \tag{2.21}$$

However, given the algorithm described above, subsequent configurations may be correlated, especially when the acceptance ratio is small. As a consequence, also the values of the local energy may be correlated and we have to consider an alternative procedure to obtain an unbiased estimation of the errorbar. A commonly used way to decrease the correlation is the so-called binning technique, in which subsequent L_b measurements are blocked together to compute partial averages over them:

$$\bar{E_b} = \frac{1}{L_b} \sum_{i=(b-1)L_b+1}^{bL_b} E_L(x_i) \tag{2.22}$$

with $b = 1, \ldots, N_{bin}$ ($N = N_{bin} \times L_b$). Whenever L_b is larger than the correlation time, the resulting variables $\bar{E}_b$ are almost uncorrelated. While, their average coincides with what can be computed without binning, namely:

$$\epsilon_N = \frac{1}{N_{bin}} \sum_{b=1}^{N_{bin}} \bar{E}_b, \tag{2.23}$$

the binned variables are much less correlated with respect to the original ones. In fact, their correlation only comes from the values of i that are close to the borders of the bin, i.e., $i = (b-1)L_b + 1$ and $i = bL_b$ in (2.22). Therefore, whenever L_b is much larger than the correlation time, we can assume that the new variables are almost uncorrelated and the error can be estimated as

$$\Delta\epsilon_N = \sqrt{\frac{1}{N_{bin}(N_{bin}-1)} \sum_{b=1}^{N_{bin}} (\bar{E}_b - E)^2} \tag{2.24}$$

2.4 The minimization algorithm: the stochastic reconfiguration method

A significant advantage of the Monte Carlo method for obtaining quantum expectation values is the possibility to consider wave functions with a large number of variational parameters $\{\alpha_k\}$ and perform an energy minimization. One possibility for this optimization is based on the zero-variance property, which relies on the fact that the variance of the random variable $E_L(x)$ goes to zero whenever the trial state coincides with an eigenstate of $\mathcal{H}$. This optimization scheme was proposed by Umrigar, Wilson, and Wilkins 1988, who developed a procedure to find the variational parameters that minimize the variance to improve the trial wave function. The aim of VMC, however, consists in dealing with the lowest possible energy. Unlike variance minimization, where the minimum value (equal to zero) is evident, the minimum of the energy is not known a priori. Nevertheless, it has been noticed (Snajdr and Rothstein 2000) that, for a given form of the trial wave function, energy-minimized wave functions yield more accurate values of expectation values than wave functions whose variance is minimized. Moreover, a lower value of the energy is associated with a higher quality wave function (Casula and Sorella 2003). This fact holds for both continuous and lattice problems (Umrigar and Filippi 2005). Therefore, in this thesis, we will consider an optimization method that is very efficient to get the lowest energy within Jastrow-Slater wave functions, namely the

so-called stochastic reconfiguration algorithm (Sorella 1998 and Sorella 2001).

Let the "initial" Jastrow-Slater wave function $\left|\Psi(\alpha_k^0)\right\rangle$ depend on the variational parameters $\{\alpha_k^0\}$, with $k = 1, \ldots, p$. In the following, for the sake of simplicity, we will denote $\left|\Psi(\alpha_k^0)\right\rangle$ by $\left|\Psi^0\right\rangle$. Its variational energy can be improved by the application of the projection operator $(\Lambda - \mathcal{H})$, where Λ is an appropriate constant shift:

$$|\Psi_\Lambda\rangle = (\Lambda - \mathcal{H})\left|\Psi^0\right\rangle \tag{2.25}$$

However, in general, the new state $|\Psi_\Lambda\rangle$ will not be written in the Jastrow-Slater form. Therefore, the idea is to find the quantum state $|\Psi'\rangle \equiv |\Psi(\alpha_k')\rangle$, which gives the best possible approximation of $|\Psi_\Lambda\rangle$. In order to do that, we consider a small variation $\{\delta\alpha_k\}$ in the variational parameters $\{\alpha_k^0\}$:

$$\alpha_k' = \alpha_k^0 + \delta\alpha_k \tag{2.26}$$

This modification induces a change in the wave function, which, at first order in $\{\delta\alpha_k\}$, reads as

$$\left|\Psi'\right\rangle = \delta\alpha_0\left|\Psi^0\right\rangle + \sum_{k=1}^{p}\delta\alpha_k\frac{\partial\left|\Psi^0\right\rangle}{\partial\alpha_k} + O(\delta\alpha_k^2) \tag{2.27}$$

where $\delta\alpha_0$ has been considered to match the normalization condition. By defining the local operators $O(\alpha_k^0)$ (with $k = 1, \ldots, p$) on the configuration $|x\rangle$ as the logarithmic derivatives with respect to the variational parameters

$$O_k(x) = \frac{\partial}{\partial\alpha_k^0}\ln\left\langle x\middle|\Psi^0\right\rangle = \frac{1}{\Psi^0(x)}\frac{\partial\Psi^0(x)}{\partial\alpha_k^0} \tag{2.28}$$

and $O_0 \equiv \mathbb{1}$, it is possible to write $|\Psi'\rangle$ in a compact form:

$$\left|\Psi'\right\rangle = \delta\alpha_0\left|\Psi^0\right\rangle + \sum_{k=1}^{p}\delta\alpha_k O_k\left|\Psi^0\right\rangle = \sum_{k=0}^{p}\delta\alpha_k O_k\left|\Psi^0\right\rangle \tag{2.29}$$

Within the stochastic reconfiguration method, we impose that the projections of $|\Psi_\Lambda\rangle$ and $|\Psi'\rangle$ into the subspace defined by $O_j\left|\Psi^0\right\rangle$ (with $j = 0, \ldots, p$) are equal, namely

$$\left\langle\Psi^0\middle|O_j\middle|\Psi'\right\rangle = \left\langle\Psi^0\middle|O_j\middle|\Psi_\Lambda\right\rangle \tag{2.30}$$

This ensures that the energy computed on $|\Psi'\rangle$ is lower than the one computed on $\left|\Psi^0\right\rangle$.

By substituting the expression (2.25) and (2.29) in (2.30) we obtain:

$$\sum_{k=0}^{p} \delta\alpha_k \langle O_j O_k \rangle = \langle O_j(\Lambda - \mathcal{H}) \rangle \tag{2.31}$$

where $\langle \dots \rangle$ stands for $\langle \Psi^0 | \dots | \Psi^0 \rangle$. In particular, the equation for $j = 0$ reads as

$$\sum_{k=0}^{p} \delta\alpha_k \langle O_k \rangle = \Lambda - \langle \mathcal{H} \rangle \tag{2.32}$$

while the ones for $j = 1, \dots, p$ are given by:

$$\sum_{k=0}^{p} \delta\alpha_k \langle O_j O_k \rangle = \Lambda \langle O_j \rangle - \langle O_j \mathcal{H} \rangle \tag{2.33}$$

these can be rewritten as:

$$\delta\alpha_0 + \sum_{k=1}^{p} \delta\alpha_k \langle O_k \rangle = \Lambda - \langle \mathcal{H} \rangle \tag{2.34}$$

and

$$\delta\alpha_0 \langle O_j \rangle + \sum_{k=1}^{p} \delta\alpha_k \langle O_j O_k \rangle = \Lambda \langle O_j \rangle - \langle O_j \mathcal{H} \rangle \tag{2.35}$$

We have that $\delta\alpha_0$ is related to the normalization of the trial wave function and such parameter does not affect any physical observable of the system. Therefore, we can solve (2.34) for $\delta\alpha_0$ and substitute it in (2.35), obtaining:

$$\sum_{k=1}^{p} \delta\alpha_k \left\{ \langle O_j O_k \rangle - \langle O_j \rangle \langle O_k \rangle \right\} = \langle O_j \rangle \langle \mathcal{H} \rangle - \langle O_j \mathcal{H} \rangle \tag{2.36}$$

This linear system, in the unknowns $\{\delta\alpha_k\}$, can be written in a compact form:

$$\sum_{k=1}^{p} \delta\alpha_k S_{jk} = f_j \tag{2.37}$$

here, we have defined the $p \times p$ symmetric and (semi) positive-definite matrix

$$S_{jk} \equiv \langle O_j O_k \rangle - \langle O_j \rangle \langle O_k \rangle \tag{2.38}$$

and the vector (with p components) of the generalized forces

$$f_j \equiv \langle O_j \rangle \langle H \rangle - \langle O_j \mathcal{H} \rangle \tag{2.39}$$

The latter ones are indeed related to the derivative of the variational energy with respect to the set of the variational parameters:

$$\frac{\partial E}{\partial \alpha_j} = \frac{\partial}{\partial \alpha_j} \frac{\langle \Psi^0 \,|\, \mathcal{H} \,|\, \Psi^0 \rangle}{\langle \Psi^0 \,|\, \Psi^0 \rangle} = -2 f_j \tag{2.40}$$

Indeed, we have that:

$$\frac{\partial E}{\partial \alpha_j} = \frac{\langle \Psi^0 \,|\, (O_j \mathcal{H} + \mathcal{H} O_j) \,|\, \Psi^0 \rangle}{\langle \Psi^0 \,|\, \Psi^0 \rangle} - 2 \frac{\langle \Psi^0 \,|\, O_j \,|\, \Psi^0 \rangle \langle \Psi^0 \,|\, \mathcal{H} \,|\, \Psi^0 \rangle}{\langle \Psi^0 \,|\, \Psi^0 \rangle^2} \tag{2.41}$$

In practice, we can perform an iterative Monte Carlo simulation with *fixed* parameters, where both the covariance matrix S_{jk} and the generalized forces f_j are computed by a stochastic sampling; then, the linear system (2.37) is solved and the variational parameters are updated:

$$\begin{aligned} \delta \alpha_k &= \sum_{j=1}^{p} S_{kj}^{-1} f_j \\ \alpha_k' &= \alpha_k^0 + \tau \delta \alpha_k \end{aligned} \tag{2.42}$$

Here, the parameter τ must be chosen as large as possible to ensure rapid convergence, but small enough for the algorithm to remain stable. A sufficiently small τ ensures that the energy is not increasing (in average) at each step. Indeed, the Taylor expansion of $E(\Psi')$ to linear order in τ is:

$$E(\Psi') = E(\Psi^0) + \sum_{k}^{p} \frac{\partial E(\Psi^0)}{\partial \alpha_k} \delta \alpha_k + \mathcal{O}(\tau^2) \tag{2.43}$$

which gives

$$E(\Psi') - E(\Psi^0) = -\sum_{j,k}^{p} S_{kj}^{-1} f_j f_k + \mathcal{O}(\tau^2) \tag{2.44}$$

The fact that the matrix S_{jk} is semi-positive definite (and hence its inverse) implies that $E(\Psi') - E(\Psi^0) \leq 0$ at linear order in τ. When all the forces vanish, the energy certainly converges to a minimum.

2.5 The wave function of a two-band model

The accurate choice of the trial wave function is a key aspect of VMC since all the physical properties will descend from it. Therefore, the trial wave functions must be flexible enough to describe different phases of matter (metals, insulators, superconductors ...) but also simple to allow efficient calculations. A good compromise between efficiency and accuracy is presented by the Jastrow-Slater wave functions:

$$|\Psi\rangle = \mathcal{J}\,|\mathcal{D}\rangle \tag{2.45}$$

where $|\mathcal{D}\rangle$ is the uncorrelated part, built from an auxiliary Hamiltonian that can easily be diagonalized, and $\mathcal{J}$ is a density-density Jastrow factor, which is crucial to include correlation effects (Capello, Becca, Fabrizio, Sorella, and Tosatti 2005 and Tocchio, F. Arrigoni, Sorella, and Becca 2016).

2.5.1 Determinantal part

In the following, we will focus on the square lattice with L sites and two orbitals per site (i.e., a two-band model). The Slater determinant is built from the diagonalization of a suitable quadratic Hamiltonian $\mathcal{H}_{\text{aux}}$, defined as:

$$\mathcal{H}_{\text{aux}} = \mathcal{H}_{\text{kin}} + \mathcal{H}_{\text{sc}} + \mathcal{H}_{\text{mag}} + \mathcal{H}_{\text{orb}} \tag{2.46}$$

The kinetic term $\mathcal{H}_{\text{kin}}$ describes hopping processes of electrons within the two orbitals:

$$\mathcal{H}_{\text{kin}} = \sum_{\alpha,\beta} a^{\alpha\beta} \sum_{\langle i,j\rangle,\sigma} c^{\dagger}_{i,\alpha,\sigma} c_{j,\beta,\sigma} + \text{H.c.} \tag{2.47}$$

where $\langle i,j\rangle$ indicates nearest-neighbor sites, α and β the orbitals and σ the spin component along the z axis. The hopping parameters $a^{\alpha\beta}$ are variational parameters that can be optimized (one of them can be always fixed, in order to set the energy scale of the auxiliary Hamiltonian). Then, $\mathcal{H}_{\text{sc}}$ contains BCS pairing terms:

$$\begin{aligned}\mathcal{H}_{\text{sc}} = &\sum_{\langle i,j\rangle,\alpha} \Delta^{\alpha}_{i,j} \left(c^{\dagger}_{i,\alpha,\uparrow} c^{\dagger}_{j,\alpha,\downarrow} + c^{\dagger}_{j,\alpha,\uparrow} c^{\dagger}_{i,\alpha,\downarrow} \right) + \text{H.c.} \\ &+ \Delta_{\perp} \sum_{i} \left(c^{\dagger}_{i,1,\uparrow} c^{\dagger}_{i,2,\downarrow} - c^{\dagger}_{i,2,\uparrow} c^{\dagger}_{i,1,\downarrow} \right) + \text{H.c.} \\ &+ \sum_{\alpha} \mu^{\alpha} \sum_{i,\sigma} c^{\dagger}_{i,\alpha,\sigma} c_{i,\alpha,\sigma}\end{aligned} \tag{2.48}$$

This term allows us to take into account different superconductive gaps. First of all, a nearest-neighbor intra-orbital singlet. It may exhibit a $d_{x^2-y^2}$ symmetry, i.e., $\Delta^{\alpha}_{\boldsymbol{q}} = 2\Delta^{\alpha}_{d}[\cos(q_x) - \cos(q_y)]$, stabilized by strong Hubbard-U interactions, as in the single-band model (Tocchio, Becca, and Sorella 2016); then, also an on-site inter-orbital triplet pairing $\Delta_{\perp}$ (with different spins along z), which is expected to exist in the presence of a finite Hund coupling J (Tocchio, F. Arrigoni, Sorella, and Becca 2016). In addition, a chemical potential μ^{α} is also considered. All these parameters (i.e., μ^{α}, Δ^{α}_{d}, and $\Delta_{\perp}$) are optimized to minimize the variational energy. We would like to mention that a finite pairing amplitude is also important to capture the essence of the resonating-valence bond state, which may be relevant to describe Mott insulators and high-temperature superconductors (Anderson 1987).

Finally, $\mathcal{H}_{\text{mag}}$ and $\mathcal{H}_{\text{orb}}$ incorporate magnetic and orbital orders:

$$\begin{aligned}\mathcal{H}_{\text{mag}} = &\sum_{\alpha} \Delta^{\alpha}_{\text{AFM}} \sum_{i} (-1)^{\mathbf{R}_i} \left(c^{\dagger}_{i,\alpha,\uparrow} c_{i,\alpha,\uparrow} - c^{\dagger}_{i,\alpha,\downarrow} c_{i,\alpha,\downarrow} \right) \\ &+ \sum_{\alpha} h^{\alpha}_{\text{FM}} \sum_{i} \left(c^{\dagger}_{i,\alpha,\uparrow} c_{i,\alpha,\uparrow} - c^{\dagger}_{i,\alpha,\downarrow} c_{i,\alpha,\downarrow} \right)\end{aligned} \tag{2.49}$$

$$\begin{aligned}\mathcal{H}_{\text{orb}} = &\Delta_{\text{AFO}} \sum_{i,\sigma} (-1)^{\mathbf{R}_i} \left(c^{\dagger}_{i,1,\sigma} c_{i,1,\sigma} - c^{\dagger}_{i,2,\sigma} c_{i,2,\sigma} \right) \\ &+ h_{\text{FO}} \sum_{i,\sigma} \left(c^{\dagger}_{i,1,\sigma} c_{i,1,\sigma} - c^{\dagger}_{i,2,\sigma} c_{i,2,\sigma} \right)\end{aligned} \tag{2.50}$$

here, $\Delta^{\alpha}_{\text{AFM}}$,$h^{\alpha}_{\text{FM}}$, Δ_{AFO} and h_{FO} are further variational parameters to include (staggered and uniform) magnetic and orbital orders.

The auxiliary Hamiltonian $\mathcal{H}_{\text{aux}}$ can be easily diagonalized (in real space) to define the uncorrelated state; in the presence of the pairing terms, its ground state is not a Slater determinant, but a BCS state. Still, whenever the superconducting terms couple only opposite spins, it is possible to perform a simple transformation that leads to a Slater determinant defined in terms of single-particle orbitals. Indeed, we can perform a particle-hole transformation on electron operators with spin down:

$$\begin{aligned} d^{\dagger}_{i,\alpha,\uparrow} &= U c^{\dagger}_{i,\alpha,\uparrow} U^{\dagger} \\ d_{i,\alpha,\downarrow} &= U c^{\dagger}_{i,\alpha,\downarrow} U^{\dagger} \end{aligned} \tag{2.51}$$

Thus we can rewrite the BCS part (2.48) as (apart from constant terms)

$$\begin{aligned}\mathcal{H}_{\text{sc}} = &\sum_{\langle i,j\rangle,\alpha} \Delta_{i,j}^{\alpha} \left(d_{i,\alpha,\uparrow}^{\dagger} d_{j,\alpha,\downarrow} + d_{j,\alpha,\uparrow}^{\dagger} d_{i,\alpha,\downarrow} \right) + \text{H.c.} \\ &+ \Delta_{\perp} \sum_{i} \left(d_{i,1,\uparrow}^{\dagger} d_{i,2,\downarrow} - d_{i,2,\uparrow}^{\dagger} d_{i,1,\downarrow} \right) + \text{H.c.} \\ &+ \sum_{i,\alpha} \mu^{\alpha} \left(d_{i,\alpha,\uparrow}^{\dagger} d_{i,\alpha,\uparrow} - d_{i,\alpha,\downarrow}^{\dagger} d_{i,\alpha,\downarrow} \right)\end{aligned} \tag{2.52}$$

In addition, the kinetic term $\mathcal{H}_{\text{kin}}$ turns out into the following form:

$$\mathcal{H}_{\text{kin}} = \sum_{\alpha,\beta} a^{\alpha\beta} \sum_{\langle i,j\rangle} \left(d_{i,\alpha,\uparrow}^{\dagger} d_{j,\beta,\uparrow} - d_{i,\alpha,\downarrow}^{\dagger} d_{j,\beta,\downarrow} \right) + \text{H.c.} \tag{2.53}$$

Similarly, for $\mathcal{H}_{\text{mag}}$ and $\mathcal{H}_{\text{orb}}$:

$$\begin{aligned}\mathcal{H}_{\text{mag}} = &\sum_{\alpha} \Delta_{\text{AFM}}^{\alpha} \sum_{i} (-1)^{\mathbf{R}_i} \left(d_{i,\alpha,\uparrow}^{\dagger} d_{i,\alpha,\uparrow} + d_{i,\alpha,\downarrow}^{\dagger} d_{i,\alpha,\downarrow} \right) \\ &+ \sum_{\alpha} h_{\text{FM}}^{\alpha} \sum_{i} \left(d_{i,\alpha,\uparrow}^{\dagger} d_{i,\alpha,\uparrow} + d_{i,\alpha,\downarrow}^{\dagger} d_{i,\alpha,\downarrow} \right)\end{aligned} \tag{2.54}$$

$$\begin{aligned}\mathcal{H}_{\text{orb}} = &\Delta_{\text{AFO}} \sum_{i} (-1)^{\mathbf{R}_i} \left(d_{i,1,\uparrow}^{\dagger} d_{i,1,\uparrow} - d_{i,2,\uparrow}^{\dagger} d_{i,2,\uparrow} - d_{i,1,\downarrow}^{\dagger} d_{i,1,\downarrow} + d_{i,2,\downarrow}^{\dagger} d_{i,2,\downarrow} \right) \\ &+ h_{\text{FO}} \sum_{i} \left(d_{i,1,\uparrow}^{\dagger} d_{i,1,\uparrow} - d_{i,2,\uparrow}^{\dagger} d_{i,2,\uparrow} - d_{i,1,\downarrow}^{\dagger} d_{i,1,\downarrow} + d_{i,2,\downarrow}^{\dagger} d_{i,2,\downarrow} \right)\end{aligned} \tag{2.55}$$

Notice that the density operators of the new operators are simply related to the ones before the particle-hole transformation:

$$\begin{aligned}N_{\alpha,\uparrow}^{c} &= \sum_{i} c_{i,\alpha,\uparrow}^{\dagger} c_{i,\alpha,\uparrow} = \sum_{i} d_{i,\alpha,\uparrow}^{\dagger} d_{i,\alpha\uparrow} = N_{\alpha,\uparrow}^{d} \\ N_{\alpha,\downarrow}^{c} &= \sum_{i} c_{i,\alpha,\downarrow}^{\dagger} c_{i,\alpha,\downarrow} = L - \sum_{i} d_{i,\alpha,\downarrow}^{\dagger} d_{i,\alpha,\downarrow} = L - N_{\alpha,\downarrow}^{d}\end{aligned} \tag{2.56}$$

The total density (summed over the orbitals and the spin components) and the z component of the spin are given by:

$$\begin{aligned}\sum_{\alpha} \left(N_{\alpha,\uparrow}^{c} + N_{\alpha,\downarrow}^{c} \right) &= \sum_{\alpha} (N_{\alpha,\uparrow}^{d} - N_{\alpha,\downarrow}^{d}) + 2L \\ \sum_{\alpha} \left(N_{\alpha,\uparrow}^{c} - N_{\alpha,\downarrow}^{c} \right) &= \sum_{\alpha} (N_{\alpha,\uparrow}^{d} + N_{\alpha,\downarrow}^{d}) - 2L\end{aligned} \tag{2.57}$$

Therefore, whenever before the particle-hole transformation there is an equal number of electrons with up and down spins, after it, the total number of particles is equal to $2L$ (i.e., the system is half filled).

Now we can rewrite $\mathcal{H}_{\text{aux}}$ in a simple quadratic form:

$$\mathcal{H}_{\text{aux}} = \mathbf{d}^\dagger \mathbf{T} \mathbf{d} \tag{2.58}$$

where $\mathbf{d}^\dagger = (\mathbf{d}_\uparrow^\dagger, \mathbf{d}_\downarrow^\dagger)$ is a vector with $4L$ componets ($\mathbf{d}_\sigma^\dagger = d_{1,1,\sigma}^\dagger, \ldots, d_{L,1,\sigma}^\dagger, d_{1,2,\sigma}^\dagger, \ldots, d_{L,2,\sigma}^\dagger$) and $\mathbf{T}$ a $4L \times 4L$ matrix. Using a suitable unitary matrix $\mathbf{V}$ we can diagonalize $\mathcal{H}_{\text{aux}}$:

$$\mathcal{H}_{\text{aux}} = \mathbf{d}^\dagger \, \mathbf{V}\mathbf{V}^\dagger \, \mathbf{T} \, \mathbf{V}\mathbf{V}^\dagger \mathbf{d} = \mathbf{f}^\dagger \, \mathbf{E} \, \mathbf{f} \tag{2.59}$$

where $\mathbf{E}$ contains the eigenvalues of $\mathbf{T}$. Then, the Slater determinant that is used in (2.45) is obtained by filling the N_s lowest-energy levels of the auxiliary Hamiltonian ($N_s = 2L$ whenever the particle-hole transformation is considered and the numbers of up and down spins are equal):

$$|\mathcal{D}\rangle = \Pi_\alpha f_\alpha^\dagger \, |0\rangle \tag{2.60}$$

where $\alpha = 1, \ldots, N_s$.

2.5.2 Jastrow factor

In order to include electron-electron correlations within the variational wave function, we consider the density-density Jastrow factor. For simplicity, let us start from the single-band Hubbard model:

$$\mathcal{H} = -t \sum_{\langle i,j \rangle, \sigma} c_{i,\sigma}^\dagger c_{j,\sigma} + U \sum_i n_{i,\uparrow} n_{i,\downarrow} \tag{2.61}$$

The effect of the on-site repulsion U is to reduce the number of doubly occupied sites, since they become energetically unfavoured. As a consequence, within the ground-state wave function, the amplitudes of all configurations with one or more doubly occupied sites will be reduced with respect to the non-interacting case with $U = 0$. With this idea in mind, Gutzwiller 1963 suggested a simple and elegant variational state, where, starting from the non-interacting many-body state, a "penalty" is associated to these energetic configurations:

$$|\Psi_G\rangle = e^{-g \sum_i^L n_{i,\uparrow} n_{i,\downarrow}} \, |\mathcal{D}_0\rangle \tag{2.62}$$

here, g is a variational parameter that depends upon U and $|\mathcal{D}_0\rangle$ is the Slater determinant constructed from plane waves (more generally, $|\mathcal{D}_0\rangle$ can be substituted by any other non-interacting state). When expanding $|\Psi_G\rangle$ in the basis set with electrons localized on every site, we can appreciate the effect of the Gutwiller factor:

$$|\Psi_G\rangle = \sum_x e^{-gN_d(x)} \langle x \,|\, \mathcal{D}_0\rangle \, |x\rangle \tag{2.63}$$

where $N_d(x)$ is the number of doubly-occupied sites in the configuration $|x\rangle$.

Of course, for $U = 0$, the exact ground state is obtained by taking $g = 0$. By contrast, far from $U/t \to \infty$ the Gutzwiller parameter diverges (i.e., $g \to \infty$), corresponding to a state with no doubly-occupied sites. When the number of electrons equals the number of sites (i.e., $N_e = L$), the fully-projected Gutzwiller state corresponds to an insulator, where the charge degrees of freedom are frozen (while the spin degrees of freedom are still dynamical). Instead, for any finite values of g, the Gutzwiller state corresponds to a metal. Indeed, whenever a positive background is considered to compensate the electron charges, empty (doubly) occupied sites carry a positive (negative) charge. The Gutzwiller factor gives a penalty for the creation of such objects, which, however, can move freely without any further obstacle. Therefore, they give rise to electrical conduction in the presence of an external field (Capello, Becca, Fabrizio, Sorella, and Tosatti 2005). Only when $g \to \infty$, there is no conduction, since the creation of empty and doubly occupied sites is prohibited. In this regard, a few improvements have been achieved in the past (Fazekas and Penc 1988 and Yokoyama and Shiba 1990), by allowing nearest-neighbor correlations between an empty and a double occupied site. However, to have a faithful description of a Mott insulator, it is crucial (Capello, Becca, Fabrizio, Sorella, and Tosatti 2005) to take into account all the spatial correlations. This can be realized by applying a long-range Jastrow $\mathcal{J}$ factor to the uncorrelated wave function:

$$\mathcal{J} = \exp\left(-\frac{1}{2}\sum_{i,j} v_{i,j} n_i n_j\right), \tag{2.64}$$

where $n_i = \sum_\sigma n_{i,\sigma}$ is the electron density on site i and $v_{i,j}$ are the pseudo-potential that depend upon the distance $|\mathbf{R}_i - \mathbf{R}_j|$ and may be optimized in order to minimize the variational energy. The Jastrow factor can be easily generalized to include multi-orbital effects:

$$\mathcal{J} = \exp\left(-\frac{1}{2}\sum_{i,j,\alpha,\beta} v_{i,j}^{\alpha,\beta} n_{i,\alpha} n_{j,\beta}\right), \tag{2.65}$$

where $n_{i,\alpha} = \sum_\sigma n_{i,\alpha,\sigma}$ is the electron density on site i and orbital α. We will indicate the terms $v_{ij}^{\alpha\beta}$ as v_{ij}^{intra} whenever $\alpha = \beta$ and v_{ij}^{inter} if $\alpha \neq \beta$.

In the next section we will see that the psudopotentials $v_{i,j}^{\alpha,\beta}$, under some circumstances, can be used to detect the insulating or metallic character of the wave function.

2.6 Metals and Insulators

The physical states of matter we are trying to describe are metals (or superconductors) and insulators. At zero temperature, they can be distinguished by looking at their conductivity, which is finite for a metal (or infinite for a superconductor) and vanishing for an insulator. Unfortunately, a straightforward computation of the conductivity would require the knowledge of the low-energy spectrum and not only the ground-state wave function. Therefore, we have to identify another quantity which must be relatively easy to evaluate by having only the ground state. This quantity is the static structure factor $N(\mathbf{q}) = N_\mathbf{q}$ (in the following, for simplicity, we will refer to a single-band model; the generalization to a multi-band case is straightforward):

$$N_\mathbf{q} = \frac{\langle\Psi|\, n_\mathbf{q} n_{-\mathbf{q}} \,|\Psi\rangle}{\langle\Psi|\Psi\rangle} \tag{2.66}$$

where $n_\mathbf{q}$ is the Fourier-transformed particle density summed over spin and orbital indices. Its behavior at small momenta (or, equivalently, at large wavelengths) reveals us the nature of the state associated with that wave function (Capello, Becca, Yunoki, and Sorella 2006). To show this, let us recall the Feynman single-mode approximation, originally formulated in the context of collective excitations in liquid Helium (Feynman 1954). At long wavelength, these systems show a linearly dispersive collective (sound) mode. In the Feynman idea, the variational excited-state $|\Psi_\mathbf{q}\rangle$ for the density wave is:

$$|\Psi_\mathbf{q}\rangle = n_\mathbf{q} \,|\Psi\rangle \tag{2.67}$$

where $|\Psi\rangle$ is the exact ground state. The variational estimator of the excitation energy is then given by:

$$E_\mathbf{q} - E_0 = \frac{\langle\Psi_\mathbf{q}\,|\,(\mathcal{H} - E_0)\,|\,\Psi_\mathbf{q}\rangle}{\langle\Psi_\mathbf{q}\,|\,\Psi_\mathbf{q}\rangle} = \frac{\langle\Psi\,|\,n_{-\mathbf{q}}[\mathcal{H}, n_\mathbf{q}]\,|\,\Psi\rangle}{N_\mathbf{q}\,\langle\Psi|\Psi\rangle} \tag{2.68}$$

The commutator can be evaluated once the specific form of the Hamiltonian is given (the non-trivial terms come from the kinetic part, while the interaction usually commutes with

$n_{\mathbf{q}}$ (Tocchio, Becca, and Gros 2011), giving:

$$\frac{\langle \Psi \,|\, n_{-\mathbf{q}}[\mathcal{H}, n_{\mathbf{q}}] \,|\, \Psi \rangle}{\langle \Psi | \Psi \rangle} \approx \text{const} \times \mathbf{q}^2 \tag{2.69}$$

Therefore, the variational expression for the excitation energy is found to be:

$$E_{\mathbf{q}} - E_0 \approx \frac{\text{const} \times \mathbf{q}^2}{N_{\mathbf{q}}} \tag{2.70}$$

Then, whenever $N_{\mathbf{q}}$ is linear in $\mathbf{q}$ the energy spectrum is gapless, suggesting that the system is metallic; by contrast, if $N_{\mathbf{q}} \approx \mathbf{q}^2$ this construction gives a finite gap, leading to an insulator. In this latter case, we cannot exclude that other kind of excitations are gapless; still, we will always assume that the low-energy excitations are collective plasmonic excitations (Tocchio, Becca, and Gros 2011).

There is a relation between $N_{\mathbf{q}}$ and the Fourier-transformed pseudopotentials of the Jastrow factor $v_{\mathbf{q}}$, which can be derived calculating the correlation function within a Gaussian approximation. The explicit relation that we are going to prove is:

$$N_{\mathbf{q}} = \frac{N^0_{\mathbf{q}}}{1 + 2\, v_{\mathbf{q}} N^0_{\mathbf{q}}} \tag{2.71}$$

where $N^0_{\mathbf{q}}$ is the static structure factor computed with the uncorrelated wave function. Even tough this formula is rigorously valid in the weak-coupling regime, it still holds in the strong-coupling regime when $\mathbf{q} \to 0$, see Fig. (2.1). Given the definition of our wave function

$$|\Psi\rangle = \mathcal{J}\,|\mathcal{D}\rangle \tag{2.72}$$

we consider

$$N_{ij} = \frac{\langle \Psi \,|\, n_i n_j \,|\, \Psi \rangle}{\langle \Psi \,|\, \Psi \rangle} = \frac{\langle \mathcal{D} \,|\, \mathcal{J}^2 n_i n_j \,|\, \mathcal{D} \rangle}{\langle \mathcal{D} \,|\, \mathcal{J}^2 \,|\, \mathcal{D} \rangle} \tag{2.73}$$

which is valid since $[\mathcal{J}, n_i] = 0$. The Jastrow factor (squared) can be rewritten by using the Hubbard-Stratonovich transformation (Altland and Simons 2010):

$$\mathcal{J}^2 = \frac{1}{W} \int \mathrm{d}\boldsymbol{\theta}\, \exp\left[-\frac{1}{4} \sum_{k,l} \theta_k v^{-1}_{kl} \theta_l - \mathrm{i} \sum_k n_k \theta_k \right] \tag{2.74}$$

where $d\boldsymbol{\theta} = d\theta_1 \dots d\theta_L$ (L being the number of sites) and W is a normalization constant.

The structure factor becomes:

$$N_{ij} = \frac{1}{Z}\int \mathrm{d}\boldsymbol{\theta}\ \exp\left[-\frac{1}{4}\sum_{k,l}\theta_k v_{kl}^{-1}\theta_l\right]\left\langle \mathcal{D}\,\middle|\, n_i n_j e^{-\mathrm{i}\sum_k n_k\theta_k}\,\middle|\,\mathcal{D}\right\rangle \tag{2.75}$$

Then, by denoting

$$F(\boldsymbol{\theta}) = \left\langle \mathcal{D}\,\middle|\, e^{-\mathrm{i}\sum_k n_k\theta_k}\,\middle|\,\mathcal{D}\right\rangle \tag{2.76}$$

we have that

$$-\partial_{\theta_i}\partial_{\theta_j}F(\boldsymbol{\theta}) = \left\langle \mathcal{D}\,\middle|\, n_i n_j e^{-\mathrm{i}\sum_k n_k\theta_k}\,\middle|\,\mathcal{D}\right\rangle \tag{2.77}$$

Therefore

$$N_{ij} = -\frac{1}{Z}\int \mathrm{d}\boldsymbol{\theta}\ \exp\left[-\frac{1}{4}\sum_{k,l}\theta_k v_{kl}^{-1}\theta_l\right]\partial_{\theta_i}\partial_{\theta_j}F(\boldsymbol{\theta}) \tag{2.78}$$

where Z comes from the normalization condition $\left\langle \mathcal{D}\,\middle|\, \mathcal{J}^2\,\middle|\,\mathcal{D}\right\rangle$.
This expression can be further manipulated by integrating by parts (and using the fact that the boundary terms are vanishing):

$$\begin{aligned} N_{ij} = -\frac{1}{Z}\int \mathrm{d}\boldsymbol{\theta}\ \exp&\left[\ln F(\boldsymbol{\theta}) - \frac{1}{4}\sum_{k,l}\theta_k v_{kl}^{-1}\theta_l\right] \\ &\left[\frac{1}{4}\left(\sum_k v_{ki}^{-1}\theta_k\right)\left(\sum_l v_{jl}^{-1}\theta_l\right) - \frac{v_{ij}^{-1}}{2}\right] \end{aligned} \tag{2.79}$$

So far everything is exact. Now, we consider the Gaussian approximation and make an expansion around a suitable saddle point $\boldsymbol{\theta}^\star$ such that

$$\partial_{\theta_i}\left[\ln F(\boldsymbol{\theta}) - \frac{1}{4}\sum_{k,l}\theta_k v_{kl}^{-1}\theta_l\right]\Bigg|_{\theta^\star} = 0 \tag{2.80}$$

Then, we will indicate $\phi_i = \theta_i - \theta_i^\star$ and

$$N_{ij}^0 = -\partial_{\theta_i}\partial_{\theta_j}F(\boldsymbol{\theta})\Big|_{\theta^\star} \tag{2.81}$$

Then, the integral (2.79) can be rewritten as

$$N_{ij} \approx -\frac{1}{Z}\int \mathrm{d}\boldsymbol{\phi}\, \exp\left[-\frac{1}{2}\sum_{k,l}\phi_k\left(N^0_{kl}+\frac{v^{-1}_{kl}}{2}\right)\phi_l\right]\left[\frac{1}{4}\left(\sum_k v^{-1}_{ki}\phi_k\right)\left(\sum_l v^{-1}_{jl}\phi_l\right)-\frac{v^{-1}_{ij}}{2}\right] \tag{2.82}$$

Finally, by using the relation:

$$\int \mathrm{d}\boldsymbol{\phi}\, \exp\left[-\frac{1}{2}\sum_{k,l}\phi_k\left(N^0_{kl}+\frac{v^{-1}_{kl}}{2}\right)\phi_l\right]\phi_i\phi_j \approx \left(\mathbf{N}^0+\frac{1}{2}\boldsymbol{v}^{-1}\right)^{-1}_{ij} \tag{2.83}$$

We get:

$$N_{ij} \approx \left(\frac{\mathbf{N^0}}{1+2\boldsymbol{v}\mathbf{N^0}}\right)_{ij} \tag{2.84}$$

which, coincides with the Reatto and Chester formula found in Random Phase Approximation (Reatto and Chester 1967).

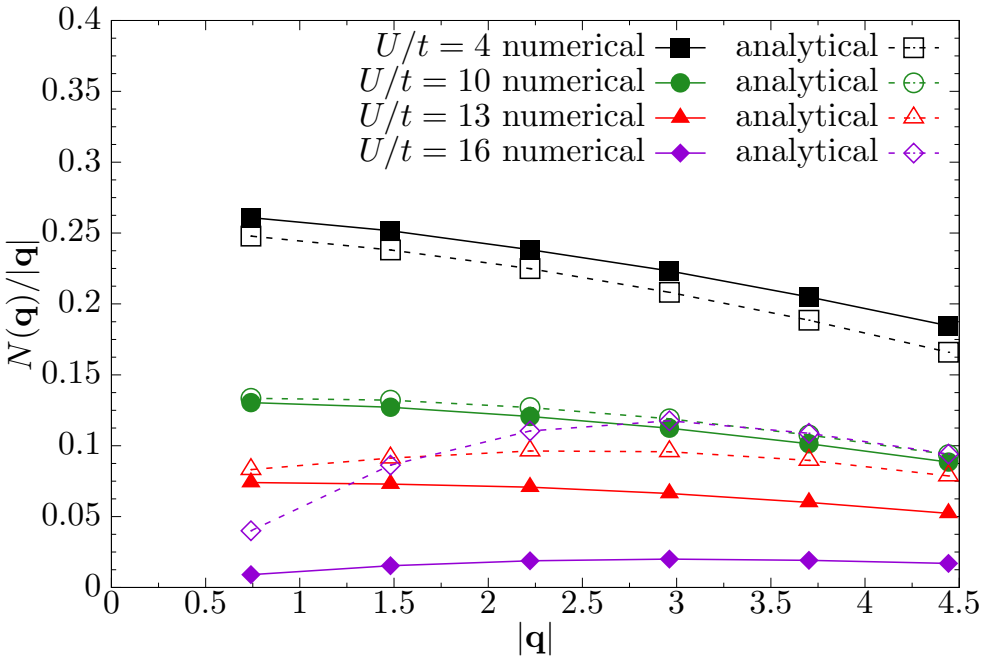

Figure 2.1: Trend of the density-density structure factor divided by $|\mathbf{q}|$ obtained by the analytical formula (2.71) (empty symbols) and by VMC (solid symbols) for the two-band Hubbard model on the 12×12 square lattice at half filling. Different values of U/t are reported, the metal-insulator transition is located at $U_{MIT}/t = 13 \pm 1$.

Chapter 3

Results: The Two-Band Hubbard Model

In this chapter we explore the ground-state properties of the two-band Hubbard model with degenerate electronic orbitals, as described previously in Chap. 1. For the sake of clarity, we remind here the Hamiltonian:

$$\begin{aligned}\mathcal{H} = & -t \sum_{\langle i,j\rangle,\alpha,\sigma} c^{\dagger}_{i,\alpha,\sigma} c_{j,\alpha,\sigma} + \text{H.c.} \\ & + U \sum_{i,\alpha} n_{i,\alpha,\uparrow} n_{i,\alpha,\downarrow} + (U-2J) \sum_{i,\sigma\neq\sigma'} n_{i,1,\sigma} n_{i,2,\sigma'} + (U-3J) \sum_{i,\sigma} n_{i,1,\sigma} n_{i,2,\sigma} \\ & - J \sum_{i,\sigma\neq\sigma'} c^{\dagger}_{i,1,\sigma} c_{i,1,\sigma'} c^{\dagger}_{i,2,\sigma'} c_{i,2,\sigma} \\ & - J \sum_{i} (c^{\dagger}_{i,1,\uparrow} c^{\dagger}_{i,1,\downarrow} c_{i,2,\uparrow} c_{i,2,\downarrow} + \text{H.c.})\end{aligned} \tag{3.1}$$

where t is the nearest-neighbor hopping parameter, U and U' define the intra- and inter-orbital Coulomb repulsion and $J > 0$ is the Hund coupling.

By means of Jastrow-Slater wave functions, we will first detect the occurrence of the Mott transition in the paramagnetic and paraorbital case at half filling and quarter filling, then we analyze the occurrence of magnetic and orbital order and the existence of superconductivity in the presence and in the absence of magnetic/orbital orders.

Unless specifically told, all simulations reported in this chapter refer to a square lattice of $L = 12 \times 12$ sites, with periodic boundary conditions on one axis and anti-periodic on the other, in order to ensure that the eigenstates of the mean-field Hamiltonian (for $U = J = 0$) form a closed shell, i.e., a non degenerate ground state.

3.1 The metal-insulator transitions in the absence of magnetic/orbital orders

3.1.1 $J > 0$ case

Let us start to study the MIT at commensurate electron densities, $n = 2$ and $n = 1$; at the moment we shall not consider any magnetic or orbital order within the variational wave function:

$$|\Psi\rangle = \mathcal{J}\,|\mathcal{D}\rangle \tag{3.2}$$

Therefore in the auxiliary Hamiltonian of $\mathcal{H}_{\text{aux}}$ of Eq. (2.46) we consider a kinetic term:

$$\mathcal{H}_{\text{kin}} = \sum_{\alpha,\beta} a^{\alpha\beta} \sum_{\langle i,j\rangle,\sigma} c^{\dagger}_{i,\alpha,\sigma} c_{j,\beta,\sigma} + \text{H.c.} \tag{3.3}$$

where, in order to set the energy scale, we have fixed $a^{11} = a^{22} = 1$ and $a^{12} = a^{21} = 0$. In addition to $\mathcal{H}_{\text{kin}}$, we take into account also an on-site interband spin triplet term,

$$\mathcal{H}_{\text{sc}} = \Delta_{\perp} \sum_{i} \left(c^{\dagger}_{i,1,\uparrow} c^{\dagger}_{i,2,\downarrow} - c^{\dagger}_{i,2,\uparrow} c^{\dagger}_{i,1,\downarrow} \right) + \text{H.c.} \tag{3.4}$$

This term is necessary to correctly describe the Mott phase in the presence of a finite Hund's coupling J (Tocchio, F. Arrigoni, Sorella, and Becca 2016; Bünemann and Spałek 2014). Indeed, it promotes the formation of localized (on-site) inter-orbital spin triplets. The results for $n = 2$ and $J > 0$ are reported in Fig. 3.1. For $J/U = 0.01$, 0.05, and 0.1, the Mott transition is first order, since two different wave functions, whose energies cross at $U = U_{\text{MIT}}$, can be stabilized in the vicinity of the MIT. In particular for $J/U = 0.01$ the transition is located at $U_{\text{MIT}}/t = 10.8 \pm 0.2$, for $J/U = 0.05$ is at $U_{\text{MIT}}/t = 8.3 \pm 0.4$, while $U_{\text{MIT}}/t = 6.9 \pm 0.1$ for $J/U = 0.1$. In Fig. 3.2 it is reported the behavior of the static structure factor as defined in Sec. 2.6 for wave functions having the lowest variational energy of Fig. 3.1. While for small values of the Coulomb interaction, the best variational state is metallic with $N(\boldsymbol{q}) \propto |\boldsymbol{q}|$ in the limit of $|\boldsymbol{q}| \to 0$, for large U/t, the lowest-energy state is insulating with $N(\boldsymbol{q}) \propto |\boldsymbol{q}|^2$. As explained in Sec. 2.6, this modification in the density-density correlations is triggered by the Jastrow factor, e.g., $v^{\text{intra}}(\boldsymbol{q}) \propto 1/|\boldsymbol{q}|$ in the metal, while $v^{\text{intra}}(\boldsymbol{q}) \propto 1/|\boldsymbol{q}|^2$ in the insulator.

We mention that the region where metastable solutions can be stabilized, shrinks as J increases, thus suggesting that the transition may become second order for a large enough value of the Hund coupling (Facio, Vildosola, Garcia, and Cornaglia 2017; Lechermann, Georges, Kotliar, and Parcollet 2007; de'Medici and Capone 2017). Indeed, for $J/U =$

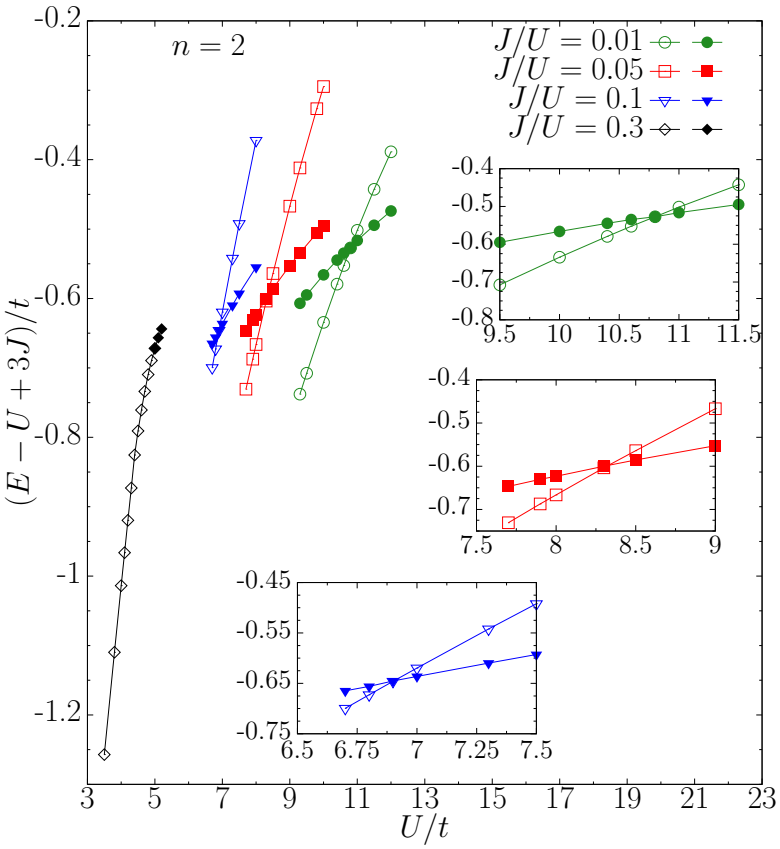

Figure 3.1: Energies (per site) of the metallic (empty symbols) and insulating (full symbols) states as a function of U/t for $n = 2$ and different values of the Hund coupling J. For clarity a constant shift of $U - 3J$, which is the ground-state energy (per site) in the $U/t \to \infty$ limit, has been considered. Insets: zoom around the metal insulator transitions.

0.3, the MIT appears to be continuous, with no metastable solutions that can be obtained (see Fig. 3.1). Still, the small-$\mathbf{q}$ behavior of the Jastrow factor is different for $U < U_{\mathrm{MIT}} = 4.9 \pm 0.1$ and $U > U_{\mathrm{MIT}}$ (see Fig. 3.2 (d)), as in the single-band Hubbard model, where the Mott transition is continuous (Capello, Becca, Yunoki, and Sorella 2006). We mention that, at least up to $J/U = 0.25$, the metal to Mott insulator transition is first order also in a model with three degenerate bands (modeled by Eq. (1.35)) at half filling. The behavior of U_{MIT} as a function of the Hund coupling J was studied by means of different computational methods such as Quantum Monte Carlo (Han, Jarrell, and Cox 1998), Dynamical Mean Field Theory (Koga, Imai, and Kawakami 2002; Pruschke and Bulla 2005) or slave-spin mean field method (de'Medici 2011).

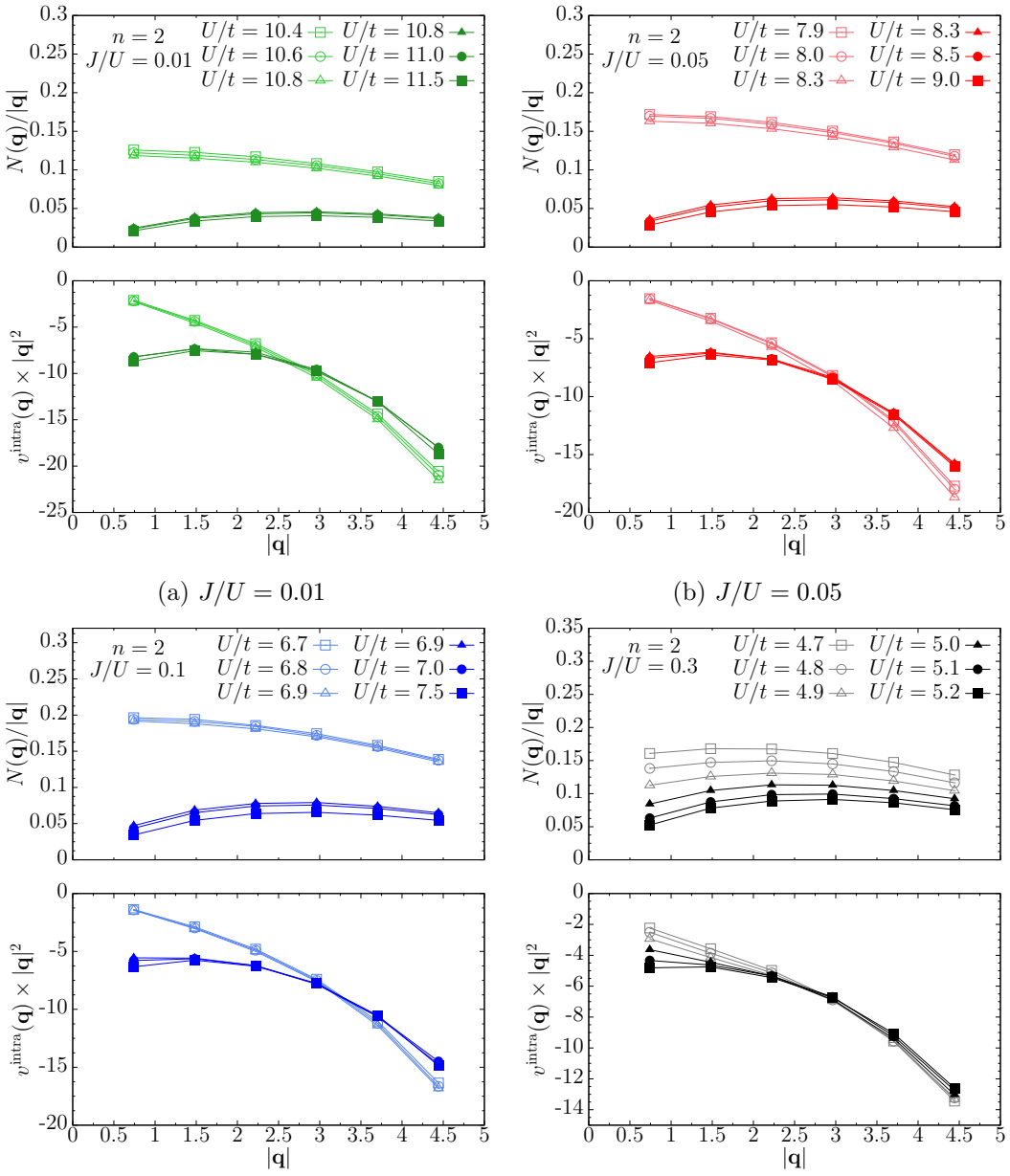

(a) $J/U = 0.01$ (b) $J/U = 0.05$

(c) $J/U = 0.1$ (d) $J/U = 0.3$

Figure 3.2: Upper panels: Density-density structure factor $N(\mathbf{q})$ (divided by $|\mathbf{q}|$) for various values of U/t for the lowest energy solutions of Fig. 3.1. Lower panels: The Fourier transform of the intra-orbital Jastrow factor $v^{\text{intra}}(\mathbf{q})$ (multiplied by $|\mathbf{q}|^2$) for the same set of parameters as in the upper panels. The results for metallic (insulating) wave functions are denoted by empty (full) symbols. Data are reported for $J/U = 0.01(a)$, $J/U = 0.05(b)$, $J/U = 0.1(c)$ and $J/U = 0.3(d)$

In all these studies J is shown to reduce the $U_{\rm MIT}/t$ needed for the Mott transition since the Mott insulator with localized moments may take advantage of the Hund coupling. Also our variational approach reproduces this evidence.
Remarkably, a strong (on-site inter-orbital) triplet pairing $\Delta_\perp$ is stabilized by the presence of a finite Hund coupling, giving a sizable gain in the variational energy with respect to the case with no pairing (see also Sec. 3.4).
For small values of J/U (and also $J = 0$, see Sec. 3.1.2) the energy of the insulating phase can be further lowered by adding a nearest-neighbor intra-orbital singlet pairing with $d_{x^2-y^2}$ symmetry (see Fig. 3.3) that in the auxiliary Hamiltonian reads:

$$\mathcal{H}_{\rm sc} = \sum_{\langle i,j\rangle,\alpha} \Delta_{i,j} \left(c^\dagger_{i,\alpha,\uparrow} c^\dagger_{j,\alpha,\downarrow} + c^\dagger_{j,\alpha,\uparrow} c^\dagger_{i,\alpha,\downarrow} \right) + \text{H.c.} \tag{3.5}$$

where $\Delta_q = 2\Delta_d(\cos q_x - \cos q_y)$ is the Fourier transform of $\Delta_{i,j}$. Nonetheless, we must emphasize that the Jastrow factor with $v^{\rm intra}(\boldsymbol{q}) \propto 1/|\boldsymbol{q}|^2$ and $v^{\rm inter}(\boldsymbol{q}) \propto 1/|\boldsymbol{q}|^2$, typical of a Mott insulator, is able to destroy the superconducting long-range order that is present in the uncorrelated wave function $|\mathcal{D}\rangle$ (Pitaevskii and Stringari 1991). Therefore, the presence of electronic pairing in $|\mathcal{D}\rangle$ leads to the existence of "preformed pairs" without phase coherence in the full correlated wave function $|\Psi\rangle$ of Eq. (3.2), as in the single-band Hubbard model. As discussed also in Sec. 3.4, the relevant difference with respect to the latter case is that, when doping, in the two-orbital Hubbard model "preformed pairs" do not form singlets with $d_{x^2-y^2}$ symmetry (except for small values of J/U) but triplets with s (on-site) symmetry.

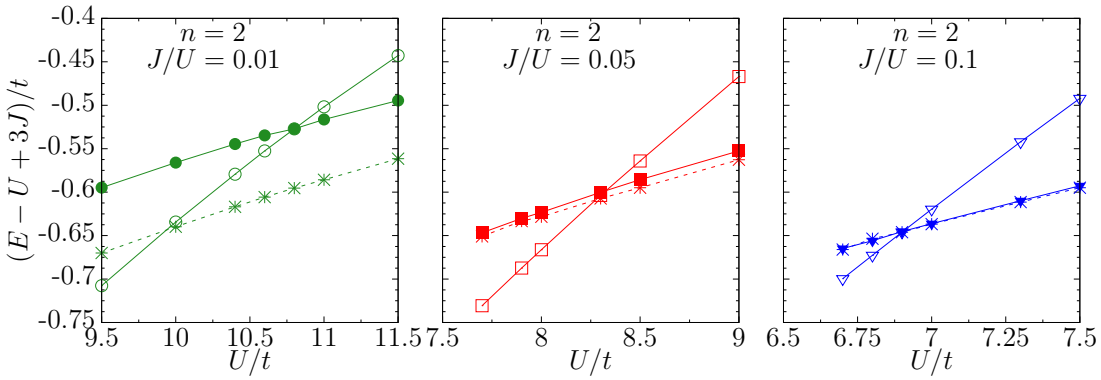

Figure 3.3: Energies (per site) of the metallic (empty symbols) and insulating (full symbols) states as a function of U/t for $n = 2$ and different values of the Hund coupling J. The stars denote the energies of the insulating state when Δ_d is allowed. All the Energies are shifted by $U - 3J$.

Within the metallic regime, there is no appreciable gain when including superconducting pairing (either singlet or triplet); a similar result has been obtained in the paramagnetic solution of the single-band Hubbard model, where the metallic phase at half filling has vanishingly small pairing correlations (Capello, Becca, Yunoki, and Sorella 2006; Tocchio, Becca, and Gros 2012; Dayal, Clay, and Mazumdar 2012). In addition, in this metallic phase, the intra- and inter-orbital Jastrow pseudopotentials are approximately equal for every distance, indicating that the correlation between two electrons on the same orbital is similar to the one between two electrons on different orbitals. By contrast, in the insulating phase the intra-orbital Jastrow factor is larger than the inter-orbital one, implying that configurations with two electrons on the same orbital are penalized with respect to the ones with two electrons on different orbitals, as expected in the presence of a finite value of J.

The results for $J/U = 0.1$, 0.15 and 0.2 at quarter-filling, $n = 1$, are shown in Fig. 3.4. In contrast to the half-filled case, here the Mott transition is always continuous (see Fig. 3.4 (a)) and is marked by a progressive change in the small-$\mathbf{q}$ behavior of the Jastrow factor (see Fig. 3.4 (b), (c) and (d)).
When no magnetic or orbital order are allowed, the effect of the Hund coupling J at $n = 1$ is to shift upward the MIT, as already pointed out by slave-spin mean field calculations (de'Medici 2011) and Dynamical Mean Field Theory (Georges, de'Medici, and Mravlje 2013). Indeed, the insulator with one electron per site does not have any substantial advantage from the presence of the Hund coupling, while the metallic phase, where the number of double occupancies is higher than in the insulator, gains potential energy when two electrons with the same spin are on the same site (and different orbitals).

Remarkably, no gain in the variational energy is detected by allowing (on-site inter-orbital) triplet or (nearest-neighbor intra- or inter-orbital) singlet pairings, both in the metallic and the insulating phases. In addition, the intra- and inter-orbital Jastrow pseudopotentials are very similar, implying that the variational wave function $|\Psi\rangle$ remains fully symmetric.

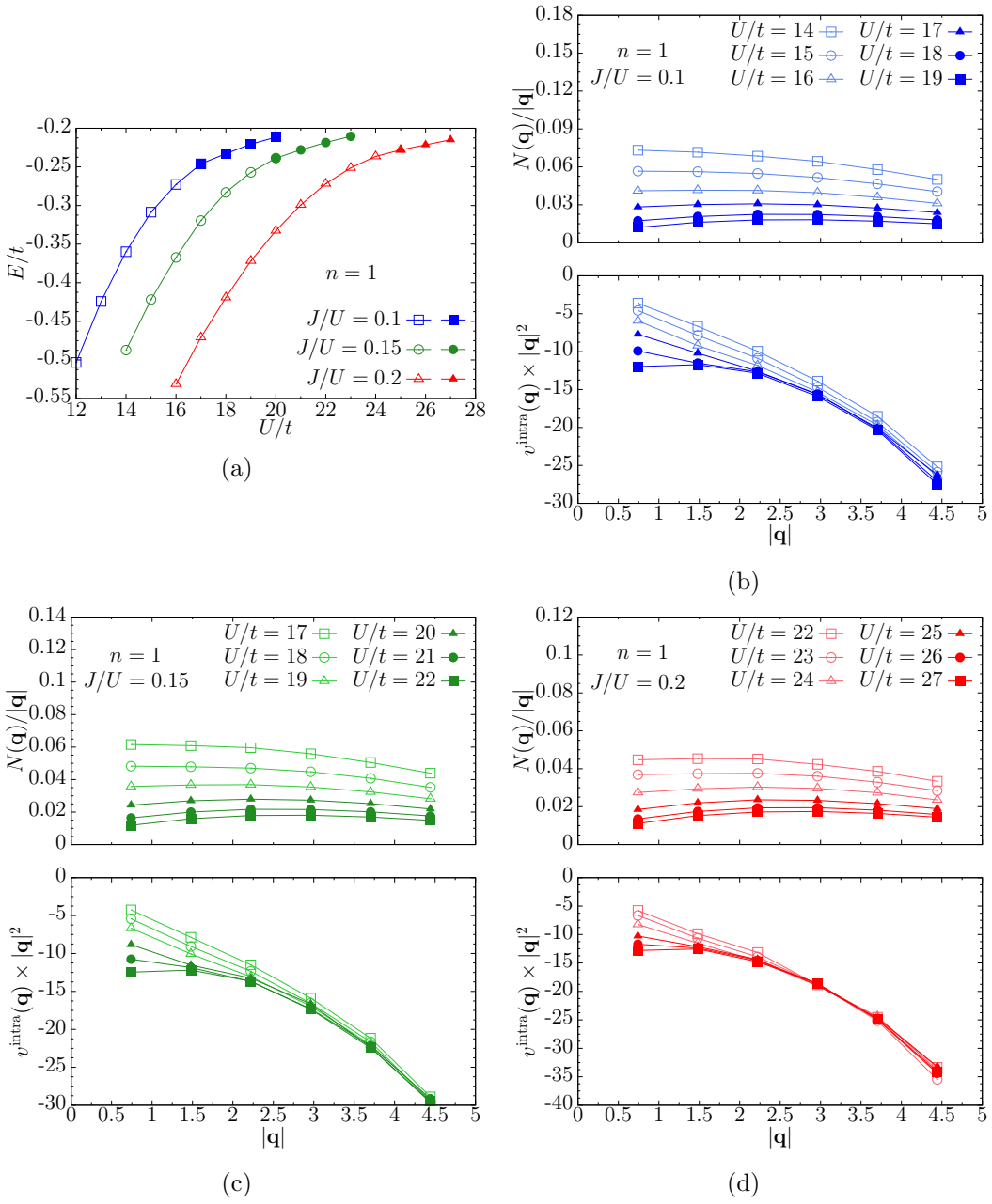

Figure 3.4: (a): Energy (per site) of the metallic and insulating states as a function of U/t for $n = 1$ and different values of the Hund coupling J. (b), (c), (d): Density-density structure factor $N(\mathbf{q})$ (divided by $|\mathbf{q}|$) for various values of U/t and J/U (upper panels) and the Fourier transform of the intra-orbital Jastrow factor $v^{\text{intra}}(\mathbf{q})$ (multiplied by $|\mathbf{q}|^2$) (lower panels) for the same set of parameters as in the upper panels. The results for metallic (insulating) wave functions are denoted by empty (full) symbols.

3.1.2 $J = 0$ case

In the $J = 0$ limit the model with degenerate bands possesses an enlarged SU(4) symmetry, which is generated by spin and orbital degrees of freedom. At $n = 2$, whenever the variational wave function is taken to have a full SU(4) symmetry (i.e., by only considering the kinetic term in the auxiliary Hamiltonian and imposing $v_{i,j}^{\text{intra}} = v_{i,j}^{\text{inter}}$), the transition appears to be continuous (at $U_{\text{MIT}}/t = 15 \pm 1$), with no metastable solutions in the energy optimization (see Fig. 3.5 (a)).
By allowing different intra- and inter-orbital Jastrow factors in the variational optimization, we break the full SU(4) symmetry and another insulating solution appears, which is energetically favorable for $U/t \gtrsim 13$ (see Fig. 3.5 (b)), so the transition turns out to be first order. In fact, whenever the intra-orbital Jastrow factor is different with respect to the inter-orbital one, this implies that configurations with two electrons on the same orbital are weighted in a different way in the ground state with respect to the ones with two electrons on different orbitals. In particular, in this new insulating solution, the pseudopotential v_{ij}^{intra} are, in modulus, greater than the v_{ij}^{inter} terms, while in the metallic state the two Jastrow factors remain similar.
Then, this insulating state can be further improved by considering the electron (singlet) pairing (with $d_{x^2-y^2}$ symmetry) in the auxiliary Hamiltonian, further lowering the transition to $U_{\text{MIT}}/t = 11 \pm 0.5$ (see Fig. 3.5 (c)). As before, the Jastrow factor prevents the existence of off-diagonal superconducting order.
The same considerations hold when adding another degenerate band. Also in this case at half filling, $n = 3$, the Mott metal-insulator transition is continuous when the SU(4) symmetry is not broken (see Fig. 3.6 (a)), while becoming first order allowing $v_{i,j}^{\text{intra}} \neq v_{i,j}^{\text{inter}}$ (see Fig. 3.6 (b)). Similarly to the two-band case, an energy gain in the insulating solution can be obtained by adding a singlet superconductive pairing with $d_{x^2-y^2}$ in the auxiliary Hamiltonian (see Fig. 3.6 (c)).

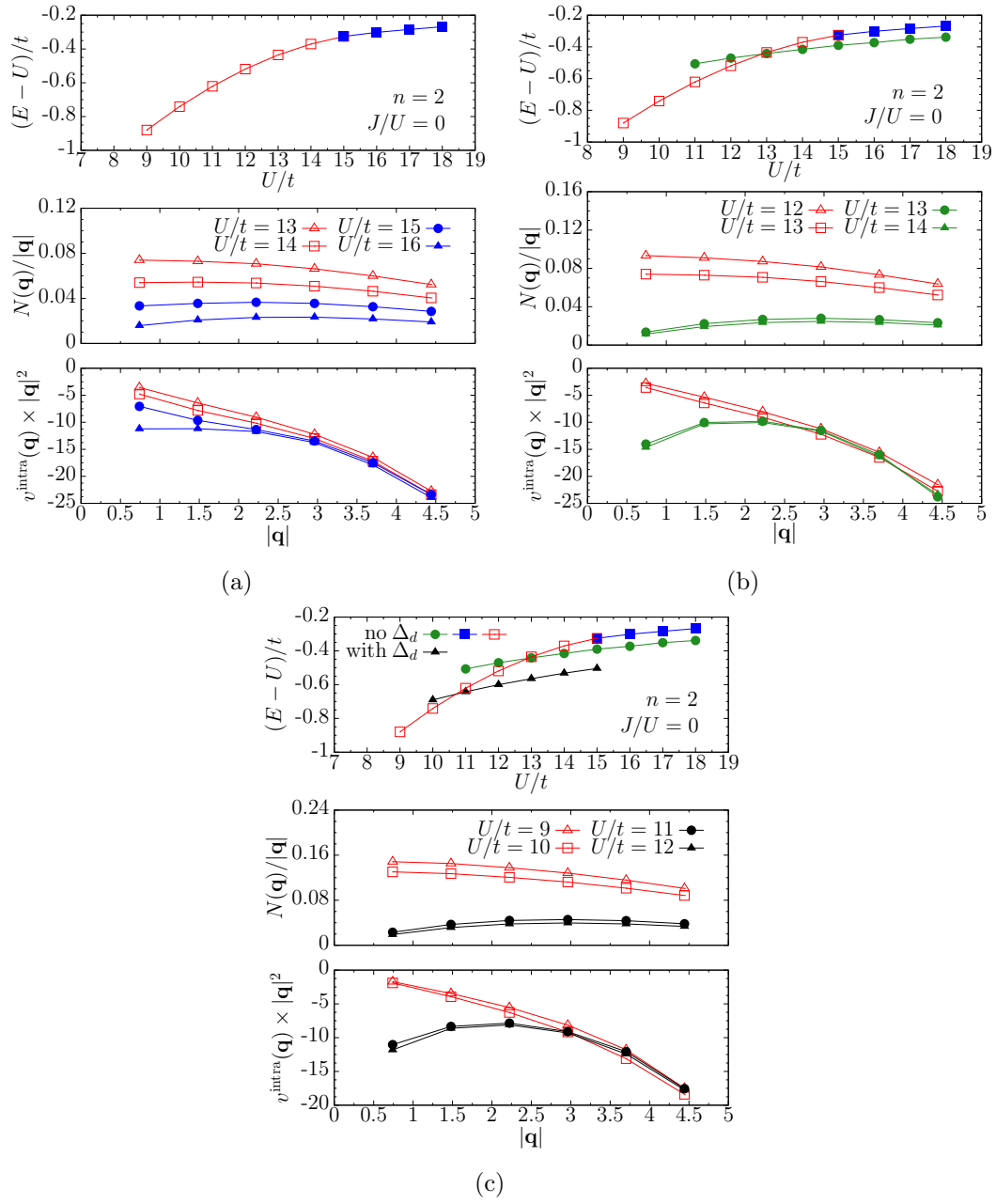

Figure 3.5: Results for $n = 2$ and $J = 0$. Upper panels: Variational energies (per site) for (a) the metallic (red empty squares) and insulating states (blue full squares) when the wave function does not break the SU(4) symmetry; (b) when the insulating state (green full circles) has no pairing but $v^{\text{inter}}(\mathbf{q}) \neq v^{\text{intra}}(\mathbf{q})$; ($c$) when the insulating state (black full triangles) has a finite Δ_d pairing. For clarity the energies are shifted by U. Middle panels: The density-density structure factor $N(\mathbf{q})$ of Eq. (2.66) (divided by $|\mathbf{q}|$) at various values of U/t, for the best variational state. Lower panels: The Fourier transform of the intra-orbital Jastrow factor (multiplied by $|\mathbf{q}|^2$) for the same set of parameters as in the middle panel. No magnetic or orbital orders are considered within the variational wave functions.

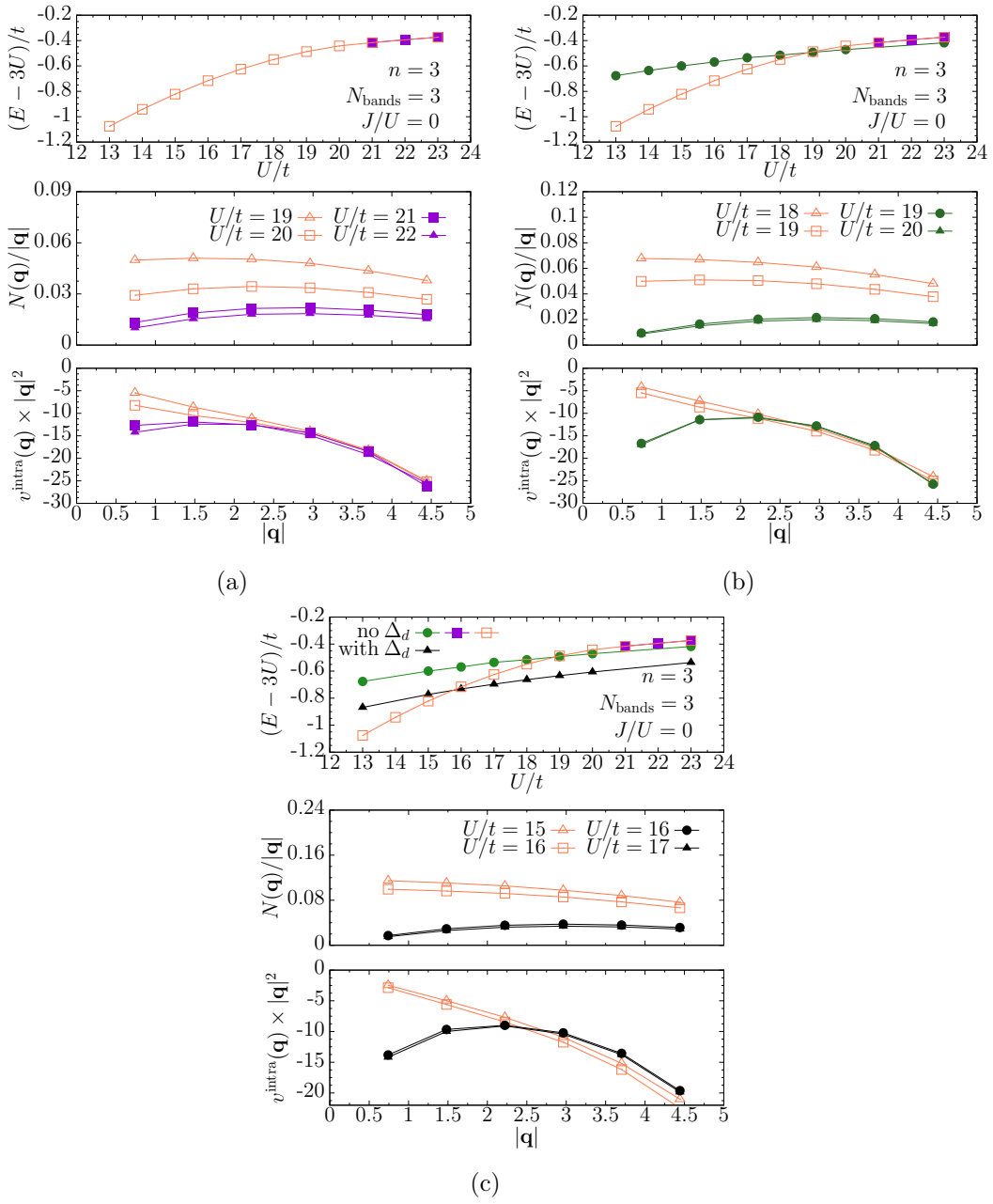

Figure 3.6: Results for three degenerate bands at half filling, $n = 3$, and $J = 0$. Upper panels: Variational energies (per site) for (a) the metallic (orange empty squares) and insulating states (violet full squares) when the wave function does not break the SU(4) symmetry; (b) when the insulating state (green full circles) has no pairing but $v^{\rm inter}(\mathbf{q}) \neq v^{\rm intra}(\mathbf{q})$; ($c$) when the insulating state (black full triangles) has a finite Δ_d pairing. For clarity the energies are shifted by $3U$. Middle panels: The density-density structure factor $N(\mathbf{q})$ of Eq. (2.66) (divided by $|\mathbf{q}|$) at various values of U/t, for the best variational state. Lower panels: The Fourier transform of the intra-orbital Jastrow factor (multiplied by $|\mathbf{q}|^2$) for the same set of parameters as in the middle panel. No magnetic or orbital orders are considered within the variational wave functions.

As for $J > 0$, also for $J = 0$ at quarter filling ($n = 1$) the variational wave function is fully symmetric and no gain in the variational energy is detected by allowing (on-site inter-orbital) triplet or (nearest-neighbor intra- or inter-orbital) singlet pairings, both in the metallic and the insulating phases. Here, we find that $U_{\mathrm{MIT}}/t = 13 \pm 1$ (see Fig. 3.7). Also when considering three degenerate band and $n = 2$ the transition appears to be continuous (see Fig. 3.8).

This result indicates that, within SU(4) symmetric solutions, the maximum value of U_{MIT} is obtained at half filling, in agreement with previous results (Lu 1994; Rozenberg 1997; Koch, Gunnarsson, and Martin 1999; Ono, Potthoff, and Bulla 2003). Instead, when we allow for a breaking of the SU(4) symmetry, the situation reverses, with the U_{MIT} being lower at half filling (where the transition is no longer continuous).

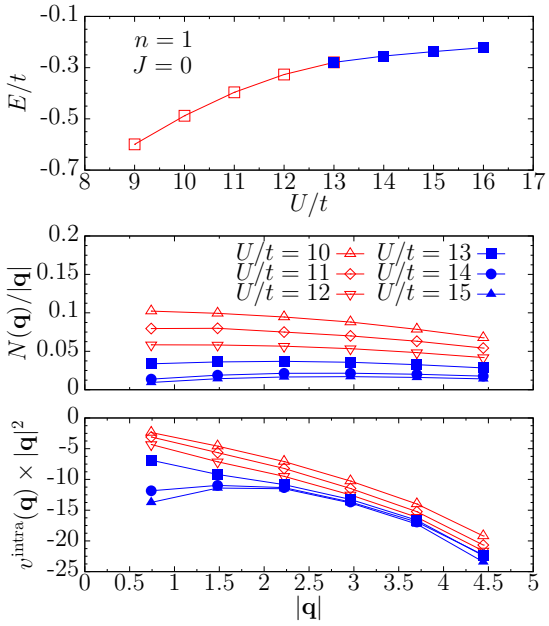

Figure 3.7: Results for $n = 1$ and $J = 0$. Upper panel: Variational energies for the metallic (empty symbols) and insulating (full symbols) states. Middle panel: density-density structure factor $N(\boldsymbol{q})$ (divided by $|\mathbf{q}|$) for various values of U/t. The results for metallic and insulating wave functions are denoted by empty and full symbols, respectively. Lower panel: The Fourier transform of the intra-orbital Jastrow factor (multiplied by $|\mathbf{q}|^2$) for the same set of parameters as in the middle panel. No magnetic or orbital orders are considered within the variational wave functions.

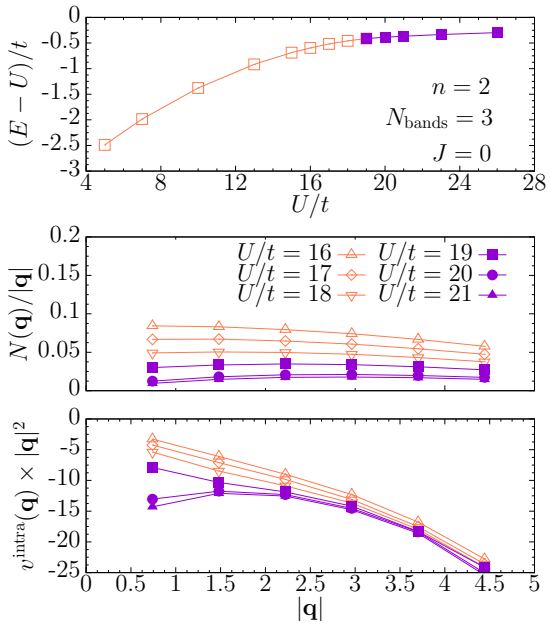

Figure 3.8: Results for three degenerate band model, with $n = 2$ and $J = 0$. Upper panel: Variational energies for the metallic (empty symbols) and insulating (full symbols) states. The energies are shifted by U. Middle panel: density-density structure factor $N(\boldsymbol{q})$ (divided by $|\mathbf{q}|$) for various values of U/t. The results for metallic and insulating wave functions are denoted by empty and full symbols, respectively. Lower panel: The Fourier transform of the intra-orbital Jastrow factor (multiplied by $|\mathbf{q}|^2$) for the same set of parameters as in the middle panel. No magnetic or orbital orders are considered within the variational wave functions.

3.2 Phase separation close to the Mott insulator

A distinctive property of metals and Mott insulators is their electronic compressibility. It is inversely proportional to the variation of the chemical potential μ with respect to the number of particles, i.e. the linear response of the chemical potential with respect to the electron density n. The inverse compressibility κ^{-1} is defined as:

$$\kappa^{-1} = \frac{\partial \mu}{\partial n} = \frac{\partial^2 E}{\partial n^2} \tag{3.6}$$

where E is the ground state energy.

In general, for a physical system in thermodynamic equilibrium, the inverse compressibility κ^{-1} is > 0, which requires the energy to be a convex function of the electron density n. When this condition is violated, the system separates into two spatially distinct re-

gions at different densities, in order to reduce the free energy. This phase separation enhances antiferromagnetic correlation, while reducing the kinetic energy. In a truly infinite system, such a phase separation would be associated with a vanishing inverse compressibility κ^{-1}, that may even become negative in finite systems. In the latter case, we can conveniently locate the density range in which phase separation occurs, by examining the energy-density diagram and looking at the slope of the secant between two different densities (Emery, Kivelson, and Lin 1990; Cosentini, Capone, Guidoni, and Bachelet 1998):

$$\frac{E(n) - E(n=2)}{n-2} \tag{3.7}$$

where a presence of a maximum at a given density $\bar{n} < 2$ marks the occurrence of phase separation between $\bar{n}$ and $n = 2$. In Fig. 3.9 we show the ratio (3.7) for the paramagnetic/paraorbital solutions. We can see that, just above the MIT, at $U/t = 10$ e $J/U = 0.1$ there is no sign of phase separation (in the paramagnetic sector below U_{MIT}, the ground-state is metallic and there is no phase separation). However, for a larger value of the Coulomb interaction, i.e. $U/t = 20$, both for $J/U = 0.1$ and $J/U = 0.2$, there is a distinctive mark of phase separation close to half-filling. This finding is similar to what was found in one- and three-orbital Hubbard models for Cuprates, where, as here, a phase separation may occur in the interaction-doping phase diagram (Emery, Kivelson, and Lin 1990; Bang, Kotliar, Castellani, Grilli, and Raimondi 1991; Imada, Fujimori, and Tokura 1998; Aichhorn, E. Arrigoni, Potthoff, and Hanke 2006).

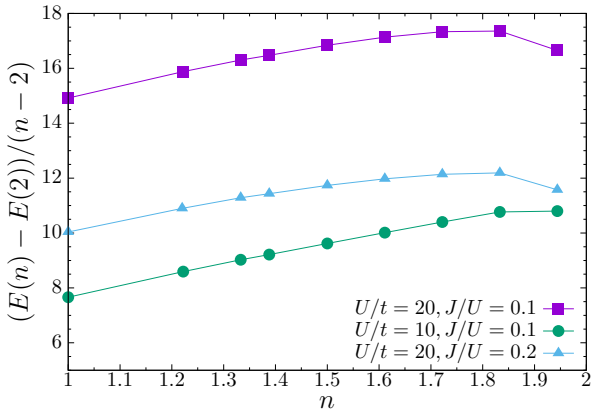

Figure 3.9: Behavior of the function of Eq.(3.7) as a function of the doping density n for $U/t = 10$ and $J/U = 0.1$ (green circles), $U/t = 20, J/U = 0.2$ (cyan triangles) and $U/t = 20, J/U = 0.1$ (violet squares).

3.3 The metal-insulator transitions with magnetic/orbital orders

The above picture for the metal-insulator transitions for the two-band model at $n = 1$ and 2 drastically changes when magnetic and/or orbital order is allowed within the non-interacting wave function i.e.:

$$\begin{aligned}\mathcal{H}_{\rm mag} = &\sum_{\alpha} \Delta^{\alpha}_{\rm AFM} \sum_{i} (-1)^{\mathbf{R}_i} \left(c^{\dagger}_{i,\alpha,\uparrow} c_{i,\alpha,\uparrow} - c^{\dagger}_{i,\alpha,\downarrow} c_{i,\alpha,\downarrow} \right) \\ &+ \sum_{\alpha} h^{\alpha}_{\rm FM} \sum_{i} \left(c^{\dagger}_{i,\alpha,\uparrow} c_{i,\alpha,\uparrow} - c^{\dagger}_{i,\alpha,\downarrow} c_{i,\alpha,\downarrow} \right)\end{aligned} \tag{3.8}$$

$$\begin{aligned}\mathcal{H}_{\rm orb} = &\Delta_{\rm AFO} \sum_{i,\sigma} (-1)^{\mathbf{R}_i} \left(c^{\dagger}_{i,1,\sigma} c_{i,1,\sigma} - c^{\dagger}_{i,2,\sigma} c_{i,2,\sigma} \right) \\ &+ h_{\rm FO} \sum_{i,\sigma} \left(c^{\dagger}_{i,1,\sigma} c_{i,1,\sigma} - c^{\dagger}_{i,2,\sigma} c_{i,2,\sigma} \right)\end{aligned} \tag{3.9}$$

where $\Delta^{\alpha}_{\rm AFM}$,$h^{\alpha}_{\rm FM}$, $\Delta_{\rm AFO}$ and $h_{\rm FO}$ include (staggered and uniform) magnetic and orbital orders.
At half filling, a finite (staggered) magnetic order can be clearly stabilized for $J \geq 0$ (while no orbital order is detected). Notice that, in the case with $J = 0$, magnetic and orbital orders are related by SU(4) symmetry and, therefore, also an orbital order can be found. The optimized antiferromagnetic parameter $\Delta_{\rm AFM}$ of Eq. (2.54) is reported in Fig. 3.10, for $J = 0$ and $J/U = 0.1$. In the former case, $\Delta_{\rm AFM}$ is significantly reduced with respect to the single-band model, which is also reported for comparison. The general trend of the antiferromagnetic parameter at $J = 0$ as a function of the number if the bands is showed in Fig. 3.11. Here we can notice that its value is reduced as the number of degenerate bands is increased.

In the presence of a finite $\Delta_{\rm AFM}$, at half-filling, the triplet pairing $\Delta_{\perp}$ is vanishing (or very small); however, a variational wave function with no magnetic order but a finite triplet pairing can be still stabilized as a local minimum at higher variational energies. Our results for $\Delta_{\rm AFM}$ in the two band-model are compatible with a finite magnetic order down to $U = 0$, with an exponentially small magnetization for $U/t \to 0$. Given the smallness of the energy gain due to $\Delta_{\rm AFM}$ in the weak-coupling limit (i.e., $U/t \lesssim 2$), we are not able to exclude the possibility that antiferromagnetism sets in at a (small) finite value of U/t and not exactly at $U = 0$. Nevertheless, our variational calculations

clearly support the existence of antiferromagnetism at half filling for intermediate values of U/t. Moreover, since the SU(4) Heisenberg model with two (fermionic) particles per site is expected to be ordered (Kim, Penc, Nataf, and Mila 2017) and since a finite Hund coupling cooperates with the super-exchange mechanism to favor staggered magnetism, we foresee that magnetic order in the two-band model should survive for any value of U/t up to $U/t \to \infty$. For the three-band model the situation is less clear and there could be a finite value of U/t for the onset of antiferromagnetic order.

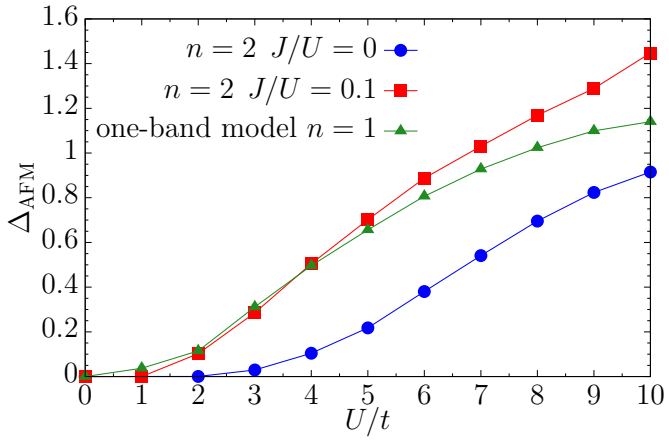

Figure 3.10: Antiferromagnetic parameter $\Delta_{\rm AFM}$ of Eq. (2.54) for $n = 2$, as a function of U/t. The cases with $J = 0$ (full circles) and $J/U = 0.1$ (full squares) are reported for the two-band Hamiltonian, as well as the results for the single-band Hubbard model (full triangles).

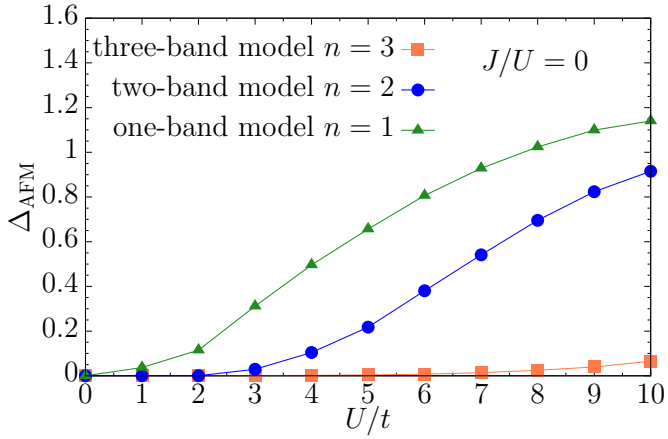

Figure 3.11: Antiferromagnetic parameter $\Delta_{\rm AFM}$ of Eq. (2.54) for the one- (green triangles),two- (blue circles) and three-band model (orange squares) as a function of U/t. In the case of two- and three-band model we set J/U=0.

A region of particular interest is that at quarter-filling, $n = 1$. Here, there is not evidence for antiferromagnetic order, at least for $U/t \lesssim 25$. Instead, in the presence of a finite Hund coupling, a considerable energy gain is found in the strong-coupling regime by allowing both ferromagnetic and antiferro-orbital order, since virtual-hopping processes favor configurations in which two electrons on neighbor sites have parallel spins and reside on different orbitals. Indeed, for sufficiently large electron-electron repulsion, the best variational state is insulating with saturated magnetization $m = (n_\uparrow - n_\downarrow)/(n_\uparrow + n_\downarrow) = 1$ (where $n_\sigma = \sum_{i,\alpha} n_{i,\alpha,\sigma}$) and a finite $\Delta_{\rm AFO}$ in Eq. (3.9). By contrast, for small values of U/t, a fully-symmetric metal with $m = 0$ and no orbital order is found. No intermediate values of m can be stabilized with orbital order. The results for $J/U = 0.1$ are reported in Fig. 3.12, where a first-order phase transition between a metallic state with $m = 0$ and no orbital order and an insulator with $m = 1$ appears at $U/t = 12.5 \pm 0.5$.

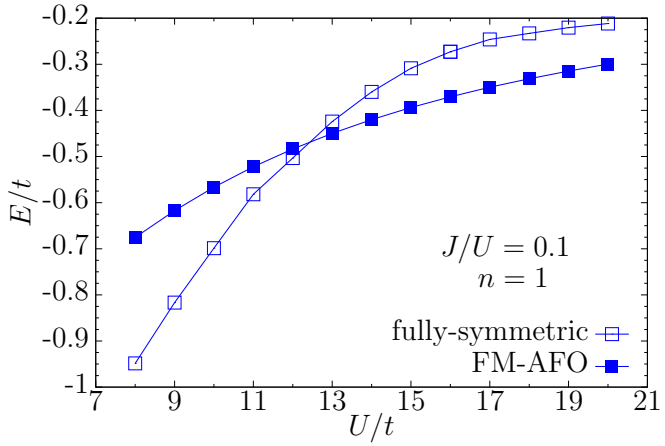

Figure 3.12: Variational energies (per site) for the fully-symmetric wave function (empty squares) and the one that contains ferromagnetic (FM) and antiferro-orbital (AFO) orders (full squares), for $n = 1$ and $J/U = 0.1$.

3.4 Superconductivity and magnetism

We already saw in Chap. 1 that a common ingredient to both Cuprates and Iron-based superconductors is the emergence of superconductivity in doping. On the other hand, the most striking difference is the multi orbital nature of the Iron-based materials. We want then to investigate how the orbitals degree of freedom affects the energetics of superconductivity.

Let us start from the single-band model, where a finite BCS pairing with d-wave symmetry can be stabilized for moderate and large values of U/t (Halboth and Metzner 2000; Maier, Jarrell, Schulthess, Kent, and White 2005; Eichenberger and Baeriswyl 2007; Gull, Parcollet, and Millis 2013; Yokoyama, Ogata, Tanaka, Kobayashi, and Tsuchiura 2012; Kaczmarczyk, Spałek, Schickling, and Bünemann 2013; Deng, Kozik, Prokof'ev, and Svistunov 2015; Tocchio, Becca, and Sorella 2016). This picture becomes less robust in the multi orbital Hubbard model with degenerate electronic bands. For very small values of the Hund coupling (including $J = 0$), a finite pairing amplitude Δ_d with $d_{x^2-y^2}$ symmetry can be stabilized at half filling (see Fig. 3.3 and 3.5); however, Δ_d drops to zero for very small doping, i.e., around $n \approx 1.95$. Singlet pairing is not present at finite doping also when different symmetries of the gap function are taken into account; in this respect, we have considered also an extended s-wave pairing with nearest- and next-nearest-neighbor coupling. In addition, for $J/U \gtrsim 0.1$, no intra-orbital pairing can be stabilized in the wave function, even at half filling (see Fig. 3.3).

We would like to mention that one way to recover a finite singlet pairing at reasonably large dopings is to break the symmetry between the inter- and the intra-orbital Coulomb repulsion, e.g., considering $J = 0$ but still $U \gg U'$. In this case, orbital fluctuations are reduced (since configurations with two electrons on different orbitals are favored over the ones with a doubly-occupied orbital) and the resulting physical behavior can be assimilated to the one of two (weakly-coupled) single-band Hubbard models (one for each orbital). Therefore, a finite d-wave pairing can be stabilized at finite dopings (see Fig. 3.13).

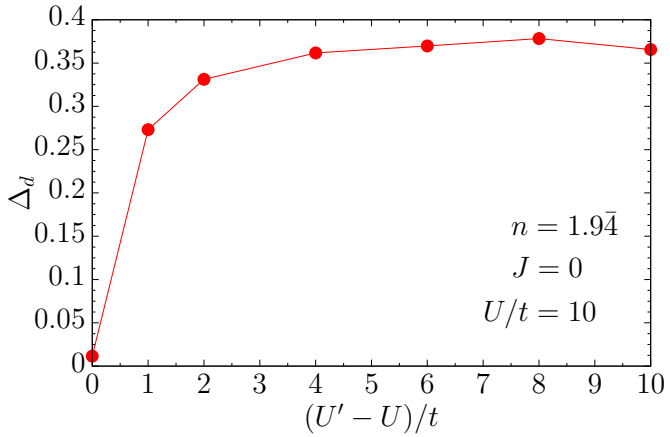

Figure 3.13: Δ_d with $d_{x^2-y^2}$ symmetry at doping $n = 1.9\bar{4}$ for $J = 0$ and $U/t = 10$ when the inter orbital Coulomb coupling U' is varied.

We also mention that, in the opposite limit with $U \ll U'$, an on-site s-wave pairing is present close to half filling, since doubly-occupied orbitals are favored over singly-occupied ones. Remarkably, these two kinds of pairings compete with each other and no singlet pairing can be stabilized away from half filling in the isotropic case with $U = U'$.

Unlike what happens when a singlet pairing is considered in the auxiliary Hamiltonian, a sizable interband triplet pairing $\Delta_\perp$ can be stabilized when no magnetic and orbital order are considered. The state with pairing $\Delta_\perp$ is present in the vicinity of $n = 2$ for $J > 0$ and sufficiently large Coulomb repulsion U, see Fig. 3.14. An s-wave spin triplet state has been already suggested as a possible pairing state in the two degenerate orbital Hubbard model by means, for instance, of Gutzwiller approximation (Bünemann and Spałek 2014), Fluctuation Exchange Approximation (Kubo 2007) or Dynamical Mean Field Theory (Han 2004). Indeed the emergence of spin-triplet superconductivity is a consequence of the fact that, on each site, $S = 1$ states are favored when $J > 0$. As expected, the strength of triplet superconductivity is proportional to

the Hund coupling, thus implying that the doping region in which $\Delta_\perp \neq 0$ enlarges with increasing J (see Fig. 3.14). It is worth mention that, in principle, to analyze the existence of the superconductive order, one should compute the off-diagonal long-range order correlator

$$\langle S_{i,\mu}\, S^\dagger_{j,\mu} \rangle \tag{3.10}$$

where $S^\dagger_{i,\mu} = c^\dagger_{i\uparrow} c^\dagger_{i+\mu\downarrow} + c^\dagger_{i+\mu\uparrow} c^\dagger_{i\downarrow}$ creates an electron singlet pair in the neighboring sites $(i, i+\mu)$. However, in our variational picture, a necessary condition for having finite superconducting correlations is the presence of a finite pairing amplitude in the auxiliary Hamiltonian of Eq. 2.52. It must be emphasized that, away from half filling, the presence of a finite electron pairing in the uncorrelated wave function implies a true long-range order, since the Jastrow pseudopotential has $v^{\text{intra}}(\boldsymbol{q}) \approx v^{\text{inter}}(\boldsymbol{q}) \propto 1/|\boldsymbol{q}|$.
A sizable $\Delta_\perp$ can be stabilized also with the three degenerate bands Hubbard model (see Fig. 3.16). The generalization of $\mathcal{H}_{\text{sc}}$ for multi-orbital models reads:

$$\mathcal{H}_{\text{sc}} = \Delta_\perp \sum_i \sum_{\alpha \neq \beta} \left(c^\dagger_{i,\alpha,\uparrow} c^\dagger_{i,\beta,\downarrow} - c^\dagger_{i,\beta,\uparrow} c^\dagger_{i,\alpha,\downarrow} \right) + \text{H.c.} \tag{3.11}$$

This kind of pairing has also been found as the best candidate of superconductivity in a three-band model by Dynamical Mean Field Theory calculations (Hoshino and Werner 2015). However, in contrast to the latter work, which found that an Ising anisotropy in the Hund coupling is important to stabilize triplet superconductivity, we have evidence that a finite triplet pairing is present also in the isotropic case, which is modeled by the Hamiltonian of Eq. (1.35).

In several Iron-based superconductors, similar to what happens in Cuprates, superconductivity emerges from the suppression of the static antiferromagnetic order in their parent compounds (Dai 2015). In this respect, it is very important to scrutinize a global stability of the spin-triplet phase against the presence of antiferromagnetism, when both magnetism and pairing are treated on an equal footing, being simultaneously optimized in the auxiliary Hamiltonian. We have found that, when including magnetism in the variational wave function, superconductivity is largely suppressed, with antiferromagnetic correlations being strong for electron densities close to half filling. The results are shown in Fig. 3.15 for $J/U = 0.1$. When Δ_{AFM} is present, triplet pairing is strongly reduced close to half filling, leading to an antiferromagnetic metal with no pairing correlations. For $U/t = 15$, a tiny triplet superconductivity emerges around $n = 1.5$, where antiferromagnetism is still present, thus leading to a coexistence between these two order parameters. The pairing amplitude becomes much stronger when increasing the value

of the Coulomb interaction, e.g., for $U/t = 20$, where $\Delta_\perp$ displays a dome-like feature with a broad maximum at $n \approx 1.6$. However, in the presence of a finite Hund coupling also ferromagnetism becomes competitive in energy, especially when U/t is large (see the discussion in the next section).

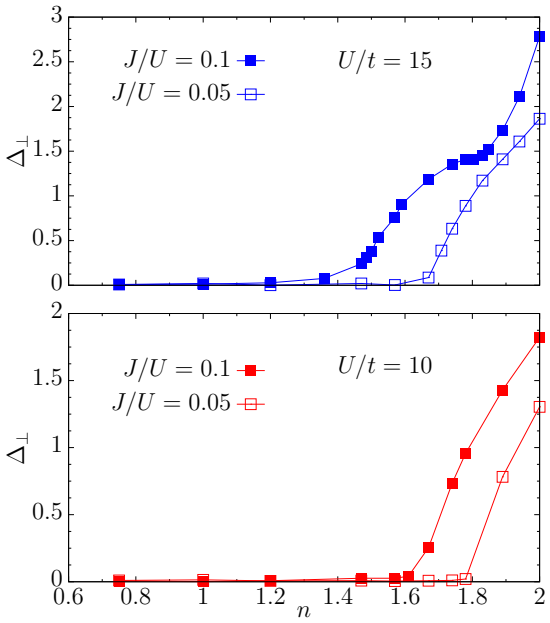

Figure 3.14: Triplet pairing $\Delta_\perp$ in the auxiliary Hamiltonian of Eq. (2.46) when no magnetic or orbital order is considered. Results are reported for $U/t = 15$ (upper panel) and $U/t = 10$ (lower panel) for two values of the Hund coupling $J/U = 0.05$ (empty squares) and $J/U = 0.1$ (full squares).

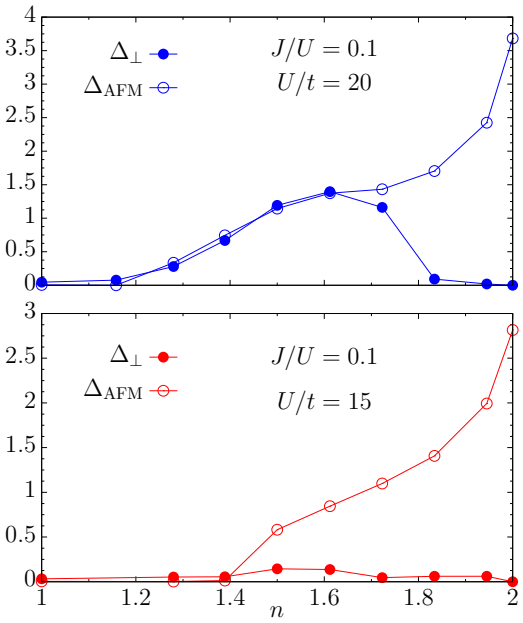

Figure 3.15: Triplet pairing $\Delta_\perp$ (full circles) and antiferromagnetic order parameter $\Delta_{\rm AFM}$ (empty circles) in the auxiliary Hamiltonian of Eq. (2.46). Results are reported for $U/t = 20$ (upper panel) and $U/t = 15$ (lower panel), for $J/U = 0.1$.

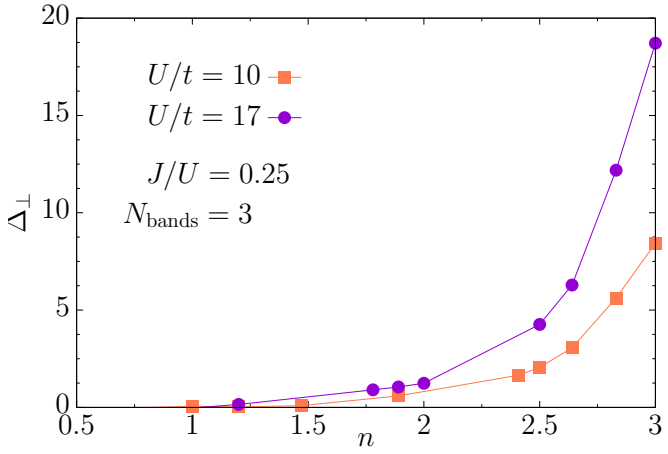

Figure 3.16: Triplet pairing $\Delta_\perp$ in the auxiliary Hamiltonian of Eq. (2.46) when no magnetic or orbital order is considered in tre three-band Hubbard model. Results are reported for $U/t = 10$ (orange squares) and $U/t = 17$ (violet circles) for the Hund coupling $J/U = 0.25$.

3.5 Phase Diagram

In contrast to what happens in the one-orbital Hubbard model, in a multi-orbital system the ferromagnetism based on Hund coupling is expected to be relevant, as suggested by Slater 1936 in the context of ferromagnetism in d-orbital systems. A direct comparison between the superconducting state (with or without antiferromagnetic order) and the ferromagnetic one (with or without orbital order) allows us to draw the two phase diagrams of Fig. 3.17 for $J/U = 0.1$ and $J/U = 0.2$.

In both cases, in the strong-coupling regime ($U/t \geq 13$ and $U/t \geq 14$ respectively) at $n = 1$, the best variational state has ferromagnetic and antiferro-orbital order. The occurrence of both these kind of orders at quarter filling in one dimension was proposed by Harthree-Fock calculations (Roth 1966), Monte Carlo method (Gill and Scalapino 1987), Lanczos diagonalization (Kuei and Scalettar 1997) and density-matrix renormalization-group (Sakamoto, Momoi, and Kubo 2002); in two dimensions by Variational Monte Carlo (Kubo 2009) and by Dynamical Mean Field Theory (Held and Vollhardt 1998; Peters and Pruschke 2010).

Starting from quarter filling, the ferromagnetic state with antiferro-orbital order extends up to (at least) $n \approx 1.1$ for $J/U = 0.2$. On the largest cluster that we considered (i.e., 18×18), $n \approx 1.1$ is is the closest available density to quarter filling that allows a direct comparison between ferromagnetic and paramagnetic states. The orbital order close to

$n \approx 1$ should survive also when $J/U = 0.1$, even if at $n \approx 1.1$ the ferromagnetic wave function has a slightly higher energy than the paramagnetic one. Away from quarter-filling, a uniform ferromagnetic phase without orbital order occurs, as already proposed in one dimension by Density Matrix Renormalization Group (Sakamoto, Momoi, and Kubo 2002), and in two dimensions by VMC (Kubo 2009) and by Dynamical Mean Field Theory (Held and Vollhardt 1998; Peters and Pruschke 2010). For $J/U = 0.2$ the uniform ferromagnetic region is connected with the state with antiferro-orbital order and extends up to $n \approx 1.8$. For $J/U = 0.1$ a paramagnetic metal intrudes between the uniform ferromagnet and the one with orbital order. These results confirm the role of Hund coupling in favoring the ferromagnetic phase. Note that at $J/U = 0.1$ a phase separation takes place close to the first order transition between the paramagnetic and the ferromagnetic metal. Finally, a large region of antiferromagnetism is present at half filling, extending up to intermediate filling, i.e. $n \approx 1.5$. Here, a small region of co-existence of antiferromagnetism and triplet superconductivity is found. Notice that for $J/U = 0.2$ triplet superconductivity is present in a region closer to $n = 2$ and at larger values of the Coulomb repulsion U/t, with respect to the $J/U = 0.1$ case.

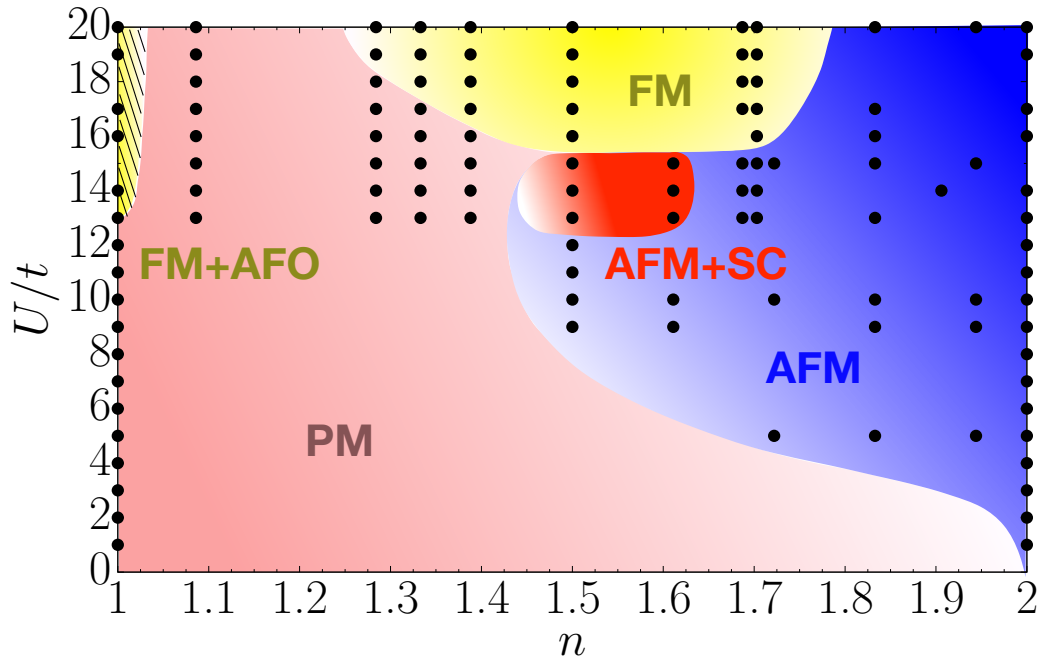

(a) $J/U = 0.1$

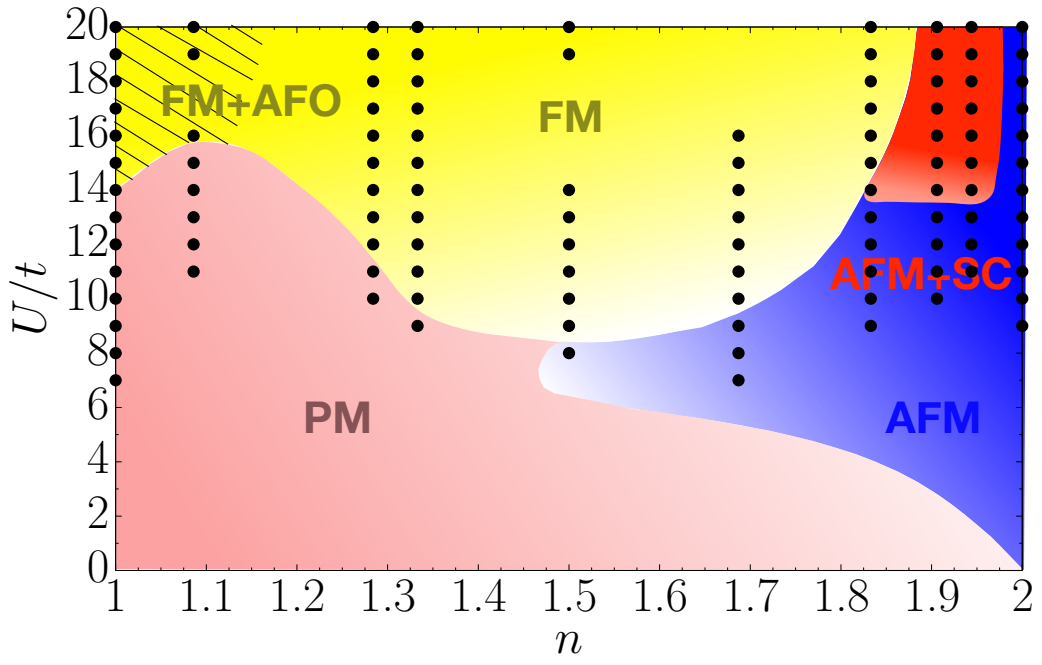

(b) $J/U = 0.2$

Figure 3.17: Schematic phase diagrams of the two-band Hubbard model in the $(n, U/t)$ plane, for $J/U = 0.1$, (a), and $J/U = 0.2$, (b). The yellow region denotes ferromagnetism (FM), which includes also antiferro-orbital order (AFO) in a region close to $n = 1$ (shaded region). The blue region has an antiferromagnetic ground state (AFM), while the red one shows a coexistence of antiferromagnetism and superconductivity with triplet pairing (AFM+SC). Finally, the pink region is a paramagnetic metal (PM). Data, shown as black points, are obtained on clusters with 12×12, 16×16, and 18×18 sites.

Chapter 4

Concluding Remarks

4.1 Summary of the thesis

In this thesis we have considered the two-band Hubbard model with degenerate electronic bands. Ground states of different nature have been investigated by using variational wave functions and Monte Carlo techniques.

At integer fillings with $n = 1$ and $n = 2$, we have first investigated the metal-insulator transitions in the paramagnetic phase. In this regime, our results for the determination of the MIT as a function of the Hund coupling J, are qualitatively in agreement with previous Dynamical Mean Field Theory and slave-particle approaches (de'Medici, Mravlje, and Georges 2011; de'Medici 2011). At half filling for $J > 0$, the transition is first (second) order for small (large) values of the Hund coupling, with a sizable triplet pairing within the Mott insulator (still, no superconducting long-range order is established at half filling, because of the strongly repulsive Jastrow factor). At quarter filling, the transition is second order with no finite pairing neither in the metallic nor in the insulating phase. We have also showed that the addition of another degenerate band does not change qualitatively these results.

Then we have included the possibility of stabilizing magnetic and/or orbital orders. At half filling, a clear evidence for antiferromagnetic order has been obtained for $J \geq 0$. In particular, the qualitative behavior of the magnetic variational parameter resembles the one of the single-band Hubbard model, where antiferromagnetic order sets at $U = 0$; therefore, our results suggest that the ground state for $n = 2$ is antiferromagnetically ordered for any positive value of the Coulomb interaction U. At quarter filling, no sign of antiferromagnetic order is detected (up to $U/t = 25$); instead for $J > 0$, the ground state shows a first-order phase transition from a metallic state for small values

of the electron-electron interaction to an insulator with staggered orbital order and ferromagnetic correlations in the strong-coupling regime.

At intermediate electron dopings with $1 < n < 2$, when both magnetic and orbital order are not included, a sizable triplet pairing is present for finite values of the Hund coupling and sufficiently large electron-electron interactions, *i.e.*, when the Mott insulator at $n = 2$ is doped. Analogously, for electron filling between $n = 2$ and $n = 3$, an appreciable triplet pairing is detectable also in the three-band model. When magnetic order is also considered within the variational wave function, triplet superconductivity is strongly suppressed by antiferromagnetic order close to $n = 2$; furthermore, the region where superconductivity can be stabilized is also reduced by the presence of ferromagnetism, which is competitive in a wide range of densities for large Coulomb repulsions. Finally, Two main tendencies have been identified. First of all the fundamental part played by Hund coupling in determining the properties of the two-band Hubbard model. Second, the presence of multiple competing magnetic states in the phase diagram, indicative of a complex landscape of energies. Our results attest the validity of Jastrow-Slater variational wave function in detecting ground states of different phase diagram sectors.

4.2 Future problems

Concerning future work, there are some issues that we would like to mention.
Throughout the thesis we have discussed the phase diagram of the two-band Hubbard model in which, for the sake of simplicity, we have assumed the orbitals having the same dispersion. For real materials, the situation is more complicated. For instance, the d orbitals have anisotropic lobes, which give preferential directions for the kinetic processes (namely, the presence of hopping terms that would in general depend on the orbitals and the directions). This fact is expected to have important consequences. Indeed it is possible that the superconducting state of the Iron-based superconductors is intrinsically sensitive to the electronic structure, both in "tuning" the pairing interaction and in the determination of pairing symmetry (Kemper, Maier, Graser, Cheng, Hirschfeld, and Scalapino 2010).

We would like to emphasize that the physical properties of a multi-band Hubbard model may crucially depend on the number of bands and their filling. Indeed, there are aspects that should be common to all of them, such as the nature of the Mott transition and the presence of antiferromagnetic order at half-filling. Instead, other properties, related to a possible orbital ordering, can be typical of a particular value of the band degeneracy. For example, while the antiferro-orbital order is clearly obtained in the

two-band model at quarter filling, it is not obvious whether it may be stabilized within a three-band model away from half filling.

Finally, our variational Monte Carlo analysis was based on the definition of a set of distinct wave functions describing different phases, e.g., magnetic, superconducting etc. The comparison of their energies led to the construction of the ground state phase diagram. The main drawback of this approach is that transitions between these phases are often first order (as for instance the transition between the ferromagnetic metal and the triplet superconductor), leading to large regions of phase separation. A possible improvement is given by the definition of variational wave functions describing states with coexisting orders. However this kind of *ansatz* may require a non-trivial generalization of the Monte Carlo method: a Pfaffian wave function is necessary whenever triplet superconductivity is present on top of a ferromagnetic order (Spanu, Lugas, Becca, and Sorella 2008). Within this context, we could also check the real occurrence of phase separation close to the Mott insulator, which was widely discussed for Cuprates materials (Emery, Kivelson, and Lin 1990) as well as for Manganite oxides (Yunoki, Hu, Malvezzi, Moreo, Furukawa, and Dagotto 1998; Dagotto, Burgy, and Moreo 2003) and Iron-based superconductors (de'Medici 2017), and its connection with superconductivity.

Bibliography

Aichhorn, M., E. Arrigoni, M. Potthoff, and W. Hanke (2006). "Antiferromagnetic to superconducting phase transition in the hole- and electron-doped Hubbard model at zero temperature". In: *Physical Review B* 74 (2), p. 024508.

Altland, A. and B. D. Simons (2010). *Condensed matter field theory*. Cambridge University Press, p. 103.

Anderson, P. W. (1973). "Resonating valence bonds: A new kind of insulator?" In: *Materials Research Bulletin* 8 (2), pp. 153–160.

— (1987). "The Resonating Valence Bond State in La_2CuO_4 and Superconductivity". In: *Science* 235 (4793), pp. 1196–1198.

Ashcroft, N. W. and N. D. Mermin (2011). *Solid State Physics*. Cengage Learning.

Bang, Y., G. Kotliar, C. Castellani, M. Grilli, and R. Raimondi (1991). "Phase separation, charge-transfer instability, and superconductivity in the three-band extended Hubbard model: Weak-coupling theory". In: *Physical Review B* 43 (16), pp. 13724–13727.

Bardeen, J., L. N. Cooper, and J. R. Schrieffer (1957). "Theory of superconductivity". In: *Physical Review* 108 (5), p. 1175.

Becca, F. and S. Sorella (2017). "Quantum Monte Carlo Approaches for Correlated Systems". In: Cambridge University Press.

Bednorz, J. G. and K. A. Müller (1986). "Possible high Tc superconductivity in the Ba-La- Cu- O system". In: *Zeitschrift für Physik B Condensed Matter* 64 (2), pp. 189–193.

Brinkman, W. F. and T. M. Rice (1970). "Application of Gutzwiller's Variational Method to the Metal-Insulator Transition". In: *Physical Review B* 2 (10), pp. 4302–4304.

Bünemann, J. and J. Spałek (2014). "Even-parity spin-triplet pairing by purely repulsive interactions for orbitally degenerate correlated fermions". In: *New Journal of Physics* 16 (3), p. 33001.

Bünemann, J. and W. Weber (1997). "Generalized Gutzwiller method for n⩾2 correlated bands: First-order metal-insulator transitions". In: *Physical Review B* 55 (7), pp. 4011–4014.

Bünemann, J., W. Weber, and F. Gebhard (1998). "Multiband Gutzwiller wave functions for general on-site interactions". In: *Physical Review B* 57 (12), p. 6896.

Capello, M., F. Becca, M. Fabrizio, S. Sorella, and E. Tosatti (2005). "Variational description of Mott insulators". In: *Physical Review Letters* 94 (2), p. 26406.

Capello, M., F. Becca, S. Yunoki, and S. Sorella (2006). "Unconventional metal-insulator transition in two dimensions". In: *Physical Review B* 73 (24), p. 245116.

Casula, M. and S. Sorella (2003). "Geminal wave functions with jastrow correlation: A first application to atoms". In: *The Journal of Chemical Physics* 119.13, pp. 6500–6511.

Cooper, L. N. (1956). "Bound electron pairs in a degenerate Fermi gas". In: *Physical Review* 104 (4), p. 1189.

Cosentini, A. C., M. Capone, L. Guidoni, and G. B. Bachelet (1998). "Phase separation in the two-dimensional Hubbard model: A fixed-node quantum Monte Carlo study". In: *Physical Review B* 58 (22), R14685–R14688.

Dagotto, E., J. Burgy, and A. Moreo (2003). "Nanoscale phase separation in colossal magnetoresistance materials: lessons for the cuprates?" In: *Solid State Communications* 126 (1-2), pp. 9–22.

Dai, P. (2015). "Antiferromagnetic order and spin dynamics in iron-based superconductors". In: *Rev. Mod. Phys.* 87 (3), pp. 855–896.

Dayal, S., R. T. Clay, and S. Mazumdar (2012). "Absence of long-range superconducting correlations in the frustrated half-filled-band Hubbard model". In: *Physical Review B* 85 (16), p. 165141.

de'Medici, L. (2011). "Hund's coupling and its key role in tuning multiorbital correlations". In: *Physical Review B* 83 (20), p. 205112.

— (2017). "Hund's Induced Fermi-Liquid Instabilities and Enhanced Quasiparticle Interactions". In: *Physical Review Letters* 118 (16), p. 167003.

de'Medici, L. and M. Capone (2017). "Modeling Many-Body Physics with Slave-Spin Mean-Field: Mott and Hund's Physics in Fe-Superconductors". In: *The Iron Pnictide Superconductors: An Introduction and Overview*. Ed. by Ferdinando Mancini and Roberta Citro. Cham: Springer International Publishing, pp. 115–185.

de'Medici, L., G. Giovannetti, and M. Capone (2014). "Selective Mott physics as a key to iron superconductors". In: *Physical Review Letters* 112 (17), p. 177001.

de'Medici, L., J. Mravlje, and A. Georges (2011). "Janus-faced influence of Hund's rule coupling in strongly correlated materials". In: *Physical Review Letters* 107 (25), p. 256401.

Deng, Y., E. Kozik, N. V. Prokof'ev, and B. V. Svistunov (2015). "Emergent BCS regime of the two-dimensional fermionic Hubbard model: Ground-state phase diagram". In: *EPL (Europhysics Letters)* 110 (5), p. 57001.

Eichenberger, D. and D. Baeriswyl (2007). "Superconductivity and antiferromagnetism in the two-dimensional Hubbard model: A variational study". In: *Physical Review B* 76 (18), p. 180504.

Emery, V. J. and S. Kivelson (1995). "Superconductivity in bad metals". In: *Physical Review Letters* 74 (16), p. 3253.

Emery, V. J., S. Kivelson, and H. Q. Lin (1990). "Phase separation in the t-J model". In: *Physical Review Letters* 64 (4), p. 475.

Erb, A., M. Lambacher, A. Habel, and R. Gross (2018). *P4 Crystal Growth of Superconducting Cuprates*. URL: http://for538.wmi.badw-muenchen.de//projects/P4_crystal_growth/index.htm.

Facio, J. I., V. Vildosola, D. J. Garcia, and P. S. Cornaglia (2017). "On the nature of the Mott transition in multiorbital systems". In: *Physical Review B* 95 (8), p. 85119.

Fazekas, P. and P. W. Anderson (1974). "On the ground state properties of the anisotropic triangular antiferromagnet". In: *Philosophical Magazine* 30 (2), pp. 423–440.

Fazekas, P. and K. Penc (1988). "Generalized Gutzwiller Ansatz for the Half-filled Hubbard Model". In: *International Journal of Modern Physics B* 02 (05), pp. 1021–1034. ISSN: 1793-6578.

Fernandes, R. M. and A. V. Chubukov (2016). "Low-energy microscopic models for iron-based superconductors: a review". In: *Reports on Progress in Physics* 80 (1), p. 14503.

Feynman, Richard P. (1954). "Atomic theory of the two-fluid model of liquid helium". In: *Physical Review* 94 (2), p. 262.

Georges, A., L. de'Medici, and J. Mravlje (2013). "Strong Correlations from Hund's Coupling". In: *Annual Review of Condensed Matter Physics* 4 (1), pp. 137–178.

Georges, A., G. Kotliar, W. Krauth, and M. J. Rozenberg (1996). "Dynamical mean-field theory of strongly correlated fermion systems and the limit of infinite dimensions". In: *Reviews of Modern Physics* 68 (1), p. 13.

Gill, W. and D. J. Scalapino (1987). "Monte Carlo study of a one-dimensional degenerate Hubbard model". In: *Physical Review B* 35 (1), pp. 215–218.

Giuliani, G. and G. Vignale (2005). *Quantum theory of the electron liquid*. Cambridge university press.

Gros, C. (1988). "Superconductivity in correlated wave functions". In: *Physical Review B* 38 (1), pp. 931–934.

Gros, C., D. Poilblanc, T. M. Rice, and F. C. Zhang (1988). "Superconductivity in correlated wavefunctions". In: *Physica C: Superconductivity* 153, pp. 543–548.

Gubernatis, J., N. Kawashima, and P. Werner (2016). *Quantum Monte Carlo Methods*. Cambridge University Press.

Gull, E., O. Parcollet, and A. J. Millis (2013). "Superconductivity and the pseudogap in the two-dimensional Hubbard model". In: *Physical Review Letters* 110 (21), p. 216405.

Gutzwiller, M. C. (1963). "Effect of correlation on the ferromagnetism of transition metals". In: *Physical Review Letters* 10 (5), p. 159.

Halboth, C. J. and W. Metzner (2000). "d-wave superconductivity and Pomeranchuk instability in the two-dimensional Hubbard model". In: *Physical Review Letters* 85 (24), p. 5162.

Han, J. E. (2004). "Spin-triplet s-wave local pairing induced by Hund's rule coupling". In: *Physical Review B* 70 (5), p. 054513.

Han, J. E., M. Jarrell, and D. L. Cox (1998). "Multiorbital Hubbard model in infinite dimensions: Quantum Monte Carlo calculation". In: *Physical Review B* 58 (8), R4199.

Hardy, W. N., D. A. Bonn, D. C. Morgan, R. Liang, and K. Zhang (1993). "Precision measurements of the temperature dependence of λ in $YBa_2Cu_3O_{6.95}$: strong evidence for nodes in the gap function". In: *Physical Review Letters* 70 (25), p. 3999.

Held, K. and D. Vollhardt (1998). "Microscopic conditions favoring itinerant ferromagnetism: Hund's rule coupling and orbital degeneracy". In: *The European Physical Journal B - Condensed Matter and Complex Systems* 5 (3), pp. 473–478. ISSN: 1434-6036.

Hoshino, S. and P. Werner (2015). "Superconductivity from Emerging Magnetic Moments". In: *Physical Review Letters* 115 (24), p. 247001.

Hosono, H. et al. (2015). "Exploration of new superconductors and functional materials, and fabrication of superconducting tapes and wires of iron pnictides". In: *Science and Technology of Advanced Materials* 16 (3), p. 33503.

Hu, J. (2016). "Identifying the genes of unconventional high temperature superconductors". In: *Science bulletin* 61 (7), pp. 561–569.

Hubbard, J. (1963). "Electron correlations in narrow energy bands". In: *Proc. R. Soc. Lond. A* 276 (1365), pp. 238–257.

— (1964). "Electron correlations in narrow energy bands III. An improved solution". In: *Proc. R. Soc. Lond. A* 281 (1386), pp. 401–419.

Imada, M., A. Fujimori, and Y. Tokura (1998). "Metal-insulator transitions". In: *Reviews of modern physics* 70 (4), p. 1039.

Kaczmarczyk, J., J. Spałek, T. Schickling, and J. Bünemann (2013). "Superconductivity in the two-dimensional Hubbard model: Gutzwiller wave function solution". In: *Physical Review B* 88 (11), p. 115127.

Kamihara, Y., T. Watanabe, M. Hirano, and H. Hosono (2008). "Iron-based layered superconductor $La[O_{1-x}F_x]FeAs$ ($x = 0.05 - 0.12$) with Tc= 26 K". In: *Journal of the American Chemical Society* 130 (11), pp. 3296–3297.

Kanamori, J. (1963). "Electron correlation and ferromagnetism of transition metals". In: *Progress of Theoretical Physics* 30 (3), pp. 275–289.

Kaneko, R., L. F. Tocchio, R. Valentì, F. Becca, and C. Gros (2016). "Spontaneous symmetry breaking in correlated wave functions". In: *Physical Review B* 93 (12), p. 125127.

Kemper, A. F., T. A. Maier, S. Graser, H. P. Cheng, P. J. Hirschfeld, and D. J. Scalapino (2010). "Sensitivity of the superconducting state and magnetic susceptibility to key aspects of electronic structure in ferropnictides". In: *New Journal of Physics* 12 (7), p. 073030.

Kim, F. H., K. Penc, P. Nataf, and F. Mila (2017). "Linear flavor-wave theory for fully antisymmetric SU(N) irreducible representations". In: *Physical Review B* 96 (20), p. 205142.

Koch, E., O. Gunnarsson, and R. M. Martin (1999). "Filling dependence of the Mott transition in the degenerate Hubbard model". In: *Physical Review B* 60 (23), p. 15714.

Koga, A., Y. Imai, and N. Kawakami (2002). "Stability of a metallic state in the two-orbital Hubbard model". In: *Physical Review B* 66 (16), p. 165107.

Kotliar, G. and J. Liu (1988). "Superexchange mechanism and d-wave superconductivity". In: *Physical Review B* 38 (7), p. 5142.

Kubo, K. (2007). "Pairing symmetry in a two-orbital Hubbard model on a square lattice". In: *Physical Review B* 75 (22), p. 224509.

— (2009). "Variational Monte Carlo study of ferromagnetism in the two-orbital Hubbard model on a square lattice". In: *Physical Review B* 79 (2), p. 20407.

Kuei, J. and R. T. Scalettar (1997). "Ferromagnetism in an orbitally degenerate Hubbard model". In: *Physical Review B* 55 (22), pp. 14968–14974.

Lechermann, F., A. Georges, G. Kotliar, and O. Parcollet (2007). "Rotationally invariant slave-boson formalism and momentum dependence of the quasiparticle weight". In: *Physical Review B* 76 (15), p. 155102.

Lee, P. A., N. Nagaosa, and X. G. Wen (2006). "Doping a Mott insulator: Physics of high-temperature superconductivity". In: *Reviews of modern physics* 78 (1), p. 17.

Lu, J. P. (1994). "Metal-insulator transitions in degenerate Hubbard models and A_xC_{60}". In: *Physical Review B* 49 (8), p. 5687.

Maier, T. A., M. Jarrell, T. C. Schulthess, P. R. C. Kent, and J. B. White (2005). "Systematic study of *d*-wave superconductivity in the 2D repulsive hubbard model". In: *Physical Review Retters* 95 (23), p. 237001.

Maxwell, E. (1950). "Isotope effect in the superconductivity of mercury". In: *Physical Review* 78 (4), p. 477.

Metropolis, N., A. W. Rosenbluth, M. N. Rosenbluth, A. H. Teller, and E. Teller (1953). "Equation of state calculations by fast computing machines". In: *The journal of chemical physics* 21 (6), pp. 1087–1092.

Momoi, T. and K. Kubo (1998). "Ferromagnetism in the Hubbard model with orbital degeneracy in infinite dimensions". In: *Physical Review B* 58 (2), R567.

Monthoux, P., D. Pines, and G. G. Lonzarich (2007). "Superconductivity without phonons". In: *Nature* 450 (7173), p. 1177.

Mott, N. F. (1949). "The basis of the electron theory of metals, with special reference to the transition metals". In: *Proceedings of the Physical Society. Section A* 62 (7), p. 416.

Mott, N. F. and R. Peierls (1937). "Discussion of the paper by de Boer and Verwey". In: *Proceedings of the Physical Society* 49 (4S), p. 72.

Norman, M. R. (2008). "Trend: High-temperature superconductivity in the iron pnictides". In: *Physics* 1, p. 21.

Ono, Y, M. Potthoff, and R. Bulla (2003). "Mott transitions in correlated electron systems with orbital degrees of freedom". In: *Physical Review B* 67 (3), p. 035119.

Peters, R. and T. Pruschke (2010). "Orbital and magnetic order in the two-orbital Hubbard model". In: *Physical Review B* 81 (3), p. 35112.

Pitaevskii, L. and S. Stringari (1991). "Uncertainty principle, quantum fluctuations, and broken symmetries". In: *Journal of low temperature physics* 85 (5-6), pp. 377–388.

Pruschke, T. and R. Bulla (2005). "Hund's coupling and the metal-insulator transition in the two-band Hubbard model". In: *Eur. Phys. J. B* 44 (2), pp. 217–224.

Reatto, L. and G. V. Chester (1967). "Phonons and the properties of a Bose system". In: *Physical Review* 155 (1), p. 88.

Reynolds, C. A., B. Serin, W. H. Wright, and L. B. Nesbitt (1950). "Superconductivity of isotopes of mercury". In: *Physical Review* 78 (4), p. 487.

Roth, L. M. (1966). "Simple narrow-band model of ferromagnetism due to intra-atomic exchange". In: *Physical Review* 149 (1), p. 306.

Rozenberg, M. J. (1997). "Integer-filling metal-insulator transitions in the degenerate Hubbard model". In: *Physical Review B* 55 (8), R4855.

Sakamoto, H., T. Momoi, and K. Kubo (2002). "Ferromagnetism in the one-dimensional Hubbard model with orbital degeneracy: From low to high electron density". In: *Physical Review B* 65 (22), p. 224403.

Si, Q., R. Yu, and E. Abrahams (2016). "High-temperature superconductivity in iron pnictides and chalcogenides". In: *Nature Reviews Materials* 1 (4), p. 16017.

Slater, J. C. (1936). "The Ferromagnetism of Nickel". In: *Phys. Rev.* 49 (7), pp. 537–545.

Snajdr, M. and S. M. Rothstein (2000). "Are properties derived from variance-optimized wave functions generally more accurate? Monte Carlo study of non-energy-related properties of H_2, He, and LiH". In: *The Journal of Chemical Physics* 112 (11), pp. 4935–4941.

Song, Y. et al. (2016). "A Mott insulator continuously connected to iron pnictide superconductors". In: *Nature communications* 7, p. 13879.

Sorella, S. (1998). "Green function Monte Carlo with stochastic reconfiguration". In: *Physical Review Letters* 80 (20), p. 4558.

— (2001). "Generalized Lanczos algorithm for variational quantum Monte Carlo". In: *Physical Review B* 64 (2), p. 24512.

Spałek, J. (2012). "Coexistence of spin-triplet superconductivity with magnetic ordering in an orbitally degenerate system: Hartree-Fock-BCS approximation revisited". In: *Physical Review B* 86 (1), p. 14505.

Spałek, J. and J. Bünemann (2013). "Coexistence of spin-triplet superconductivity with magnetism within a single mechanism for orbitally degenerate correlated electrons: statistically consistent Gutzwiller approximation". In: *New Journal of Physics* 15 (7), p. 73050.

Spanu, L., M. Lugas, F. Becca, and S. Sorella (2008). "Magnetism and superconductivity in the $t-t'-J$ model". In: *Physical Review B* 77 (2), p. 024510.

Stewart, G. R. (2011). "Superconductivity in iron compounds". In: *Reviews of Modern Physics* 83 (4), p. 1589.

Suzumura, Y., Y. Hasegawa, and H. Fukuyama (1988). "Mean field theory of RVB and superconductivity". In: *Journal of the Physical Society of Japan* 57 (8), pp. 2768–2778.

Tocchio, L. F., F. Arrigoni, S. Sorella, and F. Becca (2016). "Assessing the orbital selective Mott transition with variational wave functions". In: *Journal of Physics: Condensed Matter* 28 (10), p. 105602.

Tocchio, L. F., F. Becca, and C. Gros (2011). "Backflow correlations in the Hubbard model: An efficient tool for the study of the metal-insulator transition and the large-U limit". In: *Physical Review B* 83 (19), p. 195138.

— (2012). "Strong renormalization of the Fermi-surface topology close to the Mott transition". In: *Physical Review B* 86 (3), p. 35102.

Tocchio, L. F., F. Becca, and S. Sorella (2016). "Hidden Mott transition and large-U superconductivity in the two-dimensional Hubbard model". In: *Physical Review B* 94 (19), p. 195126.

Tsuei, C. C. and J. R. Kirtley (2000). "Pairing symmetry in cuprate superconductors". In: *Reviews of Modern Physics* 72 (4), p. 969.

Tsuei, C. C., J. R. Kirtley, et al. (1994). "Pairing symmetry and flux quantization in a tricrystal superconducting ring of $YBa_2Cu_3O_{7-\delta}$". In: *Physical Review Letters* 73 (4), p. 593.

Umrigar, C. J. and C. Filippi (2005). "Energy and variance optimization of many-body wave functions". In: *Physical Review Letters* 94 (15), p. 150201.

Umrigar, C. J., K. G. Wilson, and J. W. Wilkins (1988). "Optimized trial wave functions for quantum Monte Carlo calculations". In: *Physical Review Letters* 60 (17), p. 1719.

Van Delft, D. and P. Kes (2010). "The discovery of superconductivity". In: *Physics Today* 63 (9), pp. 38–43.

Van Kampen, N. G. (1992). *Stochastic processes in physics and chemistry*. Vol. 1. Elsevier.

Wen, X. G. (2004). *Quantum field theory of many-body systems: from the origin of sound to an origin of light and electrons*. Oxford University Press on Demand.

Winter, S. M. et al. (2017). “Models and materials for generalized Kitaev magnetism”. In: *Journal of Physics: Condensed Matter* 29 (49), p. 493002.

Yokoyama, H., M. Ogata, Y. Tanaka, K. Kobayashi, and H. Tsuchiura (2012). “Crossover between BCS superconductor and doped mott insulator of d-wave pairing state in two-dimensional Hubbard model”. In: *Journal of the Physical Society of Japan* 82 (1), p. 14707.

Yokoyama, H. and H. Shiba (1990). “Variational Monte-Carlo Studies of Hubbard Model. III. Intersite Correlation Effects”. In: *Journal of the Physical Society of Japan* 59 (10), pp. 3669–3686. ISSN: 1347-4073.

Yunoki, S., J. Hu, A. L. Malvezzi, A. Moreo, N. Furukawa, and E. Dagotto (1998). “Phase Separation in Electronic Models for Manganites”. In: *Physical Review Letters* 80 (4), pp. 845–848.

Zhang, F. C., C. Gros, T. M. Rice, and H. Shiba (1988). “A renormalised Hamiltonian approach to a resonant valence bond wavefunction”. In: *Superconductor Science and Technology* 1 (1), p. 36.

Zhang, F. C. and T. M. Rice (1988). “Effective Hamiltonian for the superconducting Cu oxides”. In: *Physical Review B* 37 (7), p. 3759.